

**Link Nomenclature, Random Grid Diagrams, and Markov Chain Methods in Knot
Theory**

By

SHAWN L. WITTE
DISSERTATION

Submitted in partial satisfaction of the requirements for the degree of

DOCTOR OF PHILOSOPHY

in

MATHEMATICS

in the

OFFICE OF GRADUATE STUDIES

of the

UNIVERSITY OF CALIFORNIA

DAVIS

Approved:

Mariel Vazquez, Chair

Javier Arsuaga

Eric Babson

Committee in Charge

2019

Contents

Abstract	iv
Acknowledgments	v
Chapter 1. Introduction	1
Chapter 2. Definitions and Background	4
2.1. Combinatorics	4
2.2. Computation	4
2.3. Knot Theory	5
2.4. Markov Chains	25
2.5. Questions and Conjectures	34
Chapter 3. Link Nomenclature	39
3.1. Symmetries, Writhe and Linking Number	39
3.2. Canonical Isotopy Class	40
3.3. Numerical Writhe Results for 2-Component Links	42
3.4. Writhe and Minimum Step Conformations	46
Chapter 4. Markov Chain Methods for Lattice Links	48
4.1. Link-BFACF	49
4.2. Wang-Landau for Lattice Links	55
Chapter 5. Combinatorics and Writhe of Grid Diagrams	59
5.1. Combinatorics of Grid Diagrams	59
5.2. Grids and Writhe	65
Chapter 6. The Frisch-Wasserman-Delbrück Conjecture(FWD) for Grid Diagrams	72
6.1. Proof of the FWD Conjecture for Grid Diagrams	73
Chapter 7. Random Grid Diagrams	85

7.1. Uniformly Random $n \times n$ Grid Diagrams	85
7.2. Markov Chain Algorithms for Grid Diagrams	86
7.3. Numerical Results for Grid Diagrams	96
Chapter 8. Conclusion	102
Appendix A. Index of Notation	104
Appendix B. Link Nomenclature Data	106
Appendix C. Oriented Labeled Link Table	121
Bibliography	126

Abstract

With the support of data from BFACF Markov chain Monte Carlo sampling, conjectures are formed stating that the mean writhe of 2-component lattice links with fixed length and knot type are bounded as length increases. Further, the self-writhe of the components exhibit a similar behavior. It is further conjectured that these writhes sufficiently distinguish reflections and component relabelings of links lacking those symmetries. Guided by these conjectures and using the writhe data obtained, a set of canonical isotopy classes are proposed. Further refinements of the BFACF algorithm are also presented, including a modification into a Wang-Landau algorithm. The behavior of writhe under BFACF moves is proven to be bounded and determined precisely by the local geometry around the edge where the move is being performed.

The combinatorics of grid diagrams are explored. In particular, $n \times n$ grid diagrams representing c -component links and the total number of $n \times n$ grid diagrams are enumerated precisely. A lower bound is provided for the number of $n \times n$ grid diagrams representing a specific knot type. It is proven that the probability that an $n \times n$ grid diagram of a knot chosen uniformly at random being of knot type K decays to 0 as $n \rightarrow \infty$, i.e. the Frisch-Wasserman-Delbrück (FWD) conjecture. This proof provides an upper bound to the number of $n \times n$ grid diagrams representing a specific knot type. It is also shown that the change in writhe from performing knot-preserving grid moves is bounded and can be determined precisely from only a few entries related to where the move is being performed.

Two Markov chain algorithms for randomizing grid diagrams of fixed knot type are presented, one of which is a Wang-Landau algorithm. The Wang-Landau algorithm is used to explore the decay of the knotting probability and shows that the upper bound on the number of $n \times n$ grid diagrams representing a specific knot type given by the proof of the Frisch-Wasserman-Delbrück is not tight. Using this data, it is conjectured that this decay is exponential or faster. The Wang-Landau algorithm is also used to explore the mean writhe of $n \times n$ grid diagrams representing a fixed knot type. These results are used to conjecture that the mean writhe of $n \times n$ grid diagrams is bounded as $n \rightarrow \infty$ and can be used to distinguish a chiral knot and its mirror image.

Acknowledgments

I'd like to acknowledge the many people who made this dissertation possible. Reuben Brasher helped with getting the BFACF software running and for general knowledge about the BFACF algorithm. Rob Scharein provided a copy of KnotPlot and was available for support in using that software. Robert Stolz and I had many conversations regarding BFACF, correlation, and Markov chain sampling. Michelle Flanner collaborated on the link nomenclature work and provided invaluable technical assistance at all levels and all stages of my work. Zihao Zhu did a large amount of work in implementing a version of Wang-Landau for lattice links. Tamara Christiani was always a ready sounding board for any of my ideas. Maxime Puokam was available to consult with on statistical matters. Chris Soteros provided a constant stream of ideas. Andrew Rechnitzer presented a workshop on the Wang-Landau algorithm which inspired all of the work done from that point forward. Chaim Even-Zohar pointed out the possible extension of his FWD proof from petal diagrams to grid diagrams. Marc Culler created Gridlink from which the original versions of my grid diagram codebase were based and from which I obtained my initial conformations for each knot type. My Committee members Javier Arsuaga and Eric Babson provided useful feedback on this work. My advisor, Mariel Vazquez, provided guidance through the whole process.

I'd also like to thank the many artists who provided the soundtrack to which I wrote this dissertation: Sammus, Holly Herndon, Lingua Ignota, Carly Rae Jepsen, Mannequin Pussy, and many many others.

CHAPTER 1

Introduction

Of primary importance in knot theory is determining the equivalence or inequivalence of knots and links. This is usually done through the use of topological invariants (Section 2.3.6). Many of these invariants do not distinguish knots or links that differ only by a mirroring, orientation change, or relabeling of components, i.e. different isotopy classes of a link. This is okay for a broad study of knots and links, but these can be crucial considerations for particular applications.

Take, for example, double stranded deoxyribonucleic acid (dsDNA). In B-form dsDNA, the two sugar phosphate backbones wrap around each other forming a double helix that twists in a right-handed fashion [BBM⁺05]. Bacterial DNA is circular, meaning that the strands of the double helix form a 2-component link. For the cell to undergo mitosis, this DNA must be replicated. This operation is performed by enzymes and proteins in the cell which unzip the DNA into two complementary strands which are then synthesized back into double stranded DNA. If this operation is performed as stated, then the two new DNA molecules will necessarily be linked in the same fashion as the backbones of the original helix, preventing them from being pulled into separate daughter cells. This means that there must be unlinking machinery in the cell which resolve the linked DNA into two unlinked molecules. The machinery comes in the form of recombinases and type II topoisomerases which perform operations equivalent to diagrammatic smoothings and crossing changes (as in the skein relations in Section 2.3.6.3), respectively. It has been observed that these mechanisms unlink the DNA more efficiently than a random process would [Ryb97]. It has also been shown that topo IV, a type II topoisomerase, has a chiral bias [Cri00]. Several studies have been focused on the study of unlinking pathways, i.e. the series of intermediate links and/or knots that a pair of DNA molecules pass through as they are unlinked [SYB⁺17, BI15, VCS05]. In those studies, it is important to consider the specific isotopy classes of knots and links along the pathway, as a chiral bias could affect the appearance of links vs. their mirror images.

To communicate knot and link types of low crossing number, one usually uses Rolfsen's table [Rol76] (preferably a version without the infamous "Perko pair" [Per14]). This table is sufficient

when isotopy classes are not considered, and can be used as a reference point for the mirror of a knot or link. However, this table omits orientations and does not distinguish the components of links in any meaningful way. Further, for links which are not equivalent to their mirror images (chiral links), there is no particular mathematical reasoning for which isotopy classes are presented in the table and which are not.

Before exploring the questions raised by these facts, Chapter 2 provides the necessary background and definitions used throughout this work. A comprehensive and rigorous explanation of the questions examined here can be found in Section 2.5. Given the length and breadth of the work presented here, an index of notation is provided in Appendix A.

Markov chain Monte Carlo experiments have provided evidence that low-crossing chiral knots can be classified into “positive” and “negative” chiralities based on the sign of the mean writhe (defined in section 2.3.7) of fixed length lattice knots of that knot type [PDS⁺11, SIA⁺09]. In Chapter 3, similar methods are used to examine the writhe of 2-component links. The results are used to select a canonical isotopy class for each prime link with crossing number 9 or less. A diagram for each canonical isotopy class can be found in Appendix C.

The data used to obtain these isotopy classes was found by sampling random conformations of the links represented by unions of self-avoiding polygons embedded in the simple cubic lattice (Section 2.3.5). The samples were obtained from Markov chain Monte Carlo sampling using the BFACF algorithm (Section 2.4.4). New variations on BFACF are presented in Chapter 4, including a Wang-Landau algorithm which may be used to more directly examine the mean writhe of lattice links. An efficient way to measure change in writhe while performing these algorithms is also proven.

There are other models for which randomized knots and links may be obtained. For example, random knotting has been examined in the petal diagrams, a subset of arc diagrams (Section 2.3.3) which are themselves equivalent to grid diagrams (Figure 2.2(b), Section 2.3.4) [EZHLN16, EZHLN18]. Random knotting of grid diagrams has not been widely studied. Recently, random knots and crossing changes have been examined for grid diagrams up to grid size 20 [BCH⁺19].

Despite these explorations, the fundamental combinatorics of grid diagrams have remained unexplored until now. In Chapter 5, the number of $n \times n$ grid diagrams are enumerated along with the number of c -component $n \times n$ grid diagrams. A lower bound on the number of $n \times n$ grid

diagrams representing a fixed knot type is also given. An efficient way to measure the change in writhe while performing knot-preserving moves is also proven here.

Perhaps the most essential question in any random knotting scheme is the Frisch-Wasserman-Delbrück conjecture [FW61, Del62], which broadly states that the probability of a random knot being distinct from the unknot goes to 1 as the size of the random knot increases (Section 2.5). Chapter 6 includes the proof of this conjecture for grid diagrams. Specifically, it is shown that the probability of an $n \times n$ grid diagram of a knot chosen uniformly at random representing a given knot type is $O(n^{-1/10})$ which goes to 0 as $n \rightarrow \infty$ (Theorem 6.0.1).

Randomization models for grid diagrams are explored in Chapter 7. Section 7.1 discusses direct sampling of $n \times n$ grid diagrams of non-fixed knot type. Section 7.2 presents and discusses Markov chain methods of exploring grid diagrams. Code for these algorithms, written in Java, is maintained on GitHub [Wit19]. In Section 7.3.1, one of these models is used to explore the actual rate at which the probability of the unknot decays. Section 7.3.2 explores the behavior of writhe in grid diagrams.

Chapter 8 discusses the consequences of the work presented here as well as avenues for extending it to future research.

CHAPTER 2

Definitions and Background

This chapter lays out the required definitions and theory prerequisite to the main body of work presented in the chapters that follow.

2.1. Combinatorics

Denote the set of *permutations* on n objects by S_n . That is, $\sigma \in S_n$ is a bijective function $\sigma: \{1, 2, \dots, n\} \mapsto \{1, 2, \dots, n\}$. It is well-known that $|S_n| = n! = n \cdot (n-1) \cdot (n-2) \cdots 2 \cdot 1$. In terms of counting, one can think of $\sigma \in S_n$ as a way to rearrange the sequence $1, 2, \dots, n$ so that the number i is placed in the $\sigma(i)$ th position.

An interesting subset of S_n that comes up when enumerating grid diagrams is the set of *derangements*. A *derangement* of n objects is a permutation $\sigma \in S_n$ with no fixed points, i.e. $\sigma(i) \neq i$ for all i . The number of derangements of n objects will be denoted by $!n$. It is known that $!n \approx \frac{n!}{e}$ [KT17].

2.2. Computation

When dealing with computer-aided simulations, it is important to keep computational complexity in mind. This complexity is usually calculated on the algorithmic level. Additionally, the “big-oh” notation described here is useful for simplifying the presentation of functional upper bounds, as is done in Chapter 6.

There are several ways to evaluate algorithmic complexity, but the primary two are space complexity and time complexity. The *space complexity* of an algorithm is how much space will be used in the execution of the algorithm proportional to the size of the input data. The *time complexity* of an algorithm is how many computational steps will be executed proportional to the size of the input data.

These complexities are usually measured in “big-oh” notation [AB09]. Big-oh notation for functions $f, g: \mathbb{N} \rightarrow \mathbb{N}$:

- We say $f(n) = O(g(n))$ if there exists constants c and N such that $f(n) \leq c \cdot g(n)$ for every $n \geq N$. Hence, f is asymptotically bounded above by a constant multiple of g . This is where the notation gets its name.
- To contrast, we say $f(n) = \Omega(g(n))$ if $g(n) = O(f(n))$. Hence, f is asymptotically bounded below by a constant multiple of g .
- Finally, $f(n) = \Theta(g(n))$ if $f = O(g(n))$ and $f(n) = \Omega(g(n))$. Hence, f grows asymptotically similarly to g .

2.3. Knot Theory

2.3.1. Basic Definitions. A c -component *link* L is an embedding of the disjoint union of c circles, $\bigsqcup_{k=1}^c \mathbb{S}^1$, into either \mathbb{S}^3 , or \mathbb{R}^3 . The term *conformation* is used to refer to the specific embedding of a link. Each embedded copy of \mathbb{S}^1 is referred to as a *component* of the link. If for a link $L \subset \mathbb{S}^3$ there exists a sphere $S = \mathbb{S}^2 \subset \mathbb{S}^3$ disjoint from L such that $L \cap C_1 \neq \emptyset$, and $L \cap C_2 \neq \emptyset$ where C_1, C_2 are the connected components of $\mathbb{S}^3 \setminus S$, then L is a *split link*. A 1-component link is called a *knot*. The *unknot* is a knot which bounds a disk in \mathbb{S}^3 (or \mathbb{R}^3). Knots that are not equivalent to the unknot are called non-trivial knots. A link may be oriented or unoriented. An *oriented* link is one in which each component is assigned an *orientation* which describes a preferred direction along that component. An *unoriented* link is one in which orientations are not assigned. There are 2 possible orientations for each component, which means that, for each unoriented c -component link, there are 2^c ways that an orientation could be assigned to it.

A link may also have labeled or unlabeled components. Each component of a *labeled* c -component link is given a name so they may be uniquely identified. The components of an *unlabeled* link have no explicitly distinguishing characteristic. For the work presented here, components will be labeled with a number from $\{1, 2, \dots, c\}$. There are $c!$ ways to assign these labels.

Two links L_1 and L_2 are considered *equivalent* if there exists an ambient isotopy which transforms L_1 into L_2 [Rol76]. Colloquially, this can be thought of as moving, bending, and stretching the embedding of one link without breaking it or passing it through itself until it reaches the same embedding as the other link. If L_1 and L_2 are oriented or labeled, then the orientations and labels must match under this transformation. If two non-equivalent links become equivalent after a reflection, change of orientation, or relabeling of the components, then the links are in different *isotopy*

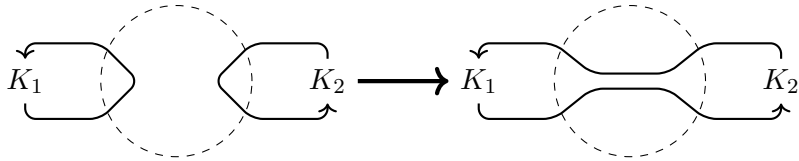


FIGURE 2.1. A demonstration of the connect sum of knots K_1 and K_2 .

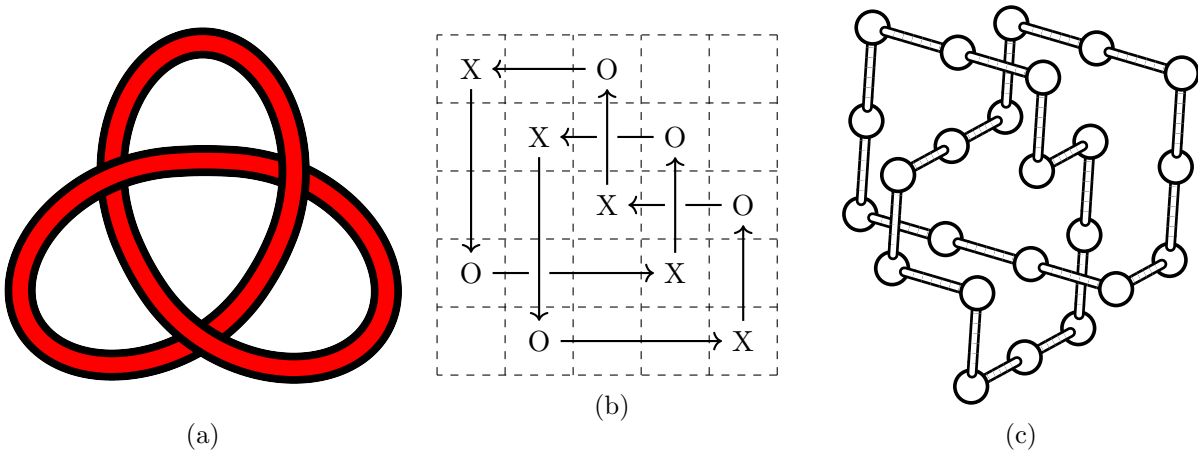


FIGURE 2.2. A regular diagram, grid diagram, and lattice link each representing the right-handed trefoil.

classes of the same *link type*. The relationships between the isotopy classes define the symmetries of a link, which are explained in detail in Section 2.3.8.

The *connect sum* of two knots is obtained by taking a sphere S which intersects each knot exactly twice such that the arcs inside the 3-ball bounded by S are both unknotted, then replacing the arcs inside the sphere with arcs connecting the two knots, respecting orientation if necessary (Figure 2.1). The operation of taking the connect sum of knots K_1 and K_2 is denoted $K_1 \# K_2$. A knot K is *prime* if there are no non-trivial knots K_1 and K_2 , such that $K_1 \# K_2 = K$.

2.3.2. Regular Diagrams. There are many ways to represent a link, but the most common is with regular diagrams. A *regular diagram* of a link is a planar projection of the link such that the preimage of every point is a single point, except for a finite set of double points where the projection crosses itself transversely [Rol76]. Each crossing is marked so that it is known which strand goes over and which strand goes under. Figures 2.2(a) and 2.3 show examples of a regular diagrams.

A regular link diagram can be encoded with a Gauss code. A *Gauss code* is obtained by numbering the crossings, then traveling along the first component of the link and marking each

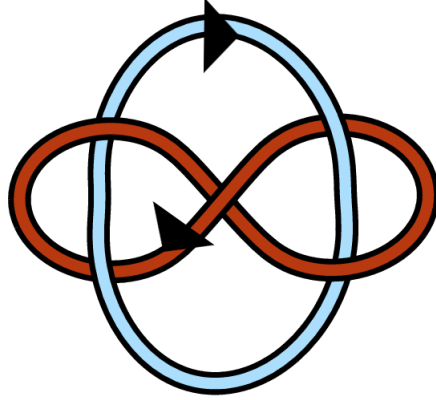


FIGURE 2.3. The 5_1^{2++} link, also known as the Whitehead link.

crossing in order and adding a negative sign if the current strand is crossing under. Then this process is repeated for each subsequent component of the link and the codes for each component are placed in order and separated by spaces. If the link is oriented, then that determines in which direction the components are traversed. As an example, take the diagram of the Whitehead link in Figure 2.3 and number the outer crossings clockwise starting with the upper left crossing as 1, then label the central crossing as 5. Assuming the lighter blue component is component 1, one Gauss code will be $-1, 2, -3, 4 \quad 1, -5, 3, -2, 5, -4$. Note that this Gauss code is not unique, as both the crossing labels and the starting point are arbitrary. Also, if the link is unoriented, then the direction is also arbitrary. Moreover, if one takes a reflection of a link by changing the over/under at each crossing, then the resulting link might not be isotopic to the original, but they may share Gauss codes (Figure 2.2(a) is an example of this).

This last point is corrected by instead using an *extended Gauss code* which is a Gauss code that includes the sign of each crossing. The sign of a crossing is determined by whether the orientations at that crossing satisfy the right-hand rule; the sign is positive if the right-hand rule is satisfied and negative otherwise. More formally, let $\mathcal{C}_{i,j}(D)$ be the set of crossings between component i and component j in a link diagram D , and define $\chi: \mathcal{C}_{i,j}(D) \rightarrow \{-1, 1\}$ as follows

$$(2.1) \quad \chi(C) = \begin{cases} 1 & \text{if } C = \begin{array}{c} \nearrow \searrow \\ \nwarrow \nearrow \end{array} \\ -1 & \text{if } C = \begin{array}{c} \nwarrow \nearrow \\ \nearrow \searrow \end{array} \end{cases}.$$

Now $\chi(C)$ can be used to extend the Gauss codes. Note that orientation does not affect the sign of intra-component crossings, but it does affect inter-component crossings, hence extended

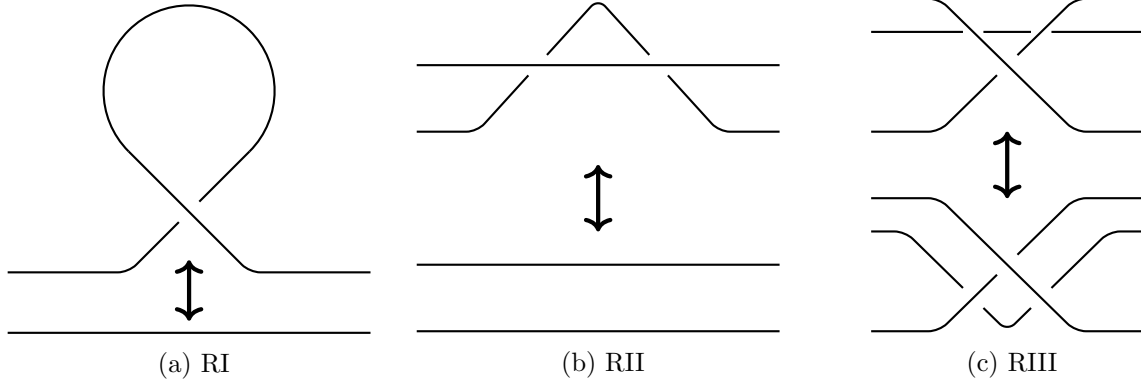


FIGURE 2.4. Reidemeister moves for regular link diagrams.

Gauss codes are well-defined for unoriented knots, but an extension to unoriented links is not well-defined. If the sign information is included by appending the sequence of signs to the code, then the extended Gauss code found for the oriented link in Figure 2.3 can be written as $-1, 2, -3, 4+--+$
 $1, -5, 3, -2, 5, -4++--++$.

Note that Knotplot and the other software used in this work use a slightly different expression of the extended Gauss code [Hyp]. In Knotplot, the extended Gauss code is constructed by using an “a” for at each overcrossing and a “b” at each undercrossing, followed by the number used to label the crossing, followed by the sign of the crossing. So extended Gauss code given above for Figure 2.3 would be written $b1+a2-b3-a4+ a1+b5+a3-b2-a5+b4+$.

While the extended Gauss code of a regular diagram isn’t unique, it does give us a way to define equivalence of regular diagrams. Namely, we can say that two regular diagrams D and D' are equivalent if the same extended Gauss code can describe both of them. This means that any equivalent regular diagrams will represent equivalent links, but each link type has infinitely many non-equivalent regular diagrams.

To see this, consider the “moves” in Figure 2.4, which transform one regular diagram into another. These are known as the Reidemeister moves [Lic97]. Performing any of these moves (in either direction) will not change the link type represented by the regular diagram. They are especially important because of the following property:

THEOREM 2.3.1 ([Rei27, AB26]). *Two regular link diagrams D and D' represent the same link if and only if there exists a finite sequence of Reidemeister moves transforming D into D' .*

Note that the number of crossings in a regular diagram changes by 1 for Reidemeister I moves, 2 for Reidemeister II moves, and 0 for Reidemeister III moves. One can obtain a diagram with an arbitrarily large number of crossings by performing a sequence of crossing-increasing Reidemeister I and/or Reidemeister II moves. By this argument, there are infinitely many regular diagrams for any given link type.

2.3.3. Arc Presentations. Another way to represent links is through arc presentations. Arc presentations were first used by Brunn in 1897 [Bru97], but seem not to have been used again for almost 100 years until a paper by Birman and Menasco [BM94]. At this point Cromwell took interest in arc presentations and proved several fundamental theorems [Cro95, CN96]. In particular, Cromwell showed that every link can be represented by an arc diagram and established an analogue to Reidemeister moves [Cro95].

Consider the extended z -axis $Z = \{(0, 0, z) \mid z \in \mathbb{R}\} \cup \{\infty\}$ in \mathbb{S}^3 and let $\{H_i\}_{i=1}^n$ be a set of half-planes, sometimes called *pages*, such that $H_i \cap H_j = \partial H_i = Z$ for all $i \neq j$. An *arc presentation* (or *arc diagram*) is constructed by the maps $f_i: [0, 1] \rightarrow H_i$ for $i = 1, \dots, n$, where f_i is an embedding of an arc in H_i with $f_i(1) = f_j(0) \in Z$ for some unique $j \neq i$. See Figure 2.5(a) for an example of an arc diagram of the knot 3_1^* .

Much of the work presented here uses grid diagrams. Grid diagrams originally arose from the work done in arc diagrams, and there is a bijection between grid diagrams and arc diagrams [Cro95]. Where useful, arc diagrams are used to help aid in explanations of the properties of grid diagrams. However, most of the results and properties applicable to arc diagrams will be presented in the context of grid diagrams.

2.3.4. Grid Diagrams. Grid diagrams are 2-dimensional representations of links introduced by Cromwell as an alternative depiction of arc presentations, although the term “grid diagram” didn’t come until later [Cro95].

DEFINITION 2.3.2. *A grid diagram is defined as an $n \times n$ lattice where each row and each column has exactly one “O” and one “X”.*

Note that the use of X’s and O’s is consistent with most literature on grid diagrams [BL12, BCH⁺19, Cro95, NT08], but any pair of symbols can be used. For example, *Manolescu et al.* [MOS09] used black and white dots to represent these vertices, and Cromwell’s original formulation used a matrix of 0’s and 1’s for unoriented diagrams [Cro95].

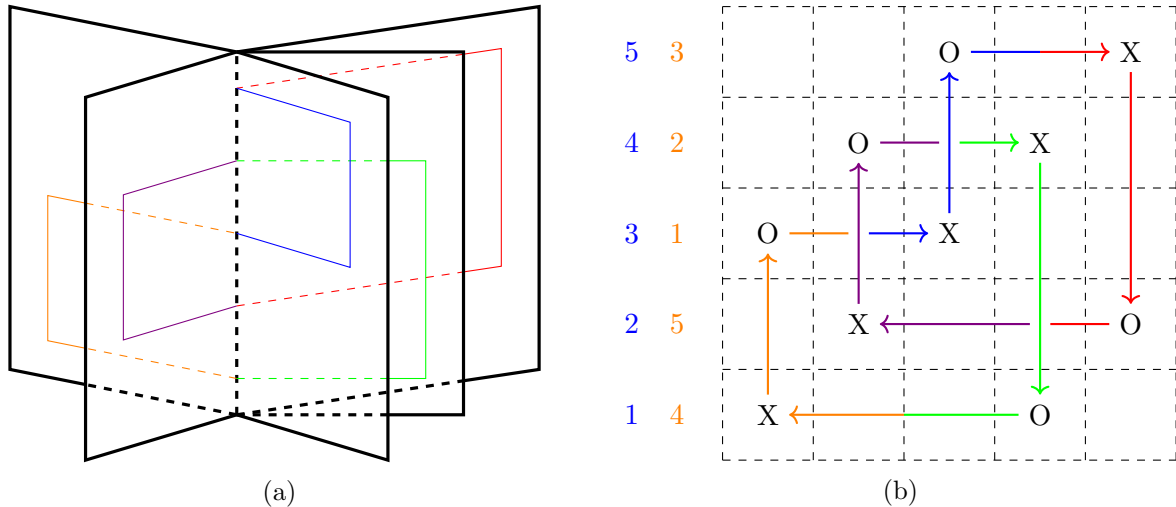


FIGURE 2.5. (a) An arc diagram with 5 pages and (b) the 5×5 grid diagram that corresponds to it as described in the text. The numbers on the left of the grid diagram denote the column indices of the X's (darker blue) and O's (lighter orange) in each row. The correspondence between (a) and (b) can be visualized here by either carefully “flattening” the arc diagram or mapping the heights in the grid diagram to the pages of the arc diagram. The arcs are colored to aid in the visualization of this correspondence.

An oriented regular diagram is obtained from a grid diagram by connecting the X and O entries in every row and column using horizontal and vertical lines, resolving crossings with the convention that vertical lines cross over the horizontal lines. Orientation is assigned from O to X horizontally and from X to O vertically, consistent with [NT08] and what [BL12] refers to as “ (x, y) orientation”. Note that the $n \times n$ grid diagram represented by the positions of the X's and O's in the grid diagram, and its corresponding regular diagram may be used interchangeably. For clarity, grid diagrams generally include oriented edges to denote the corresponding regular diagram. See Figures 2.2(b) and 2.5(b) for an example.

How rows and columns are indexed is a matter of preference. Here rows will be indexed from top to bottom and from left to right as in a matrix, and the indices will start at 1. Each entry can be defined by its row and column index. Two grid diagrams are equivalent if the exact locations of each X and O are the same in each grid.

Note that a link type can be represented by infinitely many distinct regular diagrams, and each of those regular diagrams can be represented by infinitely many distinct grid diagrams. That is, equivalence of grid diagrams is stricter than equivalence of their underlying regular diagrams, which is stricter than equivalence of their corresponding link types.

Grid diagrams correspond directly to arc diagrams. Let g be an $n \times n$ grid diagram, and let $\{H_i\}_{i=1}^n$ be a set of half-planes as in the definition given for arc diagrams where the H_i 's are arranged in numerical order counter-clockwise around Z . The arc diagram corresponding to g is constructed by using the row indices of the X and O in column i as the values for $-f_i(0)$ and $-f_i(1)$ ($f_i(0)$ and $f_i(1)$ if we instead indexed grid rows from bottom to top), respectively. Arc diagrams can be converted to a grid diagram by the inverse operation, which could also be visualized as carefully “flattening” the half-planes onto one single plane (see Figure 2.5). Given this correspondence, any result proven for grid diagrams has an immediate analogue for arc presentations and vice versa.

To discuss grid diagrams in a complete way, it is useful to introduce some extra definitions and notation.

- \mathcal{G} is the set of all grid diagrams.
- \mathcal{G}_n is the set of all $n \times n$ grid diagrams.
- $\mathcal{G}_{n,c}$ is the set of all $n \times n$ grid diagrams representing some link with c components.
- $\mathcal{G}(L)$ is the set of all grids which represent link type L .
- $\mathcal{G}_n(L)$ is the set of all $n \times n$ grids representing link type L .
- $|g|$ is the *size* of a grid diagram g , i.e. if g is an $n \times n$ grid diagram, then $|g| = n$.
- $P_n(K)$ is the probability of observing a knot type K when selecting an element of $\mathcal{G}_{n,1}$ uniformly at random, i.e. $P_n(K) = \frac{|\mathcal{G}_n(K)|}{|\mathcal{G}_{n,1}|}$.

There are four standard grid diagram transformations that preserve the link type represented by the diagram. They are cyclic permutation, commutation, stabilization, and destabilization. These are referred to as Cromwell moves [NT08], and can be inferred from the related arc diagram moves originally presented by Cromwell in [Cro95]. It is worth noting that Cromwell’s definitions didn’t include cyclic permutations, which useful in several proofs and can be constructed from the other three moves [BL12]. Here, general stabilizations/destabilizations will be used as defined by Dynnikov in [Dyn06] in place of Cromwell’s elementary version of these moves. The elementary versions of stabilizations and destabilizations are described in the definitions of the general moves below. To preserve link type under commutations, the concept of interleaving must first be defined.

DEFINITION 2.3.3. *Given columns i and j of an $n \times n$ grid, denote the row index of the first entry in column i by m_i and the second entry by M_i . Likewise denote the row indices of column j*

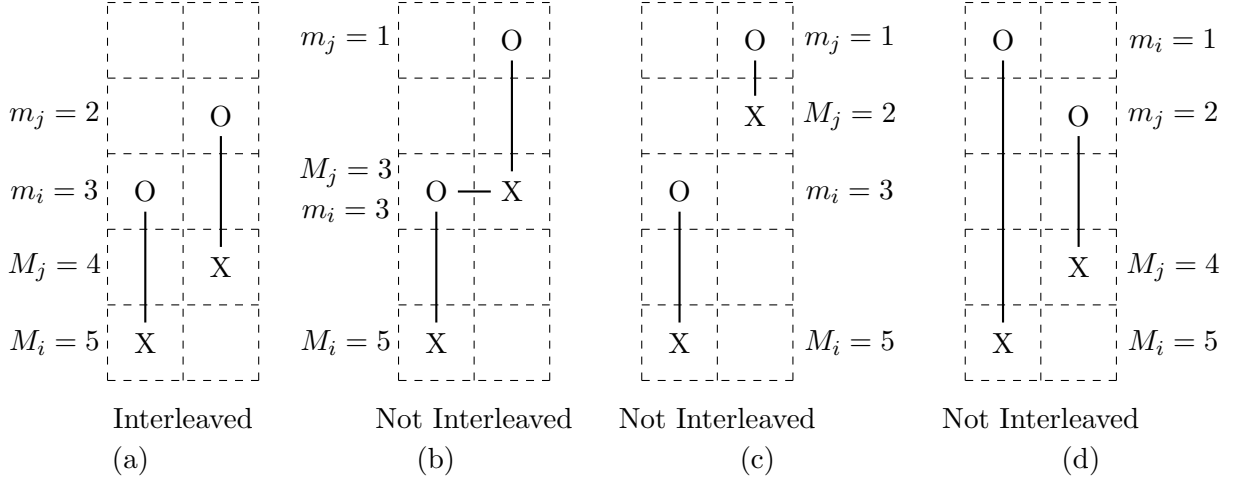


FIGURE 2.6. Columns and whether they are interleaved according to Definition 2.3.3, where the left column is column i and the right column is column j .

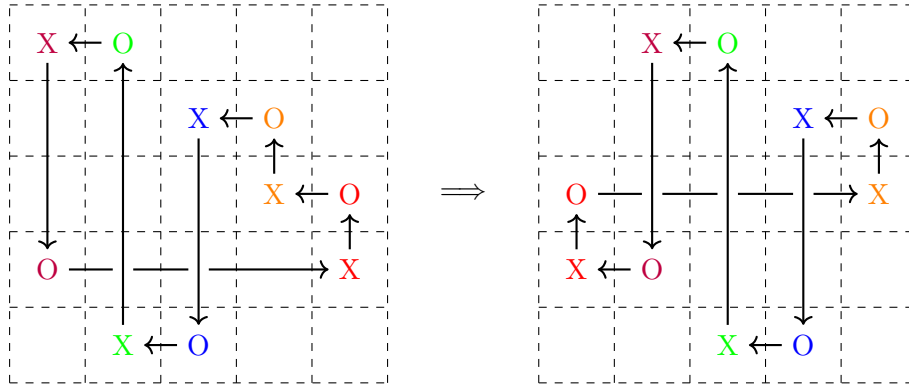


FIGURE 2.7. A cyclic permutation one unit to the right. Color included to aid in visual tracking of the columns.

as m_j and M_j , respectively. We say the two columns are interleaved if $m_i < m_j < M_i < M_j$ or $m_j < m_i < M_j < M_i$ (see Figure 2.6). Interleaving is defined analogously for rows.

The Cromwell moves are defined as follows:

- (1) *Cyclic permutation* [Dyn06, BL12] (Figure 2.7), also called *translation* [NT08], is performed by shifting every X and O up, down, left, or right by one (or more) units. Any X's or O's on the edge of the grid are moved cyclically to the opposite side of the grid.
- (2) *Commutation* [BL12, NT08] (Figure 2.8) is performed by exchanging the entries of two adjacent rows or columns that are not interleaved.
- (3) *General Stabilization* [Dyn06] (Figure 2.9) is performed by choosing a row (or column), creating a new row (column) adjacent to it, and moving one of the entries from the original

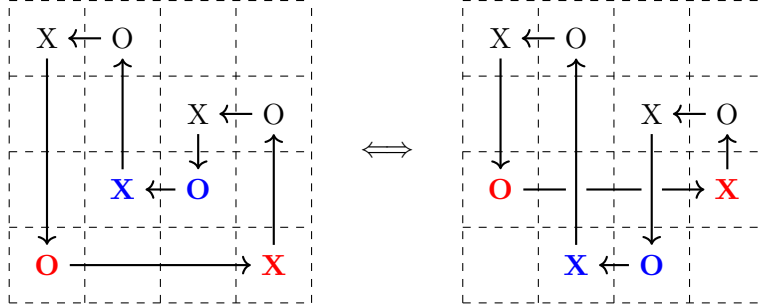


FIGURE 2.8. A commutation of the third and fourth rows.

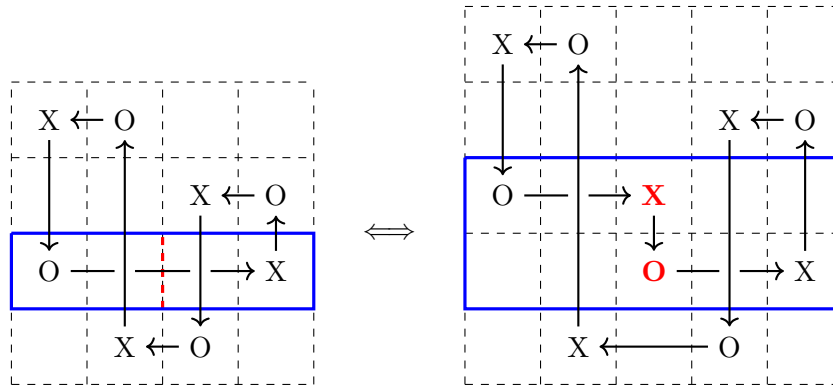


FIGURE 2.9. A general stabilization (\Rightarrow) and general destabilization (\Leftarrow)

row (column) into the new one. Then choose a vertical (horizontal) grid line and insert a new column (row) at that grid line with an X and O in the rows (columns) that are now missing them. The elementary version of this move can be achieved by selecting a grid line adjacent to an entry in the chosen row (column).

- (4) *General Destabilization* [Dyn06] (Figure 2.9) is the inverse of a general stabilization. In particular, it is performed by taking two adjacent entries and removing them by deleting their shared row/column then merging the columns/rows that they separately occupied. The elementary version of this move is achieved by performing this move where an entry is directly adjacent both vertically and horizontally to other entries (e.g. at the O in column 4 of the left-hand grid in Figure 2.9).

There are several notable properties of Cromwell moves:

- (1) Cromwell moves do not change the link type represented by a grid diagram [Cro95].
- (2) Exchanging adjacent interleaved rows or columns will result in a crossing change, which can change the link type, and hence is not a Cromwell move [BCH⁺19]. As such, the

term “commutation” as used here will only refer to exchanges of adjacent non-interleaved rows or columns.

- (3) Cyclic permutations can be performed by composing stabilizations, destabilizations, and commutations [BL12].
- (4) When performing commutations, the first and last rows or columns are considered to be adjacent.
- (5) Commutations and cyclic permutations fix the grid size, stabilizations increase the grid size by 1, and destabilizations decrease the grid size by 1.

Like Reidemeister moves, the primary property of Cromwell moves is that they do not change the link type represented by a grid diagram. The obvious question, then, is whether or not Cromwell moves connect every grid diagram of the same link in the way that Reidemeister moves do for regular diagrams (Theorem 2.3.1). The answer is that they do, which can be stated formally as Theorem 2.3.4.

THEOREM 2.3.4 ([Cro95]). *Given any link type L , and $g_1, g_2 \in \mathcal{G}(L)$, there exists a finite sequence of Cromwell moves which transforms g_1 into g_2 .*

One may have to increase grid size to transform one grid into another of the same or smaller size. For example, take the trefoil in figure 2.2(b) and reverse its orientation (switch the X’s and O’s). This yields the same knot since the trefoil is a reversible knot. One can exhaustively check that there is no way to get from one of these grids to the other by Cromwell moves without performing a stabilization, thus increasing the size of the grid. Similarly, there are grids which cannot be reduced to a minimum size grid without performing stabilizations. A very important counterpoint to this, however, is Dynnikov’s main result in [Dyn06]:

THEOREM 2.3.5 ([Dyn06]). *Let g be a grid diagram representing the unknot. There exists a finite sequence of Cromwell moves containing no stabilizations which will transform g into a 2×2 grid.*

This yields the corollary

COROLLARY 2.3.6. *Given two grid diagrams $g_1, g_2 \in \mathcal{G}(0_1)$, there exists a finite sequence of Cromwell moves which transforms g_1 into g_2 where no intermediate grid diagram is larger than g_1 or g_2 .*

PROOF. This sequence can be obtained by taking the sequence from Theorem 2.3.5 that transforms g_1 into a 2×2 grid, and then taking the inverse of the sequence that transforms g_2 into a 2×2 grid. Since $|\mathcal{G}_2| = 2$, one may need to perform a cyclic permutation by 1 unit to connect these sequences. \square

This corollary will be useful in the application of the Wang-Landau algorithm in Section 7.2.2.

2.3.5. Self-Avoiding Polygons and Lattice Links. A point $p = (x, y, z)$ is in the simple cubic lattice if its coordinates are integers. A *self-avoiding walk* (SAW) of length n in \mathbb{Z}^3 is a sequence of points, $\{p_i = (x_i, y_i, z_i)\}_{i=1}^n$, in \mathbb{Z}^3 such that $|p_i - p_{i+1}| = 1$ for all $i < n$ and $p_i \neq p_j$ (self-avoidance) for all $i \neq j$. A *self-avoiding polygon* (SAP) of length n is a self-avoiding walk of length $n - 1$ where $|p_1 - p_{n-1}| = 1$ [MS13]. Note that the length of a SAP must be even.

A knot can be constructed from a self-avoiding polygon by connecting every pair of consecutive points with an edge, and connecting p_1 and p_{n-1} with an edge as well (Figure 2.2(c)). A c -component link can be constructed by taking the disjoint union of c pairwise disjoint SAPs where each SAP represents a component of the link. SAPs, and their corresponding knots, links, and link components will be used interchangeably and may be referred to as lattice links. In general, the length of a c -component lattice link ω is taken to be the sum of the lengths of its components and is denoted $|\omega|$.

Another way to represent a SAP is with a NEWSUD sequence. A NEWSUD sequence is a sequence of letters from the set $\{N, E, W, S, U, D\}$ where each letter corresponds to an edge and its direction (North, East, West, South, Up, and Down, respectively) [SIA⁺09]. For example, the self-avoiding polygon in Figure 2.2(c) can be described by NNNUUSSDEDDWWUNUEEUSSDDW given the following framing of the cardinal directions: N is the positive y direction, E is the positive x direction, and U is the positive z direction. For links with more than one component, the sequences for each component are connected by a string of lowercase letters describing how to travel from the start of one sequence to the start of another. For example, DDEEUUWWdesDDNNUUSS describes the Hopf Link (2_1^2) . Note that multiple NEWSUD sequences correspond to the same conformation. Two lattice links are *equivalent* if they share a NEWSUD sequence.

Lattice links are genuine three-dimensional embeddings of links, contrasted with regular diagrams and grid diagrams. A valid question is whether there are analogues to Reidemeister and

typically two embeddings that differ only by rigid motions (rotations and translations) will have equivalent geometric invariants. The main geometric invariant of interest in this work is writhe (Section 2.3.7).

2.3.6.1. *Minimal Representations.* Of special interest is a set of link invariants that define the minimum complexity for a link, where complexity can be interpreted in various ways. For example, the minimum number of crossings with which a link L may be represented in a regular diagram is the *crossing number* of L . The crossing number of the unknot is 0 and the crossing number of the simplest knot, the trefoil, is 3. Most knot and link tables index the entries by crossing number. In fact, the standard notation for knots is the Alexander-Briggs notation which uses the crossing number decorated with a subscript indexing knots that share the same crossing number [Roi76]. For example, the unknot is 0_1 , the trefoil is 3_1 , and there are three knots with crossing number 6 named 6_1 , 6_2 , and 6_3 . For links with more than one component, a superscript is added to denote the number of components, e.g. 6_1^2 , 6_2^2 , and 6_3^2 are the three 2-component links with crossing number 6.

For arc diagrams, there is a related invariant called the *arc index*, which is denoted by $\alpha(L)$ and is defined as the smallest number of half-planes required to create an arc diagram representing link type L [Cro95]. Given the bijection with grid diagrams, $\alpha(L)$ can equivalently be defined as the smallest n such that $|\mathcal{G}_n(L)| \neq 0$. The reader is referred to [Cro95, CN96, Cro98] for more about arc index, particularly how it is related to crossing number.

As a note on terminology, *Baldrige & Lowrance* [BL12] use the term “grid number” to describe arc index, but [BCH⁺19, MOS09, OSS15, NT08] use “grid number” to refer to $|g|$. The term “grid number” will not be used here due to this ambiguity and the comparative clarity of the notations $|g|$ and $\alpha(L)$.

Finally, the minimum length needed to realize a link type L as a lattice link is called the *minimum step number* and is denoted $\text{msn}(L)$. It is known that $\text{msn}(0_1) = 4$, $\text{msn}(3_1) = 24$, $\text{msn}(4_1) = 30$, and $\text{msn}(5_1) = 34$, and there are numerically determined estimates for minimum step number of all prime knots through crossing number 10 [SIA⁺09]. The reader is referred to [HKON14] for the most recent bounds on minimum step number relating to crossing number and to [IPS⁺17] for studies of minimal length polygons in subsets of the simple cubic lattice.

2.3.6.2. *Linking Number.* *Linking number* is a topological invariant of oriented 2-component links. Given a 2-component link L parameterized by the closed curves γ_1 and γ_2 , linking number

can be calculated by the Gauss linking integral [Rol76]:

$$(2.2) \quad \text{lk}(L) = \frac{1}{4\pi} \int_{\gamma_1} \int_{\gamma_2} \frac{r_2 - r_1}{|r_2 - r_1|^3} \cdot (dr_2 \times dr_1).$$

The integral in Equation (2.2) can be viewed as a generalization of winding number, measuring how many times one component winds around the other. For lattice links, this integral can be evaluated as a pairwise sum over the edges of each component. Hence, this calculation takes $O(n_1 n_2)$ time where n_1 and n_2 are the lengths of components 1 and 2, respectively, of the lattice link in question.

The Gaussian integral definition of linking number requires a spatial conformation of a link to calculate. Since linking number is a topological invariant, the result will be the same for any conformation of a given link type. For regular diagrams, linking number can be calculated as half the sum over all inter-component crossings where each crossing's contribution to the sum is determined by its sign according to Equation (2.1). Then we can calculate the linking number of a c -component link from a diagram D of a 2-component link L by

$$(2.3) \quad \text{lk}(L) = \sum_{C \in \mathcal{C}_{1,2}(D)} \frac{\chi(C)}{2}.$$

For a link with c components, this can be generalized to a $c \times c$ linking matrix M where the (i, j) entry for $i \neq j$ is the linking number between the i th and j th components, $\text{lk}_{i,j}(L)$, i.e.

$$(2.4) \quad M_{i,j} = \text{lk}_{i,j}(L) = \sum_{C_\ell \in \mathcal{C}_{i,j}(D)} \frac{\chi(C_\ell)}{2}.$$

One can easily show that the linking number and linking matrix are invariant under Reidemeister moves. Reidemeister I moves do not affect inter-component crossings in any way. Inter-component crossings added or removed by Reidemeister II or III moves will change the sum in Equation (2.3) by 0.

2.3.6.3. Polynomial Invariants. There are several useful polynomial link invariants. The most famous of which is probably the Jones polynomial, but the Alexander-Conway, Kauffman, and HOMFLY-PT polynomials are all noteworthy. The latter two are generalizations of the Jones polynomial. The two polynomials used in this work are the Alexander-Conway polynomial and the HOMFLY-PT polynomial. One of the benefits of polynomial invariants is that they can be easily calculated from diagrams via so-called skein relations. A skein relation is a relationship between the polynomials of links whose diagrams differ at a single crossing.

To define a skein relation, consider an oriented link diagram D and select a crossing. Then define three new diagrams as follows: D_+ is obtained from D by replacing the crossing with , D_- is obtained from D by replacing the crossing with , and D_0 is obtained from D by replacing the crossing with . Note that either D_- or D_+ will be equivalent to D as every crossing of an oriented link must take the form  or . Then the skein relation for a polynomial P can be written in the form $F(P(D_+), P(D_-), P(D_0)) = 0$ for some particular function F which defines the specific polynomial. This relationship is then iterated recursively on different crossings to eventually obtain an expression for $P(D)$ in terms of diagrams with known polynomials, e.g. unknots which are typically given a defined polynomial value of 1.

The Alexander-Conway polynomial is used in Chapter 6. This polynomial, denoted by Δ , is defined by the skein relation

$$(2.5) \quad \Delta(D_+) - \Delta(D_-) + (t^{1/2} - t^{-1/2})\Delta(D_0) = 0,$$

with $\Delta(0_1) = 1$. The particular property of this polynomial that will be used in Chapter 6 is a skein-like relationship for $c_2(K)$, the coefficient of t^2 that is sometimes referred to as the Casson invariant [EZHLN18]. If D is a diagram representing a knot K , and $c_2(D)$ is the coefficient of t^2 in $\Delta(K) = \Delta(D)$, then for any crossing in D [Lic97],

$$(2.6) \quad c_2(D_+) - c_2(D_-) = \text{lk}(D_0).$$

The other polynomial used here is the HOMFLY-PT polynomial, which is used for knot identification (Section 7.1). The HOMFLY-PT polynomial is defined by the skein relation

$$(2.7) \quad \ell P(D_+) + \ell^{-1}P(D_-) + mP(D_0) = 0,$$

with $P(0_1) = 1$. The HOMFLY-PT polynomial has the property that if two links are mirror images of each other, then the HOMFLY-PT polynomial of one of the links can be obtained from the other by the change of variables $\ell \rightarrow \ell^{-1}$. This means that the HOMFLY-PT polynomial can distinguish mirror images in many cases, which is important when considering mirror images as distinct links. In the case of this work, all chiral (Section 2.3.8) links are considered distinct from their mirror images.

2.3.7. Writhe. Writhe is a geometric invariant used to measure the geometric complexity of a link. There are two flavors of writhe: projected writhe and space writhe. Space writhe is a measurement of a link’s specific embedding in space (as in SAPs), whereas projected writhe is defined on regular diagrams. Neither of these is a topological invariant.

2.3.7.1. *Projected Writhe.* Let D be a regular diagram of an oriented link. Each crossing in D is assigned $+1$ or -1 per the right-hand rule (Equation (2.1)) as is done when calculating linking number or writing an extended Gauss code. The *projected writhe* of D , is the sum of those contributions over all crossings,

$$(2.8) \quad w(D) = \sum_{C \in \mathcal{C}_{i,j}(D), i \leq j} \chi(C).$$

Note that for knots, the projected writhe is independent of the choice of orientation. For links with more than one component, only the inter-component crossings’ contributions to the writhe are sensitive to orientation. In some instances it is useful to consider writhe contributions of components individually. The *projected self-writhe* of component i of a link is defined as the sum of the writhe contributions from all of that component’s self-crossings,

$$(2.9) \quad s_i(D) = \sum_{C \in \mathcal{C}_{i,i}} \chi(C).$$

To distinguish the writhe obtained by using all crossings from the self-writhe, we denote the former as the *total projected writhe*. Then the relationship between total writhe and self-writhe of a c -component link is defined by

$$(2.10) \quad w(D) = \sum_{i=1}^c s_i(D) + 2 \sum_{i < j} \text{lk}_{i,j}(D).$$

Note that projected writhe is fixed under Reidemeister II and III moves, but can change by ± 1 under Reidemeister I moves. This means that for every arbitrary integer, every link has a projection which achieves that integer as its projected writhe, attained by repeated Reidemeister I moves. Despite this, there are several theorems and conjectures which make good use of the projected writhe. For example, the following is a corollary to the main result of [MT93],

THEOREM 2.3.8. *Any two reduced alternating diagrams for the same link have the same total projected writhe.*

So, the total projected writhe of a reduced alternating diagram operates as a topological invariant of that link. This does not work for non-alternating links, however, as in the case of the infamous “Perko pair” which are two minimum crossing regular diagrams of the same knot with distinct projected writhe values that were long thought to be distinct knots [Per14].

2.3.7.2. *Space Writhe.* Given the similarity of the diagrammatic computations of linking number and writhe, it might not be surprising that space writhe has a similar formula to the computation of linking number on spatial conformations. Starting with component self-writhe, consider a link ω in space where component i is parameterized by γ_i , then the self-writhe of that component can be calculated as

$$(2.11) \quad s_i(\omega) = \frac{1}{4\pi} \int_{\gamma_i} \int_{\gamma_i} \frac{r_2 - r_1}{|r_2 - r_1|^3} \cdot (dr_2 \times dr_1)$$

Similar to how linking number is an extension of winding number measuring how much one component of a link winds around another (and in which direction), self-writhe of a spatial component measures how much it winds around itself. From this, we can extend to a reasonable definition of the total space writhe of a c -component link, similar to total projected writhe:

$$(2.12) \quad w(\omega) = \sum_{i=1}^c s_i(\omega) + 2 \sum_{i < j} \text{lk}_{i,j}(\omega).$$

Note that the same notation is used for both projected writhe and space writhe. It is usually clear which kind of writhe is intended as projected writhe is only defined for regular diagrams and space writhe is only defined for spatial conformations.

2.3.7.3. *Writhe of Lattice Links.* To calculate the space writhe of a lattice link, one can find the component self-writhe by the integral in Equation (2.11) and then apply Equation (2.12) if the total space writhe is desired. This is implemented by summing over the contributions of each pair of edges to the integral. There is also another way to calculate space writhe for lattice links which will be used in Section 4.2.2 to show that writhe change is bounded under BFACF moves. For this alternative calculation, the push-offs of a SAP must first be defined.

DEFINITION 2.3.9. *Let ω be a self-avoiding polygon defined by the sequence $\{p_0, p_1, p_2, \dots, p_n\} \subset \mathbb{Z}^3$, and choose $\vec{v} \in \{-1/2, 1/2\} \times \{-1/2, 1/2\} \times \{-1/2, 1/2\}$. Then the push-off $\omega_{\vec{v}}$ is the polygon*

obtained by connecting consecutive points in the sequence $\{p_0 + \vec{v}, p_1 + \vec{v}, p_2 + \vec{v}, \dots, p_n + \vec{v}\}$ as well as connecting the first and final points.

Two push-offs are *antipodal* if they are defined by opposite vectors \vec{v} and $-\vec{v}$. The calculation of the space writhe of a self-avoiding polygon is described in Theorem 2.3.10.

THEOREM 2.3.10 ([LS91]). *Take a self-avoiding polygon, ω , and four push-offs, $\omega_{\vec{v}_1}$, $\omega_{\vec{v}_2}$, $\omega_{\vec{v}_3}$, and $\omega_{\vec{v}_4}$ of which no two are equivalent or antipodal. Then the writhe of ω may be calculated as follows ,*

$$(2.13) \quad w(\omega) = \sum_{i=1}^4 \frac{\text{lk}(\omega \sqcup \omega_{\vec{v}_i})}{4}$$

Note that Equation (2.13) is defined for a self-avoiding polygon. It may be applied to calculate the self-writhe of the components of a lattice link.

2.3.8. Link Symmetries. For an oriented c -component link with labeled components, there are up to $2 \cdot 2^c \cdot c!$ distinct isotopy classes. This number comes from the 2 reflections, 2^c choices of orientation, and the $c!$ labelings of the components. The symmetries of a link are defined by which of these isotopy classes are equivalent. These symmetries can be described by a subgroup of $\mathbb{Z}_2 \times (\mathbb{Z}_2^c \times S_c)$ where the generator from the first group represents a reflection, elements from \mathbb{Z}_2^c represent choices of orientation, and elements from S_c represent choice of component labeling [BCC⁺12].

Notation derived from that of *Doll and Hoste* [DH91] will be used to distinguish the isotopy classes of an oriented, labeled 2-component link L . First, one of the isotopy classes must be selected as a starting point, which is denoted by $L++$. If we have a link in which the i th component is reversed from $L++$, then we replace the i th $+$ with a $-$. If an oriented link is fully invertible (see below), the $+$'s and $-$'s may be omitted.

The mirror image of $L++$ is denoted by $L^{*}++$. Likewise the mirror images of $L+-$, $L-+$, and $L--$ are $L^{*}+-$, $L^{*}-+$, and $L^{*}--$, respectively. This notation extends to c -component links by appending another $+$ or $-$ for each additional component.

To account for labelings, the notation $\tau L+\dots+$ is used, where $\tau \in S_c$ to denote $L+\dots+$ with the i th component relabeled to $\tau(i)$. If τ is the identity, then τ may be omitted. Applying

Symmetry Name	Occurences for $c(L) \leq 9$	Subgroup of Γ_2	Generators of Sub- group	Equivalence Class of $L++$
Full Symmetry	1	Γ_2	$\langle \epsilon, r_1, r_2, p \rangle$	$\{L++, L+-, L-+, L--,$ $L*++, L*+-, L*-+, L*--,$ $\tau L++, \tau L+-, \tau L-+, \tau L--,$ $\tau L*++, \tau L*+-, \tau L*-+,$ $\tau L*--\}$
Purely Inv. (Pure Ex.)	25	$\Sigma_{4,1}$	$\langle r_1 r_2, p \rangle$	$\{L++, L--, \tau L++, \tau L--\}$
Purely Inv. (No Ex.)	32	$\Sigma_{2,1}$	$\langle r_1 r_2 \rangle$	$\{L++, L--\}$
Fully Inv. (Pure Ex.)	5	$\Sigma_{8,1}$	$\langle r_1, r_2, p \rangle$	$\{L++, L+-, L-+, L--,$ $\tau L++, \tau L+-, \tau L-+, \tau L--\}$
Fully Inv. (no Ex.)	22	$\Sigma_{4,2}$	$\langle r_1, r_2 \rangle$	$\{L++, L+-, L-+, L--\}$
Even Op. (Pure Ex.)	3	$\Sigma_{8,2}$	$\langle \epsilon r_1, \epsilon r_2, p \rangle$	$\{L++, L--, L*+-, L*-+,$ $\tau L++, \tau L--, \tau L*+-, \tau L*-+\}$
Even Op. (Non-Pure Ex.)	1	$\Sigma_{4,5}$	$\langle \epsilon r_1 p, \epsilon r_2 p \rangle$	$\{L++, L--, \tau L*+-, \tau L*-+\}$
No Symmetry	3	$\{e\}$	$\langle e \rangle$	$\{L++\}$

TABLE 2.1. Symmetry groups for two-component links with up to 9 crossings. Listed are names for the groups and their notation as a subgroup of Γ_2 [CCMP12, BCC⁺12]. Also listed are generators for the subgroup where ϵ is a reflection, r_1 and r_2 are reversals of components 1 and 2, respectively, and p is the exchange of the component labels. The final column indicates which of the 16 different possible isotopy classes are equivalent to $L++$ where τ is the non-trivial element of S_2 .

this notation with reversals, for example $\tau L+-$, leaves an ambiguity for what order the relabeling and component reversals happen. The convention is used that τ is applied to $L \pm \cdots \pm$ after the orientations are determined. This means that the diagrams of $L+-$ and $(12)L+-$ look identical except for the names assigned to the components. Figure 2.11 shows this notation in full for the 4_1^2 link.

Cantarella et al. discuss the subgroups of $\Gamma_2 = \mathbb{Z}_2 \times (\mathbb{Z}_2^2 \times S_2)$, the full symmetry group for 2-component links [CCMP12]. In particular there are 27 subgroups up to conjugacy where the j th subgroup of order k in the subgroup lattice (as presented in [CCMP12]) is designated $\Sigma_{k,j}$. When cross-referenced with the symmetries found in [BCC⁺12, HW92], it is seen that only 8 of the 27 subgroups occur for 2-component links with crossing number 9 or less. These particular subgroups will be important in Chapter 3, which assigns a canonical choice of $L++$ for 2-component links through 9 crossings. Details of each of these subgroups are included in Table 2.1. The symmetry names used come from [BCC⁺12] and are defined as follows:

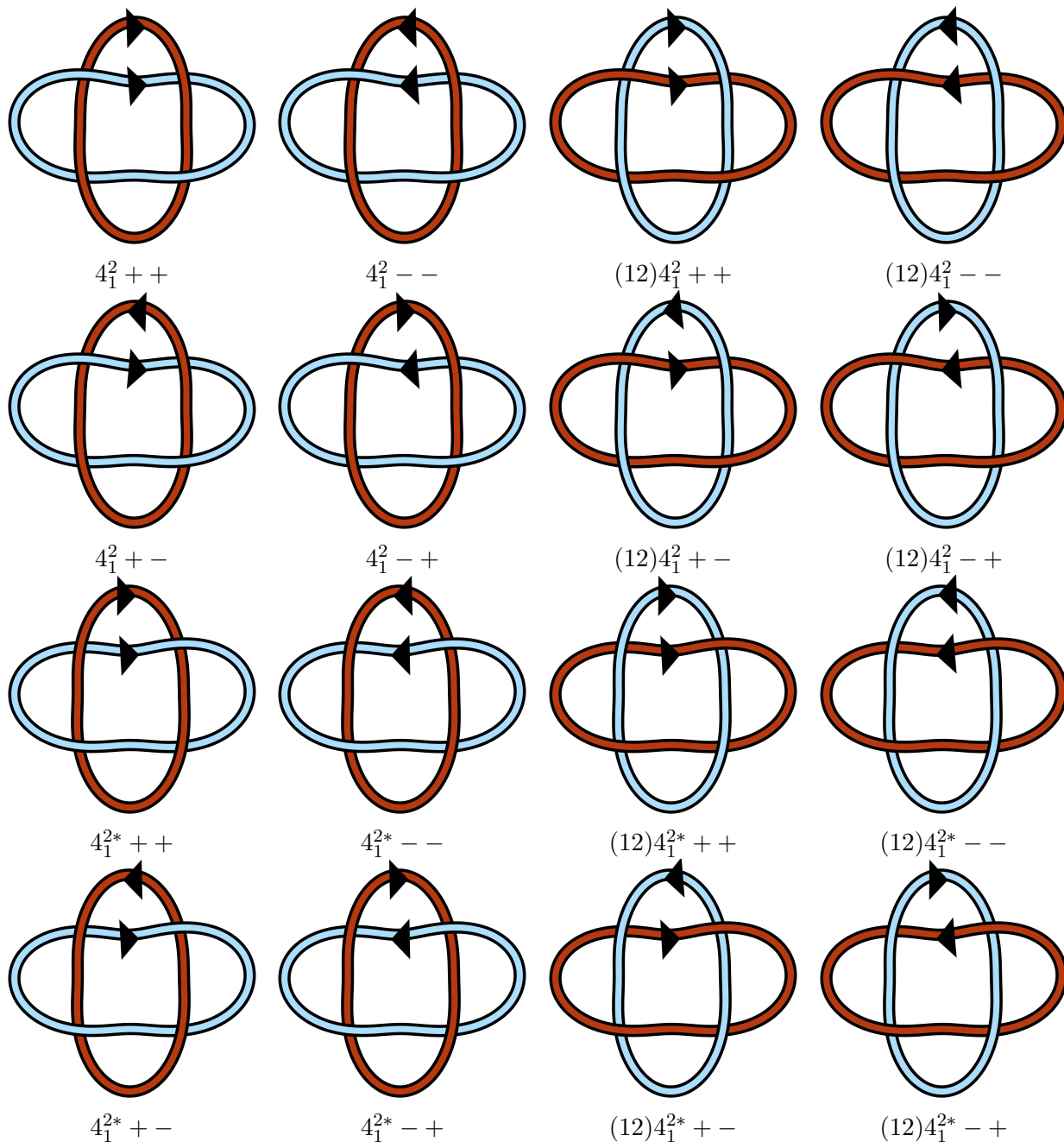


FIGURE 2.11. Link notation, adopted and modified from [DH91]. The lighter blue strand is component 1 and the darker red-orange strand is component 2. Due to the symmetry of 4_1^2 , all links sharing a row in this figure are equivalent.

- A link L is *non-invertible* or *non-reversible* if it is not isotopic to L with any other choice of orientation.
- A link L is *purely invertible* if it is isotopic to the link found by simultaneously reversing both components ($L_{++} = L_{--}$).

- A link L is *fully invertible* if it is isotopic to L with every other choice of orientation.
- A link L has *even operations* symmetry if it is isotopic to links obtained by an even number of reflections and/or component reversals.
- A link L has *pure exchange* symmetry if it is isotopic to L with every relabeling of components.
- A link L has *full symmetry* if it is isotopic to every link obtained by component relabeling, component reversal, or reflection.
- A link L has *no symmetry* if it is not isotopic to any link obtained by component relabeling, component reversal, or reflection.

Note that even operations and full symmetries are the only symmetry types here where the un-oriented versions of the links are achiral (equivalent to their mirror) as opposed to chiral (not equivalent to their mirror).

2.4. Markov Chains

A *Markov chain* is a set of states Ω , called the *state space*, combined with transition probabilities $P(\omega \rightarrow \omega') \in [0, 1]$ for each pair of states $\omega, \omega' \in \Omega$ [GS09]. The values $P(\omega \rightarrow \omega')$ are probabilities in the sense that they satisfy the property $\sum_{\omega' \in \Omega} P(\omega \rightarrow \omega') = 1$ for fixed ω . A Markov chain can be described entirely by an $n \times n$ matrix where n is the number of states and the (i, j) entry is $P(\omega_i \rightarrow \omega_j)$. A Markov chain can also be realized as a weighted directed graph in which the vertices are states and the weights are transition probabilities, i.e. the matrix described above is used as a weighted adjacency matrix. Note that a Markov chain need not have a finite number of states. In this work, Markov chains with countably infinite state spaces will be considered. For these, the matrix and graph representations may easily be extended to an infinite matrix and a graph with infinitely many vertices, respectively.

A *step* along a Markov chain is a transition from ω to ω' according to the transition probability $P(\omega \rightarrow \omega')$, visualized in the the Markov chain graph as moving from the ω node to the ω' node. A *walk of length t* along a Markov chain is a sequence of t steps. The probability of being at state ω' after taking t steps from state ω is denoted $P^t(\omega \rightarrow \omega')$. Note that each step and walk along a Markov chain only depends on the current state and not on previous states. Of primary concern for most Markov chains is the posterior distribution π and whether or not it exists. The *posterior distribution* (also *limiting*, *equilibrium*, or *stationary distribution*) is defined

as $\pi(\omega) = \lim_{t \rightarrow \infty} P^t(\omega_0 \rightarrow \omega)$ where ω_0 is an initial state. This limit may or may not exist and may or may not depend on the initial state ω_0 . Theorem 2.4.1 below guarantees that $\lim_{t \rightarrow \infty} P^t(\omega_0 \rightarrow \omega)$ exists and is independent of ω_0 as long as the conditions described below are met. All Markov chains examined here will satisfy Theorem 2.4.1.

A Markov chain is *ergodic* (or *irreducible*) if for every pair of states $\omega, \omega' \in \Omega$, there is a finite t such that $P^t(\omega \rightarrow \omega') > 0$. In other words, every state in Ω can be reached from any other state in a finite number of steps. The *period* of a state $\omega \in \Omega$ is defined as $\gcd\{t \mid P^t(\omega \rightarrow \omega) > 0\}$. If this value is 1, then ω is *aperiodic*. Being aperiodic is equivalent to saying that there exists some T such that $P^t(\omega \rightarrow \omega) > 0$ for all $t \geq T$, i.e. after T steps from ω , there is a non-zero probability that any step could return to ω . The entire Markov chain is *aperiodic* if every state in Ω is aperiodic. Note that an ergodic chain with at least one aperiodic element must be an aperiodic chain. A Markov chain satisfies *detailed balance* (or is *reversible*) with respect to a distribution π if for each pair of states $\omega, \omega' \in \Omega$ the following equation holds:

$$(2.14) \quad \pi(\omega)P(\omega \rightarrow \omega') = \pi(\omega')P(\omega' \rightarrow \omega).$$

These properties come together in the following theorem,

THEOREM 2.4.1 ([MS13]). *If a finite or countably infinite Markov chain is aperiodic, ergodic, and satisfies detailed balance with respect to π , then $\lim_{t \rightarrow \infty} P^t(\omega_0 \rightarrow \omega) = \pi(\omega)$ for all $\omega_0, \omega \in \Omega$.*

2.4.1. Monte Carlo Sampling. Markov chains have many uses, one of which is Monte Carlo sampling. *Monte Carlo sampling* is the process of taking a large number of random samples from a set of states to estimate some property of that set.

A common example of Monte Carlo sampling (without using Markov chains) is estimating the value of π (the mathematical constant, not the posterior distribution). One way to do this is to randomly sample points in $[0, 1] \times [0, 1]$ uniformly and count how many are less than 1 unit from the origin. In this work, *sampling uniformly* from a set means to randomly sample from the uniform distribution on that set. The points less than 1 unit from the origin are in the first quadrant of the unit disk centered at $(0, 0)$ in \mathbb{R}^2 . Hence these points should make up approximately $\pi/4$ of the total samples, as that is the proportion of $[0, 1] \times [0, 1]$ occupied by the unit disk. As more samples are gathered, the proportion of points within 1 unit from the origin will have higher and higher probability of being very near $\pi/4$.

Markov chains provide a way to produce the random samples for Monte Carlo estimation. In the example above, using with a reliable $O(1)$ time random number generator one can uniformly sample (x, y) points from $[0, 1] \times [0, 1]$ in $O(1)$ time by uniformly generating $x, y \in [0, 1]$ directly. For more complicated state spaces, it is not so straightforward to generate an element of the space uniformly at random. This is resolved by running a Markov chain simulation with some initial state ω_0 and large enough t so that $P^t(\omega_0 \rightarrow \omega) \approx \pi(\omega)$ for the posterior distribution π . In the cases of the Markov chains in this work, the posterior distributions are known and shown to exist via Theorem 2.4.1.

The following is a generic algorithm for obtaining n samples via Markov chain Monte Carlo (MCMC) sampling,

ALGORITHM 2.4.2.

- (1) Start with an initial state ω_0 . Let $t = 0$, $t_{\text{samp}} > 0$, and $n > 0$.
- (2) Choose a state ω' with probability $P(\omega_t \rightarrow \omega')$.
- (3) Let $\omega_{t+1} = \omega'$.
- (4) Increase t by 1
- (5) If t is divisible by t_{samp} , then sample ω_t .
- (6) If $t/t_{\text{samp}} = n$, then terminate the algorithm. Else, return to step 2.

Here, t_{samp} is the sampling rate, i.e. the number of steps taken between samples. Since the goal is to sample from as close as possible to the posterior distribution π , t_{samp} should be large enough so that $P^{t_{\text{samp}}}(\omega_t \rightarrow \omega) \approx \pi(\omega)$ for each ω . If t_{samp} is too small, then consecutive samples will be highly correlated. On the other hand if t_{samp} is too large then iterating the algorithm to gather enough samples will use extra time on unnecessary computation. The appropriate tuning of t_{samp} is dependent on the Markov chain being implemented.

2.4.2. Metropolis-Hastings. There is a class of Markov chain algorithms called Metropolis-Hastings algorithms. These defined by the implementation of a *Metropolis-Hastings step* which determines whether or not a chosen transition will be performed or not, i.e. accepted or rejected. A Metropolis-Hastings algorithm is implemented by rewriting $P(\omega \rightarrow \omega') = P_{\text{choose}}(\omega \rightarrow \omega') \cdot P_{\text{accept}}(\omega \rightarrow \omega')$, where $P_{\text{choose}}(\omega \rightarrow \omega')$ is the probability that a transition from ω to ω' is chosen in the Markov chain and $P_{\text{accept}}(\omega \rightarrow \omega')$ is the probability of accepting and performing that transition (the Metropolis-Hastings step). If the transition is not accepted, then the chain steps from ω to ω .

In practice implementing a Metropolis-Hastings algorithm tends to be more straightforward to implement than a non-Metropolis-Hastings version of the same algorithm. For an example, compare the Metropolis-Hastings version of BFACF in Section 2.4.4 to the discussion of BFACF probabilities in [MS13]. The version in [MS13] requires selecting a set of possible transitions, then choosing one or rejecting them all based on probabilities dependent on each of the selected transitions. Solving detailed balance for the transition probabilities in that implementation requires ensuring that the transition probabilities satisfy four inequalities in addition to the relationship defined by Equation (2.37). Similarly, the algorithm presented in Section 7.2.1 was originally conceived in a non-Metropolis-Hastings fashion, but selecting valid transition probabilities became even more convoluted as they had to satisfy an infinite set of inequalities. If a state-space has way to choose transitions between states where $P_{\text{choose}}(\omega \rightarrow \omega')$ can be readily calculated, then all that remains in a Metropolis-Hastings implementation is to solve for $P_{\text{accept}}(\omega \rightarrow \omega')$ from the detailed balance equation. All of the Markov chain algorithms presented in this work are Metropolis-Hastings algorithms.

2.4.3. Wang-Landau. The Wang-Landau algorithm is a generic Metropolis-Hastings MCMC algorithm used to explore the density of energies of a given state space and was introduced by *Wang and Landau* in [WL01]. It is a particularly versatile algorithm, as “energy” can be defined as any measurable value of the system. Energy can even be defined as something categorical, or as a tuple of values. In the case of lattice links energy can be defined as space writhe, total length, length of a single component, a tuple of the lengths of each component, a tuple of space writhe and total length, and any other conceivable value of interest. For grid diagrams, examples of energy are the grid size, projected writhe, and whether or not the diagram is alternating.

Also, Wang-Landau can be applied to any existing Markov chain. Let Ω be the finite state space of a Metropolis-Hastings Markov chain whose transitions are chosen with probabilities $P_{\text{choose}}(\omega \rightarrow \omega')$. The Wang-Landau algorithm is defined by the Metropolis-Hastings probabilities, $P_{\text{accept}}(\omega \rightarrow \omega')$ as described below. Before fully defining the Wang-Landau algorithm, it will be helpful to assign some notation.

Let $E: \Omega \rightarrow X$ be the chosen energy function, where X is some finite space appropriate for the energy function. Let $\mathcal{E} = \{E(\omega) \mid \omega \in \Omega\}$ be the set of all possible energy values for states in Ω .

Assuming $|\mathcal{E}| = M$, index the elements of \mathcal{E} as E_1, E_2, \dots, E_M . Let $\mu_{E_i} = |\{\omega \in \Omega \mid E(\omega) = E_i\}|$, the number of states in Ω with energy value E_i .

As a motivation for using Wang-Landau, suppose we want to use MCMC to uniformly sample from the possible energy states. That is, we want the Markov chain to converge to the distribution

$$(2.15) \quad \pi(\omega) = \frac{1}{\mu_{E(\omega)}} \cdot \frac{1}{M}.$$

Then, detailed balance yields the following,

$$(2.16) \quad \pi(\omega)P(\omega \rightarrow \omega') = \pi(\omega')P(\omega' \rightarrow \omega)$$

$$(2.17) \quad \frac{P_{\text{choose}}(\omega \rightarrow \omega')P_{\text{accept}}(\omega \rightarrow \omega')}{M\mu_{E(\omega)}} = \frac{P_{\text{choose}}(\omega' \rightarrow \omega)P_{\text{accept}}(\omega' \rightarrow \omega)}{M\mu_{E(\omega')}}.$$

$$(2.18) \quad \frac{P_{\text{accept}}(\omega \rightarrow \omega')}{P_{\text{accept}}(\omega' \rightarrow \omega)} = \frac{P_{\text{choose}}(\omega' \rightarrow \omega)}{P_{\text{choose}}(\omega \rightarrow \omega')} \cdot \frac{\mu_{E(\omega)}}{\mu_{E(\omega')}}.$$

Thus the Metropolis-Hastings probabilities can be selected as

$$(2.19) \quad P_{\text{accept}}(\omega \rightarrow \omega') = \min \left\{ 1, \frac{P_{\text{choose}}(\omega' \rightarrow \omega)}{P_{\text{choose}}(\omega \rightarrow \omega')} \cdot \frac{\mu_{E(\omega)}}{\mu_{E(\omega')}} \right\}.$$

In most of the Wang-Landau literature, it is assumed that $P_{\text{choose}}(\omega \rightarrow \omega') = P_{\text{choose}}(\omega' \rightarrow \omega)$, hence those terms disappear in the acceptance probabilities. This is not the case for the algorithms studied here.

Calculating $P_{\text{accept}}(\omega \rightarrow \omega')$ from Equation (2.19) only works if $\mu_{E(\omega)}/\mu_{E(\omega')}$ is known a priori. This is usually not the case. Wang-Landau provides a way to “train” a set of weights to estimate the ratios μ_{E_i}/μ_{E_j} for each pair i, j . Training of Wang-Landau weights is done by periodically updating the weights, W_{E_i} , from some initial guess until they converge to values with the property that

$$(2.20) \quad \frac{W_{E_i}}{W_{E_j}} \approx \frac{\mu_{E_i}}{\mu_{E_j}}$$

for every i, j . We can then adjust the posterior distribution to be

$$(2.21) \quad \pi(\omega) = \frac{1}{W_{E(\omega)}} \cdot \frac{1}{M}$$

which approximates the distribution in Equation (2.15). This yields the Wang-Landau Metropolis-Hastings probabilities of

$$(2.22) \quad P_{\text{accept}}(\omega \rightarrow \omega') = \min \left\{ 1, \frac{P_{\text{choose}}(\omega' \rightarrow \omega)}{P_{\text{choose}}(\omega \rightarrow \omega')} \cdot \frac{W_{E(\omega)}}{W_{E(\omega')}} \right\}.$$

The Wang-Landau weights, W_{E_i} , are “trained” as follows:

ALGORITHM 2.4.3.

- (1) Choose an initial state $\omega_0 \in \Omega$, set $t = 0$, choose an update factor $f \in \mathbb{R}_{>1}$ and an update frequency $t_{\text{samp}} \in \mathbb{Z}_{>0}$, and initialize each weight, $W_{E_i} > 0$.
- (2) Choose a state ω' with probability $P_{\text{choose}}(\omega_t \rightarrow \omega')$.
- (3) Set $\omega_{t+1} = \omega'$ with probability $P_{\text{accept}}(\omega_t \rightarrow \omega')$ (from Equation (2.22)), else set $\omega_{t+1} = \omega_t$.
- (4) Increment t by 1.
- (5) If t divides t_{samp} , then update $W_{E(\omega_t)} \leftarrow W_{E(\omega_t)} \cdot f$. Return to step 2.

Most sources for Wang-Landau describe the algorithm with $t_{\text{samp}} = 1$. If no prior information is known, then the weights are typically initialized as $W_{E_i} = 1$ for every i , which is often a very poor estimate. An inaccurate set of initial weights can increase the amount of time it takes for the weights to reach a good estimate, but once at least one weight training has been completed, the weights obtained can be used as the initial weights in future runs.

Zhou and Bhatt showed that for each pair of energy values E_i and E_j , the ratio W_{E_i}/W_{E_j} will converge to an interval around the true ratio μ_{E_i}/μ_{E_j} , regardless of the initial weights [ZB05]. The width of this interval is proportional to $\sqrt{\ln(f)}$ and the convergence time is inversely proportional to $\sqrt{\ln(f)}$ [ZB05, ML07]. As $f \rightarrow 1$, the weight estimates become more accurate, but the time it takes to converge to these estimates increases.

Weights are usually trained by starting with a larger value of f and then reducing f after some criterion is met. This reduction is usually $f \leftarrow \sqrt{f}$, with the initial value of $f = e^1$, as was used in the original paper [WL01]. The algorithm terminates once f has been reduced to a sufficiently small value (determined beforehand). Several criteria have been recommended for how to decide when to reduce f [WL01, BP07, ZB05]. This work will use the convention provided by *Morozov and Lin* [ML07]. Morozov and Lin found an estimation for error that is appropriate as long as

each weight, W_{E_i} , has been updated at least

$$(2.23) \quad \frac{1}{2 \ln(f)} \ln \left(\frac{a}{\gamma_i \ln(f)} \right)$$

times, where f is being updated as $f \leftarrow f^{1/a}$, and $\gamma_i = W_{E_i}/W_{E_j}$ with $W_{E_i} > W_{E_j}$. The appropriate choice of j for γ_i is somewhat vague in [ML07], but if the error of W_{E_i}/W_{E_j} is desired for any particular value of j , then that is a good choice for j . In the numerical experiments of Section 7.3, updating W_{E_i} at least as many times as indicated by Equation (2.23) is used as the condition to be met before updating f .

To calculate the error of Wang-Landau weights, define $\Delta_{i,j}$ to satisfy

$$(2.24) \quad \frac{W_{E_i}}{W_{E_j}} = \frac{\mu_{E_i}}{\mu_{E_j}} e^{\Delta_{i,j}}.$$

Then $\langle \Delta_{i,j} \rangle \rightarrow 0$ as $f \rightarrow 1$, and $\Delta_{i,j}$ can be estimated by its error [ML07],

$$(2.25) \quad \sigma \left(\ln \left(\frac{W_{E_i}}{W_{E_j}} \right) \right) = \Delta_{i,j} \approx \sigma(\Delta_{i,j}) \sim \sqrt{\ln(f) \cdot W_{E_i}/W_{E_j}}$$

as long as the weights were update enough times according to Equation (2.23). Note that the error estimate in Equation (2.25) is only a proportion which means it could potentially overestimate or underestimate the actual error. This error can be propagated to functions of weights by the general error propagation formula,

$$(2.26) \quad \sigma(f(x_1, \dots, x_m)) = \sqrt{\left(\frac{\partial f}{\partial x_1} \cdot \sigma(x_1) \right)^2 + \dots + \left(\frac{\partial f}{\partial x_m} \cdot \sigma(x_m) \right)^2}.$$

Once the ratios W_{E_i}/W_{E_j} have converged satisfactorily, the acceptance probabilities in Equation (2.22) can be used for regular MCMC sampling from the distribution in Equation (2.21) which will sample states uniformly within each energy value and will sample approximately uniformly across all energy values. For the Wang-Landau experiments in Section 7.3, the Wang-Landau weights are used directly to analyze the distribution of energies. More specifically grid size is used as energy to examine the growth rate of $|\mathcal{G}_n(K)|$ (Section 7.3.1) and writhe is added to the energy to examine the behavior of writhe as grid size increases (Section 7.3.2). It is important to keep in mind that Wang-Landau does not estimate μ_{E_i} , but only estimates the ratios μ_{E_i}/μ_{E_j} . However, if μ_{E_j} is

known (or well-estimated through other means) for some j , then we can estimate μ_{E_i} by using

$$(2.27) \quad \mu_{E_i} = \mu_{E_j} \frac{\mu_{E_i}}{\mu_{E_j}} \approx \mu_{E_j} \frac{W_{E_i}}{W_{E_j}}$$

2.4.4. The BFACF Algorithm. The BFACF algorithm is a Markov chain algorithm that can be used to generate random lattice link conformations of a fixed link type. BFACF is named for the authors of the papers in which it was introduced: Berg, Foester, Aragão, Caracciolo, and Fröhlich [BF81, AC83, ACF83]. It has been extensively used to generate ensembles of random conformations of lattice links [PDS⁺11, BSV13, SYB⁺17]. In particular, if one wishes to model DNA with lattice links, then BFACF can be used to generate random ensembles to compare to biological models.

2.4.4.1. *Distribution and Transition Probabilities.* The BFACF algorithm converges to a posterior distribution based on the canonical ensemble from statistical mechanics. Let ω be a lattice link representing link type L , then the posterior distribution of BFACF is,

$$(2.28) \quad \pi(\omega) = \frac{|\omega|z^{|\omega|}}{\Xi(z)}$$

with

$$(2.29) \quad \Xi(z) = \sum_{n=0}^{\infty} n z^n \mu_n(L)$$

for some fixed value $z \in (0, z_0)$ (discussed below), where $\mu_n(L)$ is the total number of lattice link conformations of length n which represent the link type L . One property of this distribution is that every lattice link representing the same link type with the same length will have equal probability i.e. the resulting conformations are uniformly distributed in the space of lattice links of length n and type L . More precisely, if ω_1 and ω_2 are both lattice links representing link type L , then $|\omega_1| = |\omega_2| \Rightarrow \pi(\omega_1) = \pi(\omega_2)$.

Note that the value of z must be chosen so that $\Xi(z)$ converges. By the root test, this means

$$(2.30) \quad 0 < z < \left(\lim_{n \rightarrow \infty} (n\mu_n)^{1/n} \right)^{-1} := z_0.$$

Note that μ_n grows approximately exponentially and $z_0 \approx .2134$; z is called the fugacity parameter [MS13].

A larger choice of z will increase both the expected value and the variance of the conformation length. Each of these values will tend to infinity as $z \rightarrow z_0$. Technically, every lattice link conformation of L will have a nonzero probability in π , however the probability of conformations tend to 0 as length increases, so in practice BFACF can be useful for sampling from a certain region of lengths.

As mentioned in Section 2.4.2, it is more straightforward to implement BFACF as a Metropolis-Hastings algorithm. The reader is directed to [MS13] for a complete description of a non-Metropolis-Hastings implementation. With π as selected in Equation (2.28), and the transitions defined by the BFACF moves described in Section 2.3.5, all that remains is to determine how to choose the transitions and then solve detailed balance for the Metropolis-Hastings probabilities.

Suppose the current state, ω , is a SAP with length n (links with more than one component are considered in Section 4.1). Then the BFACF move is chosen by selecting an edge uniformly at random from the set of all edges, and selecting a perpendicular direction uniformly at random, which is the direction the edge will be pushed to perform the move. This gives every possible move a $\frac{1}{4n}$ probability of being chosen. Also, every move that transforms ω into ω' has exactly one BFACF move that is inverse to it, i.e. pushing the edge back. This means that if there are k moves that transform ω into ω' , then there are k moves that transform ω' into ω .

Suppose the move is a 0-move:

$$(2.31) \quad \pi(\omega)P(\omega \rightarrow \omega') = \pi(\omega')P(\omega' \rightarrow \omega)$$

$$(2.32) \quad \frac{nz^n}{\Xi(z)} \cdot \frac{k}{4n} P_{\text{accept}}(\omega \rightarrow \omega') = \frac{nz^n}{\Xi(z)} \cdot \frac{k}{4n} P_{\text{accept}}(\omega' \rightarrow \omega)$$

$$(2.33) \quad P_{\text{accept}}(\omega \rightarrow \omega') = P_{\text{accept}}(\omega' \rightarrow \omega).$$

If we let $P_{\text{accept}}(+0)$ be the probability of accepting any 0-move in the Metropolis-Hastings step, then to maximize the number of accepted transitions we may choose

$$(2.34) \quad P_{\text{accept}}(+0) = 1.$$

Now suppose the chosen move is a +2-move:

$$(2.35) \quad \pi(\omega)P(\omega \rightarrow \omega') = \pi(\omega')P(\omega' \rightarrow \omega)$$

$$(2.36) \quad \frac{nz^n}{\Xi(z)} \cdot \frac{k}{4n} P_{\text{accept}}(\omega \rightarrow \omega') = \frac{(n+2)z^{(n+2)}}{\Xi(z)} \cdot \frac{k}{4(n+2)} P_{\text{accept}}(\omega' \rightarrow \omega)$$

$$(2.37) \quad P_{\text{accept}}(\omega \rightarrow \omega') = z^2 P_{\text{accept}}(\omega' \rightarrow \omega).$$

Since this expression only depends on the fact that $\omega \rightarrow \omega'$ is a +2-move and $\omega' \rightarrow \omega$ is a -2-move, we can let $P_{\text{accept}}(+2)$ and $P_{\text{accept}}(-2)$ represent the probability of accepting any +2-move and any -2-move, respectively. Since $0 < z < z_0 < 1$ we may maximize the accepted transitions by choosing

$$(2.38) \quad P_{\text{accept}}(+2) = z^2$$

$$(2.39) \quad P_{\text{accept}}(-2) = 1.$$

2.4.4.2. BFACF and Split Links. Note that BFACF fails for split links. Consider a link conformation $\omega = \omega_1 \sqcup \omega_2$ of a split 2-component link L . Since L is a split link, one could simply translate ω_2 to one of infinitely many locations in \mathbb{Z}^3 and get the same link type. Hence, for all n either $\mu_n(L) = \infty$ or $\mu_n(L) = 0$. Therefore the sum in Equation (2.29) cannot converge and the distribution in Equation (2.28) is not well-defined. This issue does not occur for split links in confinement, but confinement problems are not considered here.

2.5. Questions and Conjectures

As this work covers many topics, some more related than others, it is beneficial to outline the specific problems being addressed.

2.5.1. Link Nomenclature. How does one clearly communicate the different isotopy classes (Section 2.3.1) of a link? One method is to draw an explicit representation of the link every time, but this is not an efficient way to describe large amounts of experimental data.

One attempt to classify isotopy classes of links was presented in [LCM96], which classified alternating links into chiral designations of either D or L based on a method called *writhe profiles* which is related to projected writhes. While writhe profiles provide a useful way to classify many

alternating knots and links, they do not classify non-alternating knots and links. Moreover, there is a discrepancy in [LCM96] between how oriented and non-oriented links are classified.

For non-oriented links, in [LCM96], the sign of the projected writhe is checked and the link is assigned a D for a positive value and an L for a negative value. If the sum of self-writhe is zero, writhe profiles are calculated in order to specify a designation of D or L. For oriented links, the sign of the linking number is checked first and the link is assigned a D for a positive value and an L for a negative value. If linking number is zero, the designation process for the non-oriented links is followed, with minor changes to account for orientation.

The discrepancy arises when linking number is non-zero. Chirality is a property independent of orientation but linking number depends on orientation. Thus, linking number is not a good choice for a chiral designator. To see the issue more clearly, consider the link 4_1^2 as an example. The oriented 4_1^2 link has 4 oriented symmetry classes which can be represented by 4_1^{2++} , 4_1^{2+-} , 4_1^{2*++} , and 4_1^{2*+-} (see Figure 2.11). The unoriented 4_1^2 link only has 2 unoriented symmetry classes which could be represented by 4_1^2 and 4_1^{2*} . In the classification of [LCM96], the link designated by 4_1^{2++} in Figure 2.11 would be given a D classification, while 4_1^{2+-} would get an L. However, as chirality is a property the unoriented link and since 4_1^{2++} and 4_1^{2+-} both share the same underlying unoriented link representation, 4_1^2 , then in a consistent classification scheme they should be given the same chiral designation.

Another method, presented in [PDS⁺11,BSV13], is to classify chirality using the mean writhe of lattice links. The given classifications from [PDS⁺11,BSV13] were only for knots, and writhe data was obtained with BFACF (Section 2.4.4) sampling. Using writhe data from further BFACF sampling, a method for selecting a canonical link isotopy class is proposed in Chapter 3 which is then applied to prime 2-component links of up to crossing number 9.

Let $\mathcal{Z}_n(L)$ be the set of all length n lattice conformations of L . Let the average of the self-writhe of component i of L be

$$(2.40) \quad \mathcal{S}_n(L, i) = \frac{1}{|\mathcal{Z}_n(L)|} \sum_{\omega \in \mathcal{Z}_n(L)} s_i(\omega).$$

Then, assuming L is a c -component link, the average of the sum of self-writhes of the elements of $\mathcal{Z}_n(L)$ is

$$(2.41) \quad \mathcal{S}_n(L) = \sum_{i=1}^c \mathcal{S}_n(L, i).$$

Based on the data described in Section 3.3, the following conjectures are proposed

CONJECTURE 2.5.1. *Given a c -component link L , the mean of the self-writhe for each component, $\mathcal{S}_n(L, i)$, is bounded as the total link length n varies.*

CONJECTURE 2.5.2. *If there is no exchange symmetry between components i and j of a link L , then there exists some N such that $\mathcal{S}_n(L, i) < \mathcal{S}_n(L, j)$ for all $n \geq N$, or $\mathcal{S}_n(L, j) < \mathcal{S}_n(L, i)$ for all $n \geq N$.*

CONJECTURE 2.5.3. *For any link L , the mean of the sum of self-writhes, $\mathcal{S}_n(L)$, is bounded.*

CONJECTURE 2.5.4. *If link L is chiral, then the mean of the sum of self-writhes, $\mathcal{S}_n(L)$, is either positive for every n or negative for every n .*

Conjectures 2.5.2 and 2.5.4 provide a method to distinguish mirror images and component labelings in a way that, when combined with linking number, allows a consistent way to select a candidate for $L++$ for all except five prime 2-component links with crossing number 9 or less. This is done by selecting the $L++$ such that $\mathcal{S}_n(L++) > 0$, $\mathcal{S}_n(L++, 2) < \mathcal{S}_n(L++, 1)$, and $\text{lk}(L++) > 0$. This leaves ambiguity of orientation in some cases, as detailed in Section 3.2. The canonical choices for $L++$ as determined by this process are presented for prime 2-component links with up to 9 crossings in Appendix C.

2.5.2. Markov Chains and Self-Avoiding Polygons. The BFACF algorithm (Section 2.4.4) can be used to explore properties of lattice links. One drawback of BFACF when used on links with more than one component is that the posterior distribution only depends on the sum of the lengths of the components. In some experiments, such as those modeling the action of recombinases in the unlinking of replicated DNA, it is desirable to sample conformations where the components are of relatively similar or equal length [SYB⁺17]. In other cases the model may require a different ratio of the component lengths.

Another — albeit, anecdotal — drawback of BFACF for links with more than one component is that it has a tendency to get “stuck” in regions of the state space where one component is particularly small. A possible explanation for this is that the probability of performing a BFACF move on a component is proportional to the length of that component with respect to the total conformation. That is, if n_i is the length of component i , then the probability of choosing a BFACF move on component i of a c -component lattice link is $\frac{n_i}{\sum_{j=1}^c n_j}$.

Solutions to these issues are explored in detail in Chapter 4. Alternate posterior distributions along with a modified move selection method are presented in Section 4.1 and proven to yield valid Markov chains that address these problems. Then in Section 4.2, application of Wang-Landau (Section 2.4.3) to lattice links using BFACF moves is explored.

2.5.3. Grid Diagrams. The impetus for the work done here in grid diagrams was to examine the mean writhe of knot types in a similar way to what is done with lattice links in Chapter 3 and in [BSV13, PDS⁺11]. The first step was to write a Markov chain for Monte Carlo sampling of grid diagrams. This was done initially by using Cromwell moves in a non-Metropolis-Hastings way (imitating the presentation of BFACF in [MS13]). There were two main issues with this implementation.

First, solving for detailed balance in the implementation without Metropolis-Hastings acceptance probabilities was not clear. There was a method established, but it was convoluted and is deprecated by the use of Metropolis-Hastings probabilities. This algorithm is proposed in Section 7.2.1.

There is still an issue with the algorithm as presented. There is an experimentally known critical value of z for the BFACF algorithm (Section 2.4.4). That is, the BFACF algorithm will only converge to a proper posterior distribution if the z parameter is below about .2134 [MS13]. The distribution used for the algorithm in Section 7.2.1 also has a z parameter that controls the expected value for the grid size in the posterior distribution. The issue arises with whether or not this z parameter has a critical value or not. This depends entirely on the growth rate of $|\mathcal{G}_n(L)|$ for given link type L as $n \rightarrow \infty$, which is unknown. This leads to the world of combinatorial questions for grid diagrams which includes enumeration of \mathcal{G}_n and $\mathcal{G}_{n,c}$, along with a lower bound for $|\mathcal{G}_n(K)|$ for fixed knot type K . The combinatorial questions are addressed in Section 5.1.

When restricting to only knots, the question of the growth of $|\mathcal{G}_n(K)|$ becomes equivalent to the growth of $P_n(K) = |\mathcal{G}_n(K)|/|\mathcal{G}_{n,1}|$. The Frisch-Wasserman-Delbrück (FWD) conjecture is a conjecture in most random knotting schemes which roughly states that the probability of getting an unknotted configuration goes to 0 as the size of a random knot increases. For grid diagrams, the FWD conjecture is equivalent to the following theorem with $K = 0_1$, which is proven in Chapter 6,

THEOREM 2.5.5. *For any fixed knot type K , $P_n(K) \rightarrow 0$ as $n \rightarrow \infty$.*

The proof of Theorem 2.5.5 gives a bound on the rate at which $P_n(K) \rightarrow 0$, but that bound is not necessarily tight. Luckily, Wang-Landau with $E(g) = |g|$ provides a way to examine the rate at which $P_n(K) \rightarrow 0$. Wang-Landau for grid diagrams is presented in Section 7.2.2, and is used to show that the decay of $P_n(K)$ is likely exponential or faster in Section 7.3.1.

Wang-Landau also provides a much more direct way to assess the mean writhe of grid diagrams, which was the original motivation for working with grid diagrams. The way writhe behaves under Cromwell moves is explained in Section 5.2. This is then used for Wang-Landau experiments where $E(g) = (|g|, w(g))$. In Section 7.3.2 the resulting numerical data is used to directly assess the mean writhe of grid diagrams.

CHAPTER 3

Link Nomenclature

To address the question of link nomenclature (Section 2.5.1), measurements of writhe from BFACF experiments (Section 2.4.4) will be used. Combined with linking number (Section 2.3.6.2), this will give us a clear way to denote a canonical isotopy class for a link.

3.1. Symmetries, Writhe and Linking Number

As the method described here will use writhe and linking number to distinguish isotopy classes of links, it will be important to examine how writhe and linking number behave under reflection, reversal, and component relabeling.

Consider a regular diagram $D+\cdots+$ of any c -component link, $L+\cdots+$. The reflection of $D+\cdots+$, denoted by $D^*+\cdots+$, is obtained by switching all of the over/under-crossings of $D+\cdots+$ and represents the link $L^*+\cdots+$. This changes the sign of each crossing's contribution to both projected writhe and linking number, hence

$$(3.1) \quad \text{lk}(L+\cdots+) = -\text{lk}(L^*+\cdots+),$$

$$(3.2) \quad s_i(D+\cdots+) = -s_i(D^*+\cdots+),$$

$$(3.3) \quad s(D+\cdots+) = -s(D^*+\cdots+), \text{ and}$$

$$(3.4) \quad w(D+\cdots+) = -w(D^*+\cdots+).$$

The same holds true for space writhe and reflections of spatial conformations, which can be seen by examining the argument of the writhe and linking integrals (Equations (2.2) and (2.11)). That is, if $\omega+\cdots+$ is a spatial conformation representing $L+\cdots+$, and $\omega^*+\cdots+$ is its reflection, then

$$(3.5) \quad s_i(\omega+\cdots+) = -s_i(\omega^*+\cdots+),$$

$$(3.6) \quad s(\omega+\cdots+) = -s(\omega^*+\cdots+), \text{ and}$$

$$(3.7) \quad w(\omega+\cdots+) = -w(\omega^*+\cdots+).$$

Equation (3.1) says that an oriented link with non-zero linking number cannot be equivalent to its mirror image. Note that a link with non-zero linking number could, for example, have even operations symmetry (see Table 2.1) which would make it equivalent to its mirror as an unoriented link but inequivalent as an oriented link.

Similarly, reversing the orientation of one component will change the sign of each inter-component crossing, i.e.

$$(3.8) \quad \text{lk}(L++) = \text{lk}(L--) = -\text{lk}(L-+) = -\text{lk}(L+-)$$

for two component links. For links with more than two components this means the sign of $\text{lk}_{i,j}$ will change if component i xor j is reversed, but will remain the same if component i and j are both reversed. Thus, linking number can help discern choices of orientation. Observe that linking number is dependent on both orientation and chirality, whereas self-writhe depends only on chirality.

If the components of a c -component link are relabeled according to permutation $\sigma \in S_c$ such that i is relabeled to $\sigma(i)$, then

$$(3.9) \quad s_i(L++) = s_{\sigma(i)}(\sigma L++).$$

3.2. Canonical Isotopy Class

References to links most commonly use the name listed in the Rolfsen table [Rol76]. This is effective for communicating general properties of links, but when working with oriented links, or with links with distinguished components, one must still explicitly draw a picture of the link for full clarity. Doll & Hoste provided a link table which included orientation and component labels in addition to providing a nomenclature for reversing components [DH91]. While the diagrams in the Doll & Hoste table were chosen in a systematic way (using Conway notation), there is inconsistency in which isotopy classes are actually represented for each link. For example, the two diagrams that Doll & Hoste listed for 7_3^2 are reflections of each other and are non-isotopic, since 7_3^2 lacks reflection symmetry. Here, a systematic way to identify a representative isotopy class for each link type is proposed using writhe and linking number.

3.2.1. Knots. In the case of knots, the writhe-guided nomenclature proposed by Portillo et al. and Brasher et al. is used [PDS⁺11, BSV13]. This nomenclature specified the canonical knot K as the one where $\mathcal{S}_n(K) > 0$ (where $\mathcal{S}_n(K)$ is defined in Section 2.5.1). In [PDS⁺11, BSV13],

the authors also provided numerical data in support of the conjecture that for each chiral knot K , $\mathcal{S}_n(K)$ was either consistently positive or consistently negative regardless of n (Conjecture 2.5.4 restricted to knots), thus pointing to an unambiguous designation. Note that these knots do not include orientation information, as the methods used do not discern orientations of knots.

3.2.2. 2-Component Links. The case of 2-component links is more complicated due to the extra link symmetries as detailed in Section 2.3.8 and Table 2.1. Assuming the conjectures in Section 2.5.1, self-writhes and linking number can be used to define the canonical isotopy class of a link, denoted by L_{++} . In particular, L_{++} is chosen so that $\mathcal{S}_n(L_{++}) > 0$ (Conjecture 2.5.4), $\mathcal{S}_n(L, 1) > \mathcal{S}_n(L, 2)$ (Conjecture 2.5.2), and $\text{lk}(L_{++}) > 0$ when possible. Once L_{++} is chosen, it can be used as a point of reference for obtaining all other isotopy classes of the link as described in Section 2.3.8, and illustrated in Figure 2.11.

For any n , if $\mathcal{S}_n(L_{++}) \neq 0$ then exactly half of the isotopy classes will have $\mathcal{S}_n(L_{++}) > 0$. Then, if $\text{lk}(L_{++}) \neq 0$, half of those isotopy classes will have $\text{lk}(L_{++}) > 0$. Then, as long as $\mathcal{S}_n(L, 1) \neq \mathcal{S}_n(L, 2)$, half of those isotopy classes will have $\mathcal{S}_n(L, 1) > \mathcal{S}_n(L, 2)$. This narrows down the 16 isotopy classes to two potential candidates for L_{++} . If L has pure exchange symmetry, then these candidates are equivalent and the canonical link L_{++} is chosen to be this isotopy class. There are three 2-component links with crossing number at most 9 that lack pure exchange symmetry: 9_{34}^2 , 9_{35}^2 , and 9_{39}^2 . In fact, these links have no symmetry.

The assumptions that $\mathcal{S}_n(L_{++}) \neq 0$, $\text{lk}(L_{++}) \neq 0$, and $\mathcal{S}_n(L, 1) \neq \mathcal{S}_n(L, 2)$ depend on the symmetry type of L . If there is reflection symmetry, then it is necessarily true that $\mathcal{S}_n(L_{++}) = 0$ for all n . If $\mathcal{S}_n(L_{++}) = 0$ and there is no reflection symmetry, then the link and its mirror image cannot be distinguished with the methods presented here, but this is not observed in the data (Section 3.3). If there is pure exchange symmetry, then it is necessarily true that $\mathcal{S}_n(L, 1) = \mathcal{S}_n(L, 2)$. If $\mathcal{S}_n(L, 1) = \mathcal{S}_n(L, 2)$ and there is no pure exchange symmetry, then different component labelings for L cannot be detected using the methods here, but this behavior was also not observed in the numerical data described below. For links with full inversion symmetry, it is necessarily true that $\text{lk}(L_{++}) = 0$. If $\text{lk}(L_{++}) = 0$ and L does not have full inversion symmetry (all orientations are equivalent), then orientations cannot be distinguished with these methods. This behavior is observed for only two links up to crossing number 9: 9_5^2 and 9_{41}^2 .

The BFACF algorithm is used to estimate $\mathcal{S}_n(L)$, $\mathcal{S}_n(L, 1)$, and $\mathcal{S}_n(L, 2)$ for each 2-component link through 9 crossings as detailed in Section 3.3. From this data, canonical isotopy classes were found for each link except for the 9_5^2 , 9_{34}^2 , 9_{35}^2 , 9_{39}^2 , and 9_{41}^2 links, which were each narrowed down to two potential candidates by this process, differing by the simultaneous reversal of both components. For these five links, some extra criterion is required to select a canonical link from the remaining two candidates. Diagrams for the canonical links can all be seen in Appendix C. An arbitrary choice was made for which isotopy class to include for the five ambiguous links.

3.2.3. c -Component Links. While no data is provided for links with more than 2 components, the selection of a canonical link isotopy class can be extended to c -component links, assuming the behavior of writhe stays the same for more components. That is, assuming Conjectures 2.5.4 and 2.5.2 are true for any number of components, then we choose $L+\dots+$ such that $\mathcal{S}_n(L+\dots+) > 0$ and $\mathcal{S}_n(L+\dots+, i) > \mathcal{S}_n(L+\dots+, j)$ when $i < j$. Extending the use of linking number to define orientation becomes less clear, but one method that can be used is to take the set of orientations that produces the most positive sum of the pairwise linking numbers. That is, choose the orientation that maximizes $\sum_{0 < i < j \leq c} \text{lk}_{i,j}(L+\dots+)$. The effectiveness of this method for $c > 2$ remains unexplored.

3.3. Numerical Writhe Results for 2-Component Links

Statistically independent ensembles of linked lattice polygons for the 91 prime non-split 2-component links with crossing number less than or equal to 9 were obtained from Markov Chain Monte Carlo sampling via the BFACF algorithm (Section 2.4.4). Only one isotopy class was sampled for each link, as the writhe values for other isotopy classes will be either identical or of opposite sign as described in Section 3.1. Choices of z values and sampling rates were chosen based on prior runs. These prior runs consisted of varying z , taking a sequence of samples at some sampling rate, calculating the autocorrelation of those samples, and if the autocorrelation was low then calculating the average of the lengths of those samples. This process was repeated for each link type and for many z values. The data was then used to select a z value which had the estimated expected value closest to the desired length and a sampling frequency that would cause low correlation of the samples.

Samples were taken for links of length 76, 100, 150, 200, 250, and 300. Up to 20000 independent samples were taken for most lengths of each link, with up to $2 \cdot 10^6$ and $2 \cdot 10^5$ independent samples

for lengths 100 and 150, respectively. Initial sampling was done for lengths 100 and 150, but in many cases runs were terminated before all samples were taken to free up computational resources, as analysis showed the number samples taken was sufficient to produce adequate confidence intervals. For the other lengths, 20000 was selected as a sufficiently large number of samples for the level of confidence desired. Samples were discarded and not counted if their length did not match the target length for the run.

Once the samples were obtained, the component self-writhe and the sums of self-writhe were calculated. This resulted in three data points for each conformation: the sum of self-writhe; component 1 self-writhe; and component 2 self-writhe. Batch mean analysis was then used to ensure statistical independence of this data and to calculate 95% confidence intervals for the mean of each of these values. Batch mean analysis is a method which, in short, puts sequential data into blocks, if necessary, to reduce auto-correlation and uses the average of each block as a data point [Fis13].

Before fully analyzing the results, the robustness of the sampling methods were double-checked by comparing certain results to known facts. First, every link L with reflection symmetry must have $\mathcal{S}_n(L) = 0$ for every n . Hence, the confidence interval for $\mathcal{S}_n(L)$ must contain zero for these links. This was true of each link with symmetry group $\Sigma_{8,2}$ and $\Sigma_{4,5}$ that were sampled, and can be seen in Figure 3.2(a).

Also, for each link with the pure exchange symmetry, the mean self-writhe of each component must be exactly equal, i.e. $\mathcal{S}_n(L, 1) = \mathcal{S}_n(L, 2)$. To check for this, it was ensured that the confidence intervals for $\mathcal{S}_n(L, 1)$ and $\mathcal{S}_n(L, 2)$ had non-empty intersection for links with symmetry group $\Sigma_{4,1}$, $\Sigma_{8,1}$, or $\Sigma_{8,2}$ (see Figure 3.2(b)). The samples taken for links with these symmetries matched expectations as well. So, the sampling method appears satisfactory.

Extra samples were required for the 8_{15}^2 link at lengths 200, 250, and 300. Since 8_{15}^2 lacks pure exchange symmetry, it is expected that $\mathcal{S}_n(L, 1) \neq \mathcal{S}_n(L, 2)$. The data showed this for lengths 76, 100, and 150. However, as length of a link increases, the variance of writhe also increases, which means more samples are required to maintain the same width of confidence intervals as for smaller lengths. For the 8_{15}^2 link, the self-writhe of the components are both relatively small and close together, which means they must have particularly tight confidence intervals to ensure they are disjoint. For lengths 200, 250, and 300, the confidence intervals for the self-writhe of each component were not disjoint in the original sampling of 8_{15}^2 , which meant uncertainty as to

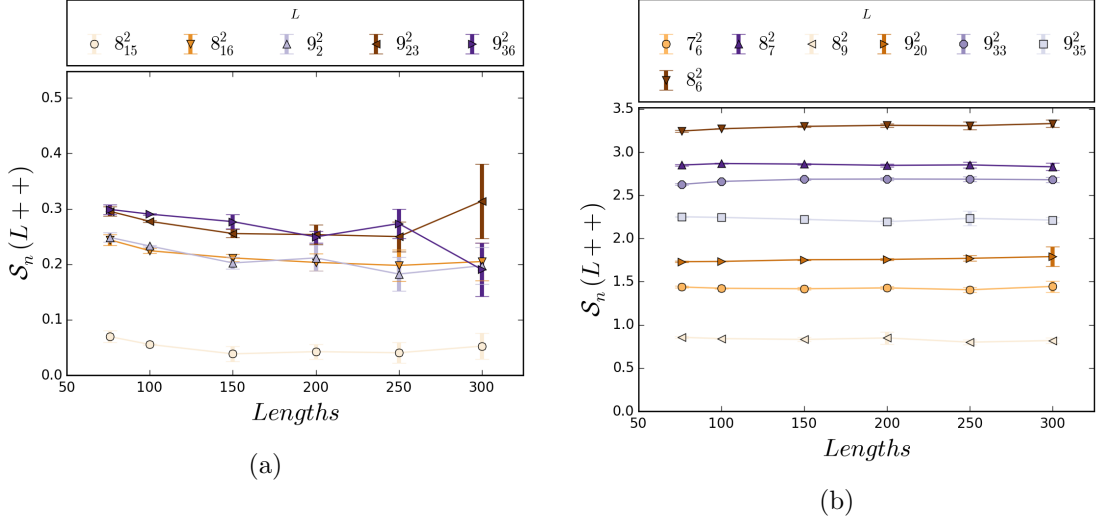


FIGURE 3.1. Estimates with 95% confidence intervals for $\mathcal{S}_n(L++)$ for a selection of links for $n \in \{76, 100, 150, 250, \text{ and } 300\}$. Data was obtained from the simulations as described in Section 3.3. The expected value of $\mathcal{S}_n(8_{15}^2)$ was the lowest among links lacking reflection symmetry. Note that even though the expected value is relatively small for all lengths examined, the confidence intervals do not include 0. Limited variability of $\mathcal{S}_n(L++)$ was observed as length increased for all prime links with up to 9 crossings. This suggests a well-behaved nature of writhe for long lattice links. Confidence intervals for all sampled links can be found in Appendix B. Values shown are transformed from the sampled links to the canonical isotopy classes seen in Appendix C.

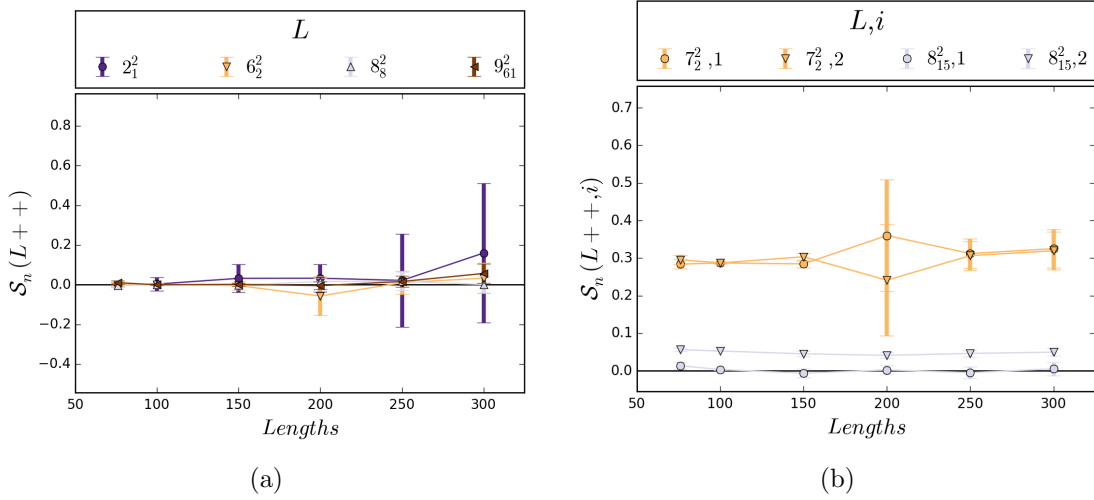


FIGURE 3.2. (a) This graph shows 95% confidence intervals for $\mathcal{S}_n(L++)$ of the four links with reflection symmetry and crossing number up to 9, for lengths 76, 100, 150, 200, 250, and 300. (b) This graph illustrates the expected behavior of $\mathcal{S}_n(L, i)$ for a link with pure exchange symmetry (7_2^2) and a link without pure exchange symmetry (8_{15}^2), where i denotes the component number. The large error bars are due to a smaller sample size for 7_2^2 at length 200, however even for low sample sizes, the error bars overlap as expected.

whether they were distinct, despite the measured estimate of $\mathcal{S}_n(8_{15}^2, 2)$ being consistently larger than $\mathcal{S}_n(8_{15}^2, 1)$ (in the component labeling of the isotopy class sampled). Extra samples were taken for lengths 200, 250, and 250, with about 45000 total samples at each length. After the extra sampling, the intervals were found to be disjoint for lengths 200 and above, matching the data for lower lengths.

The Hopf link, 2_1^2 provided another issue, in that it is difficult to sample efficiently. Analysis of the autocorrelation of writhe and length of the Hopf link under BFACF moves shows that many more steps may be required between samples. Also, a high variance of length appears to cause many samples to be rejected. Because of this, the data for 2_1^2 is somewhat sparse. However, 2_1^2 has even operations symmetry with pure exchange, which means there are only 2 isotopy classes. Since the linking numbers of these classes are 1 and -1 , we choose 2_1^{2++} such that $\text{lk}(2_1^{2++}) = 1$. It is also worth noting that due to the symmetry of 2_1^2 , it is necessary that $\mathcal{S}_n(2_1^2) = \mathcal{S}_{n,1}(2_1^2) = \mathcal{S}_{n,2}(2_1^2) = 0$, so sampling here serves only to test the robustness of our methods as described above.

The unlink, 0_1^2 , was not sampled, as BFACF fails to converge for split links without extra restrictions such as confinement (see Section 2.4.4.2). The unlink has full symmetry, so there is only one choice for isotopy class and every unlink is the canonical unlink.

For each link without reflection symmetry, each confidence interval for $\mathcal{S}_n(L)$ was found to be either entirely positive or entirely negative. Moreover, the signs of these confidence intervals are consistent across all sampled lengths for each link supporting Conjecture 2.5.4.

For links which lack pure exchange symmetry, confidence intervals for $\mathcal{S}_n(L, 1)$ and $\mathcal{S}_n(L, 2)$ are disjoint at each n . Moreover, there is a labeling of component 1 and component 2 for each link so that $\mathcal{S}_n(L, 1) > \mathcal{S}_n(L, 2)$ for $n \in \{76, 100, 150, 200, 250, 300\}$.

From this, a canonical link isotopy class can be chosen for most links as described in section 3.2. The complete set of confidence intervals for $\mathcal{S}_n(L)$, $\mathcal{S}_n(L, 1)$, and $\mathcal{S}_n(L, 2)$ for all 2-component links with 9 or less crossings can be found in Appendix B. The signs and labeling of the data in these tables are converted from the experimental data to correspond to the canonical isotopy class. A regular diagram for each canonical isotopy class can be found in Appendix C.

Table B.5 provides the link isotopy class from Rolfsen's table [Rol76] and Knotplot [Hyp] using the notation from section 2.3.8 based on the chosen canonical link, $L++$. This table also includes the mean self-writhe values at $n = 200$, linking number, and symmetry group [CCMP12] for these links.

When the estimated values of $\mathcal{S}_n(L)$ and $\mathcal{S}_m(L)$ are compared for $n, m \in \{76, 100, 150, 200, 250, 300\}$, they are found to only vary by a small amount. For each link, L , and pair of lengths, n and m , we estimated $|\mathcal{S}_n(L) - \mathcal{S}_m(L)|$. The largest difference for $\mathcal{S}_n(L)$ was found in the 8_1^2 link, where $\mathcal{S}_{250}(L)$ is estimated to be about 2.411 compared to 2.589 for $\mathcal{S}_{76}(L)$ for a difference of about 0.178. Figure 3.1 illustrates this behavior of $\mathcal{S}_n(L)$.

For individual component self-writhe, the largest difference was in $\mathcal{S}_n(9_{40}^2, 1)$, where $\mathcal{S}_{250}(9_{40}^2, 1)$ was estimated at 2.439 compared to 2.211 for $\mathcal{S}_{76}(9_{40}^2, 1)$, giving a difference of about 0.228. For comparison, writhe of a self-avoiding polygon in \mathbb{Z}^3 is always a multiple of $1/4$, so no two links or link components can differ in writhe by less than 0.25 [LS06]. In this way, $\mathcal{S}_n(L)$ and $\mathcal{S}_n(L, i)$ appear to be well-behaved, and the data supports Conjectures 2.5.3 and 2.5.1.

3.4. Writhe and Minimum Step Conformations

In [PDS⁺11], an *ideal lattice knot* of type K was defined as a minimal step number (msn) lattice embedding of K . The authors conjectured that the mean writhe of random polygons of given knot type and fixed length could be approximated by the mean writhe of the corresponding ideal msn conformation. They provided numerical evidence that there exists a constant β_K such that the mean writhe of a random lattice polygon of type K and length n belongs to $(w_I(K) - \beta_K, w_I(K) + \beta_K)$, independently of the value of n , where $w_I(K)$ is the mean writhe of the ideal lattice conformations of K .

In addition to these BFACF simulations, preliminary data produced in collaboration with Gabriel Freund yielded results for minimum length lattice links from. The data obtained was the set of all known minimum length conformations of each prime 2-component link with crossing number 9 or less. This data was obtained by running BFACF with a larger z to randomize the conformation, then reducing the z to a low value and sampling the shortest length conformations found. Reflections, component reversals, and component relabeling was then applied to obtain extra conformations for links with the proper symmetry types. Then all possible BFACF moves were performed on this set of conformations to obtain any missed conformations. The exhaustive BFACF move search was then repeated on all new conformations, including ones longer than the minimum length, until computational resources needed to be freed for other work.

The mean of the self-writhe of the minimum length conformations was calculated directly under the assumption that the set of minimum length conformations is complete. $\mathcal{S}_{\min}(L)$, $\mathcal{S}_{\min}(L, 1)$, and

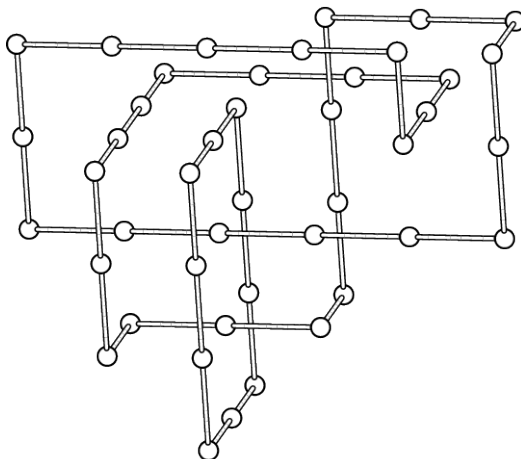


FIGURE 3.3. A minimum step conformation of 8_{15}^2 .

$\mathcal{S}_{\min}(L, 2)$ refer to the mean self-writhe of the minimum length lattice links and their components. The results through 9 crossings can be found in Table B.1.

Analysis of these values shows that $\mathcal{S}_{\min}(L)$ and $\mathcal{S}_{\min}(L, i)$ stayed reasonably close to the other values of $\mathcal{S}_n(L)$ and $\mathcal{S}_n(L, i)$. However, it is noted that $\mathcal{S}_{\min}(8_{15}^2_{++}, 1) = 0$ and $\mathcal{S}_{\min}(8_{15}^2_{++}, 2) \approx 0.2157$, while $\mathcal{S}_n(8_{15}^2_{++}, 1) > \mathcal{S}_n(8_{15}^2_{++}, 2)$ for all other sampled lengths, which shows that component self-writhe of minimum step conformations may not be a sufficient indicator of self-writhe as n increases. Examination of each minimum step conformation of 8_{15}^2 in the dataset shows that component 1 was identical in all of them; it was planar rectangle which always has 0 writhe. One of the minimum step conformations for 8_{15}^2 can be seen in Figure 3.3.

Markov Chain Methods for Lattice Links

The BFACF algorithm (as described in Section 2.4.4) generates random self-avoiding walks and self-avoiding polygons in the simple cubic lattice. When dealing with SAPs, BFACF generates conformations of a fixed knot type. For disjoint unions of SAPs, BFACF generates conformations of fixed link type. However, BFACF does not appear well-tuned for this purpose. It has been noted¹ that BFACF applied to links can have a tendency to get trapped in state regions where one component is relatively small. This can be explained by the selection of transitions being performed by first choosing an edge uniformly at random, so smaller components are less likely to get altered. Moreover, when the edges of a smaller conformation are chosen, it is more likely that any selected move will violate self-avoidance, and hence be rejected, as the smaller component is more compact and will have more nearby edges.

Additionally, another drawback of traditional BFACF comes when modeling 2-component links that arise in biology. For example, replication of a circular DNA molecule produces a 2-component link where each component has the same length. In the current implementations, the posterior distribution of BFACF (Equation (2.28)) is taken with link length defined as the sum of the component lengths. This means that the z parameter controls the expected sum of component lengths, but the probability of a particular set of component lengths is still dependent on the number of conformations with those component lengths compared to other conformations with the same sum of lengths.

Here I propose two possible solutions to these issues. The first is to change the BFACF distribution and the selection of transitions to be more appropriate for links, and is detailed in Section 4.1. The other is to apply Wang-Landau to self-avoiding polygons (and their disjoint unions) using BFACF moves. This approach is detailed in Section 4.2 along with a discussion of how Wang-Landau can help examine other questions for lattice links.

¹Ideally there would be a citation for this statement, but in actuality it comes from conversations with Robert Stolz, Andrew Rechnitzer, and others. Nonetheless, the variations of BFACF it inspired here are sound.

4.1. Link-BFACF

Link-BFACF is the algorithm described in this section. In short, it is a modification of BFACF attained by replacing the z parameter with z_i for $i = 1, 2, \dots, c$ where c is the number of components. In traditional BFACF, z controls the expected value of the sum of component lengths of the conformations, whereas z_i now controls the expected value of the length of component i . In this section, the precise changes to the distribution and transitions are given and it is proven that we get a Markov chain that converges to the new distribution.

4.1.1. Distributions. Recall that the BFACF algorithm takes two inputs: an initial conformation, and a real number $z \in (0, z_0)$ where z_0 is the “critical value” of z (from Equation (2.30)). The z value determines the precise distribution π from which to sample. The standard BFACF distribution (Equation (2.28)) is uniform within a fixed length. That is, if ω and ω' are SAPs representing the same knot and $|\omega| = |\omega'|$, then $\pi(\omega) = \pi(\omega')$. The natural extension of this is to use the sum of the components lengths. That is, if we let $\omega = \bigsqcup_{i=1}^c \omega_i$ be a c -component link in the simple cubic lattice represented as the disjoint union of self-avoiding polygons $\{\omega_i\}_{i=1}^c$, then $|\omega| = \sum_{i=1}^c |\omega_i|$. In the case of 2-component links, this interpretation causes the BFACF distribution to take the form

$$(4.1) \quad \pi(\omega) = \frac{|\omega|z^{|\omega|}}{\Xi(z)} = \frac{(|\omega_1| + |\omega_2|)z^{(|\omega_1|+|\omega_2|)}}{\Xi(z)}$$

with

$$(4.2) \quad \Xi(z) = \sum_{n=0}^{\infty} n z^n \mu_n(L) = \sum_{n_1=0}^{\infty} \sum_{n_2=0}^{\infty} (n_1 + n_2) z^{(n_1+n_2)} \mu_{n_1, n_2}(L)$$

where $\mu_{n_1, n_2}(L)$ is the number of conformations of L where component i has length n_i . Every conformation with total length n will be equally likely and larger z will yield longer links, just as in the 1-component case. However, if one is interested in links where the components have lengths of particular proportions, e.g. approximately the same length, then this distribution will produce many more undesired conformations than necessary.

Instead, we can choose the following distribution for 2-component links:

$$(4.3) \quad \pi(\omega) = \frac{|\omega_1| |\omega_2| z_1^{|\omega_1|} z_2^{|\omega_2|}}{\Xi(z_1, z_2)}$$

where

$$(4.4) \quad \Xi(z_1, z_2) = \sum_{n_1=0}^{\infty} \sum_{n_2=0}^{\infty} n_1 n_2 z_1^{n_1} z_2^{n_2} \mu_{n_1, n_2}(L).$$

This distribution is only valid if $\Xi(z_1, z_2)$ converges for some region of non-zero choices of z_i , $i = 1, 2$. Assuming, for the moment, that $\Xi(z_1, z_2)$ converges, we can note that this choice of π has the trait that if $\omega = \omega_1 \sqcup \omega_2$, $\omega' = \omega'_1 \sqcup \omega'_2$, $|\omega_1| = |\omega'_1|$, and $|\omega_2| = |\omega'_2|$, then $\pi(\omega) = \pi(\omega')$. The choices of z_i will determine the distribution of lengths of the components.

PROPOSITION 4.1.1. *If L is not a split link, then $\Xi(z_1, z_2)$ in Equation (4.4) converges for $z_1, z_2 \in (0, z_0)$ for the value of z_0 from Equation (2.30).*

PROOF. The crux of proving this statement is counting μ_{n_1, n_2} . To do this, we will count the number of conformations of each component, and then the number of ways these components can be put together into a link. Each component of the link is, itself, a knot. Denote the knot type of component i taken independently from the link by K_i . Then the number of length n_i SAPs which represent knot type K_i is $\mu_{n_i}(K_i)$.

Let ω_i be a length n_i conformation of K_i . Since $|\omega_i| = n_i$, ω_i may be embedded within an $n_i \times n_i \times n_i$ cube. In fact, there are many embeddings, so choose one specific embedding into the cube $[0, n_i] \times [0, n_i] \times [0, n_i]$. Denote the chosen embedding of length n_i conformation ω_i and its corresponding cube as $B(\omega_i)$.

Now consider $B(\omega_i)$ shifted along a vector x_i and denote it by $B(\omega_i) + \vec{x}_i$ and similarly the location of ω_i under the same shift as $\omega_i + \vec{x}_i$. Every conformation of L can be described as $(\omega_1 - \vec{x}_1) \sqcup (\omega_2 - \vec{x}_2)$ for some choice of ω_i and \vec{x}_i . Suppose $(B(\omega_1) - \vec{x}_1) \cap (B(\omega_2) - \vec{x}_2) = \emptyset$. If this is the case, then $(\omega_1 - \vec{x}_1) \sqcup (\omega_2 - \vec{x}_2)$ is necessarily a split link. For the same reasons as stated in Section 2.4.4.2, if L is a split link, then $\mu_{n_1, n_2}(L)$ will be ∞ or 0 for each pair n_1, n_2 , thus $\Xi(z_1, z_2)$ will fail to converge.

So, given that $(\omega_1 - \vec{x}_1) \sqcup (\omega_2 - \vec{x}_2)$ is a conformation of L and that L is not a split link, it must be the case that $(B(\omega_1) - \vec{x}_1) \cap (B(\omega_2) - \vec{x}_2) \neq \emptyset$. As an overestimation, we will count all possible ways to overlap $B(\omega_1)$ and $B(\omega_2)$ by first selecting integer coordinates $\vec{x}_i \in B(\omega_i)$. There are n_i^3 choices for \vec{x}_i , so there are $n_1^3 \cdot n_2^3$ ways to choose \vec{x}_1 and \vec{x}_2 . This selection covers all possible ways in which the two cubes can relatively overlap, i.e. coordinate \vec{x}_i of $B(\omega_i)$ and coordinate \vec{x}_j of $B(\omega_j)$ will both be mapped to the origin.

So, taking all possible conformations of K_1 and K_2 with lengths n_1 and n_2 , and all choices of \vec{x}_1 and \vec{x}_2 , will yield every conformation of L in which component i has length n_i . This will also yield many configurations in which the link type is not L , the components intersect, or is equivalent to another conformation constructed this way. Hence, we get an upper bound on $\mu_{n_1, n_2}(L)$, namely

$$(4.5) \quad \mu_{n_1, n_2}(L) < n_1^3 n_2^3 \mu_{n_1}(K_1) \mu_{n_2}(K_2).$$

Applying this to equation (4.4), we get

$$(4.6) \quad \Xi(z_1, z_2) = \sum_{n_1=0}^{\infty} \sum_{n_2=0}^{\infty} n_1 n_2 z_1^{n_1} z_2^{n_2} \mu_{n_1, n_2}(L)$$

$$(4.7) \quad < \sum_{n_1=0}^{\infty} \sum_{n_2=0}^{\infty} n_1 n_2 z_1^{n_1} z_2^{n_2} n_1^3 n_2^3 \mu_{n_1}(K_1) \mu_{n_2}(K_2)$$

$$(4.8) \quad = \sum_{n_1=0}^{\infty} n_1^4 z_1^{n_1} \mu_{n_1}(K_1) \sum_{n_2=0}^{\infty} n_2^4 z_2^{n_2} \mu_{n_2}(K_2)$$

We already know from the regular BFACF algorithm that $\sum_{n_i=0}^{\infty} n_i z_i^{n_i} \mu_{n_i}(K_i)$ (from Equation (2.29)) converges for $z_i \in (0, z_0)$. This means that $\sum_{n_i=0}^{\infty} n_i^4 z_i^{n_i} \mu_{n_i}(K_i)$ must also converge. Hence $\Xi(z_1, z_2)$ converges for $z_1, z_2 \in (0, z_0)$. \square

This means that as long as $0 < z_1, z_2 < z_0$, then π as defined by Equation (4.3) is a valid distribution. It is also possible that inequality (4.5) overcounts enough such that the distribution is valid for some z_i larger than the known bound on z_0 .

This distribution readily extends to c -component links. First define $\mu_{\vec{n}}(L)$ to be the number of lattice links of L where the i th component of the link has length equal to the i th component of \vec{n} . Then, for a lattice link with c components, we can use the distribution

$$(4.9) \quad \pi(\omega) = \frac{\prod_{i=1}^c |\omega_i| z_i^{|\omega_i|}}{\Xi(\vec{z})}$$

with

$$(4.10) \quad \Xi(\vec{z}) = \sum_{n_1=0}^{\infty} \cdots \sum_{n_c=0}^{\infty} \mu_{\vec{n}}(L) \prod_{i=1}^c n_i z_i^{n_i}$$

where $\vec{n} = [n_1, \dots, n_c]^T$ and $\vec{z} = [z_1, \dots, z_c]^T$. We must extend Proposition 4.1.1 to show that this is a valid distribution.

PROPOSITION 4.1.2. *If L is not a split link, then $\Xi(\vec{z})$ in Equation (4.10) converges for $z_1, z_2, \dots, z_c \in (0, z_0)$ for the value of z_0 from Equation (2.30).*

PROOF. Again, consider the $n_i \times n_i \times n_i$ cube $B_i = [0, n_i] \times [0, n_i] \times [0, n_i]$. We will again consider embeddings of the i th component into B_i and then shift each B_i by $B_i - x_i$ as was done in the proof of Proposition 4.1.1. As L is not a split link, it is a necessary condition that every B_i must intersect at least one other cube after they are shifted. Let $h: \{1, 2, \dots, c\} \rightarrow \{1, 2, \dots, c\}$ be any function. Let \mathcal{H} be the set of all possible choices of h . Note that $|\mathcal{H}| < \infty$. Now we enforce that $(B_i - x_i) \cap (B_{h(i)} - x_{h(i)})$ in the same way as before by identifying an integer coordinate in each of B_i and $B_{h(i)}$ to be translated to the same location in \mathbb{Z}^3 . There are $n_i^3 n_{h(i)}^3$ ways to make this choice. These choices of intersections are independent of the conformations inside them. There are $\prod_{i=1}^c \mu_{n_i}(K_i)$ ways to choose component conformations $\{\omega_i\}_{i=1}^c$ such that ω_i represents K_i , the knot type of component i by itself. There are $\sum_{h \in \mathcal{H}} \prod_{i=1}^c n_i^3 n_{h(i)}^3$ ways to choose the intersections of the cubes in which the ω_i are embedded. Hence,

$$(4.11) \quad \mu_{\vec{n}}(L) \leq \left(\prod_{i=1}^c \mu_{n_i}(K_i) \right) \cdot \left(\sum_{h \in \mathcal{H}} \prod_{i=1}^c n_i^3 n_{h(i)}^3 \right)$$

Now suppose p_i represents the number of times i appears as an output of h . That is $p_i = |\{j \mid h(j) = i\}|$. Applying inequality (4.11) to (4.10) yields the following:

$$(4.12) \quad \Xi(\vec{z}) = \sum_{n_1=0}^{\infty} \cdots \sum_{n_c=0}^{\infty} \mu_{\vec{n}}(L) \prod_{i=1}^c n_i z_i^{n_i}$$

$$(4.13) \quad \leq \sum_{n_1=0}^{\infty} \cdots \sum_{n_c=0}^{\infty} \left(\left(\prod_{i=1}^c n_i z_i^{n_i} \mu_{n_i}(K_i) \right) \cdot \left(\sum_{h \in \mathcal{H}} \left(\prod_{i=1}^c n_i^3 n_{h(i)}^3 \right) \right) \right)$$

$$(4.14) \quad = \sum_{h \in \mathcal{H}} \sum_{n_1=0}^{\infty} \cdots \sum_{n_c=0}^{\infty} \left(\prod_{i=1}^c n_i^{3p_i+4} z_i^{n_i} \mu_{n_i}(K_i) \right)$$

$$(4.15) \quad = \sum_{h \in \mathcal{H}} \sum_{n_1=0}^{\infty} \left(n_1^{3p_1+4} z_1^{n_1} \mu_{n_1}(K_1) \right) \cdots \left(\sum_{n_i=0}^{\infty} n_i^{3p_i+4} z_i^{n_i} \mu_{n_i}(K_i) \right) \cdots \left(\sum_{n_c=0}^{\infty} n_c^{3p_c+4} z_c^{n_c} \mu_{n_c}(K_c) \right)$$

Each sum of the form $\sum_{n_i=0}^{\infty} n_i^{3p_i+4} z_i^{n_i} \mu_{n_i}(K_i)$ converges by the convergence of Equation (2.30) as long as $z_i \in (0, z_0)$. Thus, this is a sum over finitely many finite terms, i.e. $\Xi(\vec{z})$ converges. \square

One could also use the distribution

$$(4.16) \quad \pi(\omega) = \frac{(\sum_{i=1}^c |\omega_i|) \prod_{i=1}^c z_i^{|\omega_i|}}{\Xi(\vec{z})}$$

with

$$(4.17) \quad \Xi(\vec{z}) = \sum_{n_1=0}^{\infty} \cdots \sum_{n_c=0}^{\infty} \mu_{\vec{n}}(L) \left(\sum_{i=1}^c n_i \right) \prod_{i=1}^c z_i^{n_i}.$$

Note that $(\sum_{i=1}^c n_i) \prod_{i=1}^c z_i^{n_i} \leq \prod_{i=1}^c n_i z_i^{n_i}$, so this Equation (4.17) will converge by the convergence of Equation (4.10). The choice of which distribution to use comes down to simplifying the detailed balance equation as seen in the next section. The key feature of these distributions is that $\pi(\omega)$ depends only on the lengths of the individual components and that the expected value of component i is controlled by the z_i parameter. Both the distribution in Equation (4.9) and Equation (4.16) are dominated by the exponential term with polynomial terms that serve only to cancel out terms in the detailed balance equation.

4.1.2. Choosing Transitions in Link-BFACF. The method used in BFACF to choose a transition is to select an edge uniformly at random and then choose one of the four cardinal directions orthogonal to that edge. Let $\omega = \bigsqcup_{i=1}^c \omega_i$ be a lattice conformation of a c -component link, and let n_i be the length of component i . Then the probability of choosing any specific transition is $\frac{1}{4 \sum_{i=1}^c n_i}$.

Let $\omega' = \bigsqcup_{i=1}^c \omega'_i$ be a lattice conformation of a c -component link, and let n'_i be the length of component i . Assuming there is a BFACF move that transitions ω to ω' and using the distribution from (4.16) in detailed balance, we get

$$(4.18) \quad \pi(\omega) \frac{1}{4 \sum_{i=1}^c n_i} P_{\text{accept}}(\omega \rightarrow \omega') = \pi(\omega') \frac{1}{4 \sum_{i=1}^c n'_i} P_{\text{accept}}(\omega' \rightarrow \omega)$$

$$(4.19) \quad \frac{(\sum_{i=1}^c n_i) \prod_{i=1}^c z_i^{n_i}}{\Xi(\vec{z})} \cdot \frac{P_{\text{accept}}(\omega \rightarrow \omega')}{4 \sum_{i=1}^c n_i} = \frac{(\sum_{i=1}^c n'_i) \prod_{i=1}^c z_i^{n'_i}}{\Xi(\vec{z})} \cdot \frac{P_{\text{accept}}(\omega' \rightarrow \omega)}{4 \sum_{i=1}^c n'_i}$$

$$(4.20) \quad \frac{P_{\text{accept}}(\omega \rightarrow \omega')}{P_{\text{accept}}(\omega' \rightarrow \omega)} = \prod_{i=1}^c z_i^{n'_i - n_i}$$

Which lets us use $P_{\text{accept}}(\omega \rightarrow \omega') = z_i^2$ when $\omega \rightarrow \omega'$ is a +2-move on the i th component, and $P_{\text{accept}}(\omega \rightarrow \omega') = 1$ for all other transitions. This means that the only change needed for the BFACF algorithm as stated in Section 2.4.4 is to accept moves based on the z value corresponding to the component in which that move is being performed. This is an elegant and relatively small change (depending on the actual encoded implementation of the algorithm, of course) that now allows control over the relative expected lengths of the randomly generated conformations.

This does not necessarily address the perceived issue of becoming trapped in regions of the state space with a relatively small component. It does seem to be less likely to enter one of these states unless the z_i values are set so that a smaller component is desired. However if one of these states is reached, there is still a low probability of selecting an edge from that component.

Consider the following alternative to choosing a transition in the Markov chain: choose a component uniformly at random, then choose an edge of that component uniformly at random, then choose a direction perpendicular to that edge uniformly at random. Now each component is equally as likely to be perturbed in each step. The probability of choosing a specific transition on the j th component is $\frac{1}{4cn_j}$. For this method of transition selection, we will use the distribution from Equation (4.9). Detailed balance is as follows,

$$(4.21) \quad \pi(\omega) \frac{1}{4cn_j} P_{\text{accept}}(\omega \rightarrow \omega') = \pi(\omega') \frac{1}{4cn'_j} P_{\text{accept}}(\omega' \rightarrow \omega)$$

$$(4.22) \quad \frac{\prod_{i=1}^c n_i z_i^{n_i}}{\Xi(\vec{z})} \cdot \frac{P_{\text{accept}}(\omega \rightarrow \omega')}{4cn_j} = \frac{\prod_{i=1}^c n'_i z_i^{n'_i}}{\Xi(\vec{z})} \cdot \frac{P_{\text{accept}}(\omega' \rightarrow \omega)}{4cn'_j}$$

$$(4.23) \quad \frac{P_{\text{accept}}(\omega \rightarrow \omega')}{P_{\text{accept}}(\omega' \rightarrow \omega)} = \prod_{i=1}^c z_i^{n'_i - n_i} = z_j^{n'_j - n_j}$$

Hence we get the acceptance probabilities of z_i^2 for +2-moves applied to the i th component, and 1 for all other moves. These are the same acceptance probabilities as the previous method but the Markov chain converges to a slightly different distribution.

For completeness, I will also state that one could also try to choose transitions on multiple components simultaneously. However, doing this can quickly raise issues with ergodicity and aperiodicity of the Markov chain. Additionally, this would increase complexity of the implementation, particularly with respect to self-avoidance and calculating acceptance and rejection of moves. It is not recommended to take this approach.

The two variations of link-BFACF described here should be sufficient for anyone who wishes to run BFACF sampling with more control over component length. Using Wang-Landau as described in the next section with energy defined as a tuple of component sizes can also be used for such experiments. Due to the flexibility of Wang-Landau, particularly in the ability to add other energy terms and to modify the sampling distribution, Wang-Landau is my recommendation for most random lattice link experiments.

4.2. Wang-Landau for Lattice Links

To apply Wang-Landau to lattice links, we will use BFACF moves as our transitions. Recall (from Section 2.4.3) that the posterior distribution of Wang-Landau is $\pi(\omega) = \frac{1}{M} \frac{1}{\mu_{E(\omega)}}$, where $E(\omega)$ is the chosen energy function, M is the number of valid energy states, and μ_{E_i} is the number of states in the state space, Ω , with energy equal to E_i .

Let L be the c -component link being explored by the algorithm and let $\omega = \bigsqcup_{i=1}^c \omega_i$ and $\omega' = \bigsqcup_{i=1}^c \omega'_i$ be specific conformations of L , where $n_i = |\omega_i|$ and $n'_i = |\omega'_i|$. Now we will solve for detailed balance given the two ways to choose transitions in section 4.1.2. First, if we select an edge uniformly at random from all possible edges and then choose one of the four cardinal directions orthogonal to that edge, then the probability of choosing any specific transition from ω is $\frac{1}{4 \sum_{i=1}^c n_i} = \frac{1}{4|\omega|}$. Hence, by Equation (2.22), if there exists a transition from ω to ω' , then

$$(4.24) \quad P_{\text{accept}}(\omega \rightarrow \omega') = \min \left\{ 1, \frac{4|\omega|}{4|\omega'|} \cdot \frac{W_{E(\omega)}}{W_{E(\omega')}} \right\} = \min \left\{ 1, \frac{|\omega|}{|\omega'|} \cdot \frac{W_{E(\omega)}}{W_{E(\omega')}} \right\}.$$

On the other hand, if we choose a component uniformly at random, then choose an edge of that component uniformly at random, then choose a direction perpendicular to that edge uniformly at random, we get the probability of choosing a specific transition on the j th component as $\frac{1}{4cn_j}$. Hence,

$$(4.25) \quad P_{\text{accept}}(\omega \rightarrow \omega') = \min \left\{ 1, \frac{n_j}{n'_j} \cdot \frac{W_{E(\omega)}}{W_{E(\omega')}} \right\}.$$

So either transition selection method may be used and the only mathematical difference is multiplying the acceptance probabilities by a ratio of the full link lengths vs. the changed component's length. All that remains is to choose an energy function. Wang-Landau is most useful for energy functions which are easy to calculate or at least easy to track the changes of as moves are performed. For example, total link length $E(\omega) = |\omega|$ and component lengths $E(\omega) = (|\omega_1|, |\omega_2|, \dots, |\omega_c|)$ can be used as we only need to calculate the length once and then add 2, -2, or 0, after each move is performed, based only on the local change. This means calculating the energy of a proposed step can be done in $O(1)$ time. Note that using component lengths yields an alternative to the approach proposed in Section 4.1 for handling the variability of different component lengths.

Another energy that can be used is writhe. Using $E(\omega) = (|\omega|, w(\omega))$ or $E(\omega) = (|\omega|, s_1(\omega), s_2(\omega))$ provides another possible approach to the numerical experiments in Section 3.3. The writhe change

of a BFACF move can also be calculated by the local geometry where the move is being performed, as will be described in Section 4.2.2.

4.2.1. Ergodicity of the Wang-Landau Algorithm with Lattice Links. The state space of the BFACF algorithm is the set of all lattice links representing a link type L , which is infinite. The posterior distribution of Wang-Landau, Equation (2.15), requires a finite state-space. This means that in order to run the algorithm, the state space for Wang-Landau must be restricted.

The typical way to do this is to bound the conformations by some maximum length so that length-increasing moves are all rejected if the current state is of the maximum length. However, it must be noted that this can, and likely will, cause the algorithm to no longer be fully ergodic in the state space. There will be states, particularly near the maximum length, which will not be reachable through BFACF transitions without going beyond the maximum length. With a long enough maximum length, one can expect that the lower length conformations can all be reached, hence the weights for shorter lengths can be better trusted. However, it is unknown just how long the conformations must be allowed to get to achieve every state of a particular length.

4.2.2. Writhe Change of BFACF Moves. Here it will be shown that the difference of writhe between two conformations that differ only by a BFACF move is predictable using only the local geometry around the edge where the BFACF move is performed. This is proven using the formulation of space writhe for lattice links, using push-offs, given in Theorem 2.3.10.

Recall that a BFACF move is performed by taking an edge of a self-avoiding polygon in \mathbb{Z}^3 and pushing it one unit in one of the four directions perpendicular to the direction of the edge. We will refer to the edge being pushed as the *BFACF edge*. If an endpoint of the BFACF edge traces an existing edge of the polygon during that push, then the traced edge is deleted. On the other hand, if an endpoint of the BFACF edge does not trace another edge of the polygon, then an edge is added in the traced space. With this in mind, we prove the following theorem:

THEOREM 4.2.1. *If ω and ω' are lattice links related by a single BFACF move, then $|w(\omega') - w(\omega)| \leq \frac{1}{2}$. More specifically, $(w(\omega') - w(\omega)) \in \{-\frac{1}{2}, -\frac{1}{4}, 0, \frac{1}{4}, \frac{1}{2}\}$.*

PROOF. ² Consider the BFACF move which transforms ω into ω' . Without loss of generality, we may assume that

²This proof differs from the original version of this proof published in [WFV18]. Namely, the directions of the push-offs in the original proof were not consistent, which has been corrected here.

- (1) the BFACF edge runs from $(0, 0, 0)$ to $(0, 1, 0)$,
- (2) the result of the BFACF move will push the BFACF edge to an edge from $(0, 0, -1)$ to $(0, 1, -1)$, and
- (3) the vectors used to generate the push-offs for the writhe calculation are $[1/2, 1/2, -1/2]^T$, $[1/2, -1/2, -1/2]^T$, $[-1/2, 1/2, -1/2]^T$, and $[-1/2, -1/2, -1/2]^T$.

We may rotate and translate the conformation to make these assumptions true, which will not affect the writhe of the conformations.

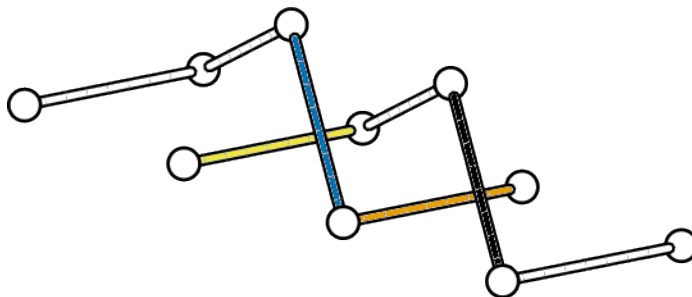


FIGURE 4.1. If a BFACF move is performed on the black edge in the direction of the orange (medium gray in grayscale) edge of the push-off beneath it, then the linking number with the push-off will change by -1 which will change the writhe by $-1/4$. This same BFACF move will also push the blue (dark gray) edge of the push-off through the yellow (light gray) edge of the link, which will cause the linking number to change by another -1 , hence this will contribute a $-1/4$ change to the writhe. So, a BFACF move pushing the black edge into the page will result in a lattice link with a writhe $1/2$ less than the current link's writhe.

Now consider the BFACF move. This move may pass the SAP through one of the push-offs from Theorem 2.3.10, changing the linking number of the polygon with that push-off. One such strand passage will change the linking number with that push-off by ± 1 , in turn changing the space writhe of the conformation by $\pm 1/4$. If the move passes the polygon through a push-off edge, then the push-off edge must have endpoints $(-1/2, 1/2, -1/2)$ and $(1/2, 1/2, -1/2)$ (e.g. the black

BFACF edge and orange push-off edge in Figure 4.1). Checking where this edge must come from in the original polygon by reversing the push-off, we see it is necessary that this edge runs in the x direction and either has an endpoint at $(0, 0, 0)$ or at $(0, 1, 0)$.

Now suppose that one of the push-offs of the BFACF edge passes through an edge of the original link when the BFACF move is performed (e.g. the blue push-off edge being pushed through the yellow edge in Figure 4.1). The four push-offs of the BFACF edge run from $(-1/2, 1/2, -1/2)$ to $(-1/2, 3/2, -1/2)$, $(1/2, 1/2, -1/2)$ to $(1/2, 3/2, -1/2)$, $(-1/2, -1/2, -1/2)$ to $(-1/2, 1/2, -1/2)$, and $(1/2, -1/2, -1/2)$ to $(1/2, 1/2, -1/2)$. We note that in each of these cases the edge that the crossing change would occur with must run in the x direction and have an endpoint at either $(0, 1, -1)$ or $(0, 0, -1)$. Then the BFACF move is only valid if there is an edge from $(0, 1, 0)$ to $(0, 1, -1)$, or from $(0, 0, 0)$ to $(0, 0, -1)$, respectively. Otherwise, the proposed BFACF move would violate self-avoidance, and any writhe change is moot because the resulting conformation is invalid.

This presents eight possible cases where writhe would change by performing the given BFACF move. Note that the two cases where there is an edge in the x direction with an endpoint at $(0, 0, 0)$, and the two cases where there is an edge in the x direction with an endpoint at $(0, 0, -1)$, are all mutually exclusive. Likewise the four cases with endpoints at $(0, 1, 0)$ or $(0, 1, -1)$ are all mutually exclusive. Hence only two of these eight cases may be true at any time, each of which contributes a writhe change of $\pm 1/4$, hence the total change in writhe from any BFACF move is in the set $\{-\frac{1}{2}, -\frac{1}{4}, 0, \frac{1}{4}, \frac{1}{2}\}$. \square

By following the proof, one can determine what the exact change in space writhe will be obtained by comparing the directions of the two edges immediately before and immediately after the edge being pushed. This means that once the space writhe of the initial conformation is calculated, it is only $O(1)$ to calculate the writhe for each subsequent conformation obtained from BFACF moves. Therefore using space writhe as part of the Wang-Landau energy is computationally inexpensive when writhe change is calculated this way.

Combinatorics and Writhe of Grid Diagrams

This section details several new statements about grid diagrams. Although some of these results are relatively simple, to the best of my knowledge they are missing from published literature. Note that, since there is a bijection between arc diagrams and grid diagrams, all results for grid diagrams presented here have an equivalent statement for arc diagrams.

5.1. Combinatorics of Grid Diagrams

At its core, the FWD conjecture for grids (Theorem 2.5.5) is a question of combinatorics. Does the number of $n \times n$ grid diagrams representing knots ($|\mathcal{G}_{n,1}|$) grow at an asymptotically faster rate than the number of $n \times n$ grid diagrams representing a specific knot ($|\mathcal{G}_n(K)|$)? Additionally, finding the number of $n \times n$ grid diagrams of a fixed knot type is a question that aids in constructing a distribution for MCMC sampling of grid diagrams, as will be seen in Section 7.2.1. This section provides bounds and the directly calculable combinatorics for these and related values.

5.1.1. Number of Grid Diagrams. The most fundamental combinatorial question regarding grid diagrams is the following: how many grid diagrams are there for a given grid size n ? The answer, $n! \cdot n$, is sequence A082491 [OEI19c] in the On-line Encyclopedia of Integer Sequences (OEIS). One of the examples that the OEIS gives for what this sequence counts is the “number of $n \times n$ matrices with exactly one 1 and one 2 in each row and column, other entries 0.” This is equivalent to the definition of a grid diagram where the grid is replaced with a matrix and the X’s and O’s are replaced with 1’s and 2’s. A constructive enumeration is given here to provide the framework for the proofs to follow.

THEOREM 5.1.1. *There are $|\mathcal{G}_n| = n! \cdot n$ size n grid diagrams.*

PROOF. Let’s enumerate $n \times n$ grids constructively. Consider an $n \times n$ grid with no entries. Start by assigning the X’s. Assign each row a distinct index from 1 to n , which represents the column where the X is placed in that row (see Figure 2.5(b)). There are $n!$ ways to do this. Each row must now be assigned an O with a distinct column index between 1 and n that is different

from the column index of the X in that row. This is equivalent to choosing a permutation with no fixed points, i.e. a derangement (Section 2.1). Hence there are $n!$ ways to choose the O's and $|\mathcal{G}_n| = n! \cdot n!$ size n grid diagrams. \square

Theorem 5.1.1 counts all $n \times n$ grid diagrams, regardless of the link type or even the number of components. If one is instead interested in only links of one component, i.e. knots, then the total count is $n!(n-1)!$ as proved in Theorem 5.1.2. The sequence defined by $n!(n-1)!$ is equivalent to a one-unit shift of sequence A010790 [OEI19b] in the OEIS. At the time of this writing there does not appear to be any obvious direct connection between the listed relations and uses of this sequence on the OEIS and the counting of grid diagrams of knots.

THEOREM 5.1.2. *There are $|\mathcal{G}_{n,1}| = n!(n-1)!$ size n grid diagrams representing 1-component links.*

PROOF. As in the proof of Theorem 5.1.1, there are $n!$ ways to first assign the X's. Once the X's are chosen, there are $n-1$ ways to assign the O in the first row. Each subsequent O will be placed in the row containing the X that shares its column with the previously placed O. There will be $n-k$ choices of which column to place the k th O for $k < n$, as it cannot occupy the same column as any of the previous O's, nor can it occupy the same column as the X in the first row. Finally, the n th O must be placed in the same column as the X in the first row to complete the knot. Thus, there are $(n-1)!$ ways to choose the O's, and $|\mathcal{G}_{n,1}| = n!(n-1)!$ ways to create an $n \times n$ grid diagram representing a 1-component link. \square

Now to generalize this argument to c -component links.

THEOREM 5.1.3. *For any $n \geq 4$ and $2 \leq c \leq \lfloor \frac{n}{2} \rfloor$, there are*

$$(5.1) \quad n!(n-1)! \sum_{k_1=2}^{n-2(c-1)} \sum_{k_2=2}^{n-2(c-2)-k_1} \cdots \sum_{k_j=2}^{n-2(c-j)-\sum_{i=1}^{j-1} k_i} \cdots \sum_{k_{c-1}=2}^{n-2-\sum_{i=1}^{c-1} k_i} \frac{1}{\prod_{l=1}^{c-1} (n - \sum_{m=1}^l k_m)}$$

$n \times n$ grid diagrams representing c -component links.

PROOF OF THEOREM 5.1.3. First place the X's. There are still $n!$ ways to do this.

We can see that the size of every component must be at least two, hence in a size n grid diagram with c components we get $2c \leq n$. Consider the component which occupies the first row. Let k_1

be the size of this component. We must have $2 \leq k_1 \leq n - 2(c - 1)$ to leave space to place the remaining $c - 1$ components.

Now place the O in the first row, there are $n - 1$ choices. If $k_1 = 2$, then the next O must be placed to close the component. If $k_1 > 2$ then we follow the logic of the proof for Theorem 5.1.2 and place the second O in the row of the X which shares its column with the first O. There are $n - 2$ choices for this placement as in the proof of Theorem 5.1.2. The pattern repeats until $(k_1 - 1)$ O's are placed, and then the final O must be placed to close the component (1 choice). In this process there are $(n - 1)!/(n - k_1)!$ possible ways to place the O's.

Now consider the component which occupies the topmost row that does not currently contain an O. Let k_2 be the size of this component. To ensure each of the remaining $c - 2$ components have at least two rows left to occupy, we need $2 \leq k_2 \leq n - 2(c - 2) - k_1$. By filling in this component as we filled in the first component, we can make $(n - k_1 - 1)$ choices for the first O, $(n - k_1 - 2)$ choices for the second O, and so on terminating at $(n - k_1 - k_2 + 1)$ choices for the second to last O. The final O must close the component (1 choice). Hence, there are $(n - k_1 - 1)!/(n - k_1 - k_2)!$ ways to construct the second component.

Proceeding in this fashion, the j th component can occupy at most $n - 2(c - j) - \sum_{i=1}^{j-1} k_i$ rows and there are $(n - 1 - \sum_{i=1}^{j-1} k_i)!/(n - \sum_{i=1}^j k_i)!$ ways to place the O's for that component. The value of k_c must be equal to the number of unoccupied rows after the previous $c - 1$ components have been constructed. Summing over all possible k_j yields the following number of c -component link diagrams in an $n \times n$ grid,

$$(5.2) \quad n! \sum_{k_1=2}^{n-2(c-1)} \sum_{k_2=2}^{n-2(c-2)-k_1} \cdots \sum_{k_j=2}^{n-2(c-j)-\sum_{i=1}^{j-1} k_i} \cdots \sum_{k_{c-1}=2}^{n-2-\sum_{i=1}^{c-1} k_i} \prod_{l=1}^c \frac{(n-1-\sum_{i=1}^{l-1} k_i)!}{(n-\sum_{i=1}^l k_i)!}$$

After carefully canceling terms in the product, this can be found to be equivalent to equation (5.1). □

For 2-component links this number is $n!(n - 1)! \sum_{k=2}^{n-2} \frac{1}{n-k}$. Dividing Equation (5.1) by $n!$ gives sequence A008306 [OEI19a] in the OEIS, which counts the “number of derangements of $1..n$ with k cycles.” Hence we get the following identity,

THEOREM 5.1.4.

$$(5.3) \quad \sum_{k_1=2}^{n-2(c-1)} \sum_{k_2=2}^{n-2(c-2)-k_1} \cdots \sum_{k_j=2}^{n-2(c-j)-\sum_{i=1}^{j-1} k_i} \cdots \sum_{k_{c-1}=2}^{n-2-\sum_{i=1}^{c-1} k_i} \frac{(n-1)!}{\prod_{l=1}^{c-1} (n - \sum_{m=1}^l k_m)} = T(n, c)$$

where $T(n, c)$ is the number of derangements of $\{1..n\}$ with c cycles.

PROOF. Assume that the X's have been placed in a size n grid diagram for a c -component link. Then the left side of the equation counts the number of ways to place the O's to complete the link, per the proof of Theorem 5.1.3. All we need to show is that placing the O's is equivalent to choosing a derangement of with c cycles.

Consider a derangement σ with c cycles. For each X, let i be its column index and place an O in column $\sigma(i)$ of the row containing that X. Each cycle of length m will then define a size m component. Since there are c cycles, there will be c components. \square

It is noted on the OEIS page for sequence A008306 that $\sum_{k=1}^{\lfloor n/2 \rfloor} T(n, c) = !n$, which is reaffirmed here, combinatorially.

5.1.2. $\mathcal{G}_n(K)$, the Set of $n \times n$ Grid Diagrams with Knot Type K . The set $\mathcal{G}_n(K)$ is naturally much more difficult to enumerate exactly, as it is highly dependent on the knot type. One fact we can say about $|\mathcal{G}_n(K)|$ is that it is a multiple of n .

LEMMA 5.1.5. $|\mathcal{G}_n(K)|/n \in \mathbb{Z}$

PROOF. Consider an $n \times n$ grid diagram g representing a knot K . Let $g \sim g'$ if g' can be obtained by a horizontal cyclic permutation of g . This defines an equivalence relation:

- $g \sim g$ by cyclically permuting n units to the right,
- if $g \sim g'$ by cyclically permuting t units to the right, then $g' \sim g$ by cyclically permuting t units to the left, and
- if $g_1 \sim g_2$ by cyclically permuting t_1 units to the right and $g_2 \sim g_3$ by cyclically permuting t_2 units to the right, then $g_1 \sim g_3$ by cyclically permuting $t_1 + t_2$ units to the right.

Let \mathcal{T}_g be the equivalence class formed by g under this equivalence relation. Every horizontal cyclic permutation by t units results is equivalent to a permutation by $t \bmod n$, hence $|\mathcal{T}_g| = n$ for any g . So, $\mathcal{G}_n(K)$ is partitioned into equivalence classes of equal size n , hence n divides $|\mathcal{G}_n(K)|$ \square

Now for a lower bound on $|\mathcal{G}_n(K)|$, starting with the special case of the unknot.

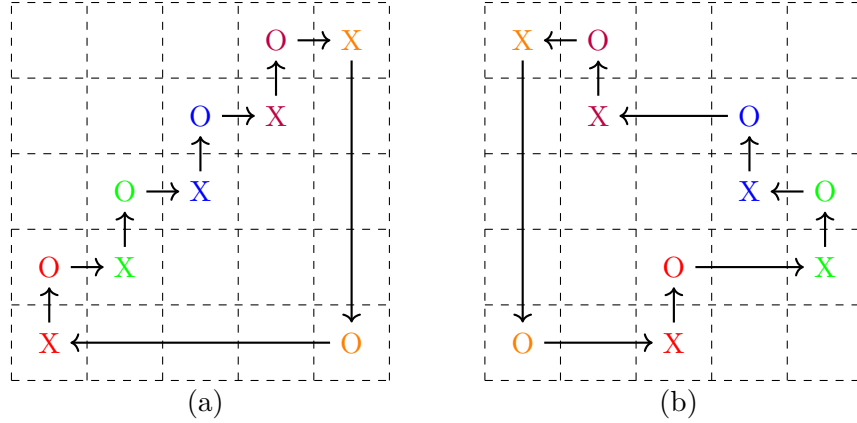


FIGURE 5.1. (a) A 5×5 “stair unknot,” and (b) the result of a sequence of column commutations applied to the grid diagram in (a). Color is added to aid visual tracking of the columns. This figure illustrates the construction of at least $n!$ unknots in grids of size n (Lemma 5.1.6).

LEMMA 5.1.6. $n! \leq \mathcal{G}_n(0_1)$

PROOF. Consider the “stair unknot” (Figure 5.1) constructed by placing an entry in the top-right corner of a grid, then placing an entry directly to the left of it. Then place an entry directly below that entry. Keep placing entries directly to the left or below the previous one until the bottom row of the grid is reached. Place the last entry in the bottom-right corner of the grid to close the component. There are no crossings in this grid, hence it is the unknot.

Now note that no two adjacent columns are interleaved. In fact, no two columns, adjacent or not, are interleaved. This means that any column can be commuted to replace any other column. There are $n!$ ways to arrange the columns, all of which can be achieved by commutations. Hence, there are at least $n!$ different $n \times n$ grid diagrams representing the unknot. \square

This can then be used to bound the number of grid diagrams for any knot by a simple concatenation argument. First, we must define a way to concatenate two grid diagrams, i.e. take the connect sum of the knots represented in them. To do this, consider two grids g_1 and g_2 such that $|g_i| = n_i$. We construct a connect sum by taking a size $n_1 + n_2 - 1$ grid and filling the first n_1 rows with entries in the same columns as g_1 except for the entries in column n_1 (see Figure 5.2). Then we fill the remaining rows with the entries from rows 2 through n_2 of g_2 shifted to the right by $n_1 - 1$ units. There are now two missing entries in this grid diagram, and only one way to fill them in to create a valid grid diagram. Namely, we place an O in the same row as the O from column n_1 of g_1 and in the column $n_1 - 1$ units to the right of the column containing the O in row 1 of g_2 .

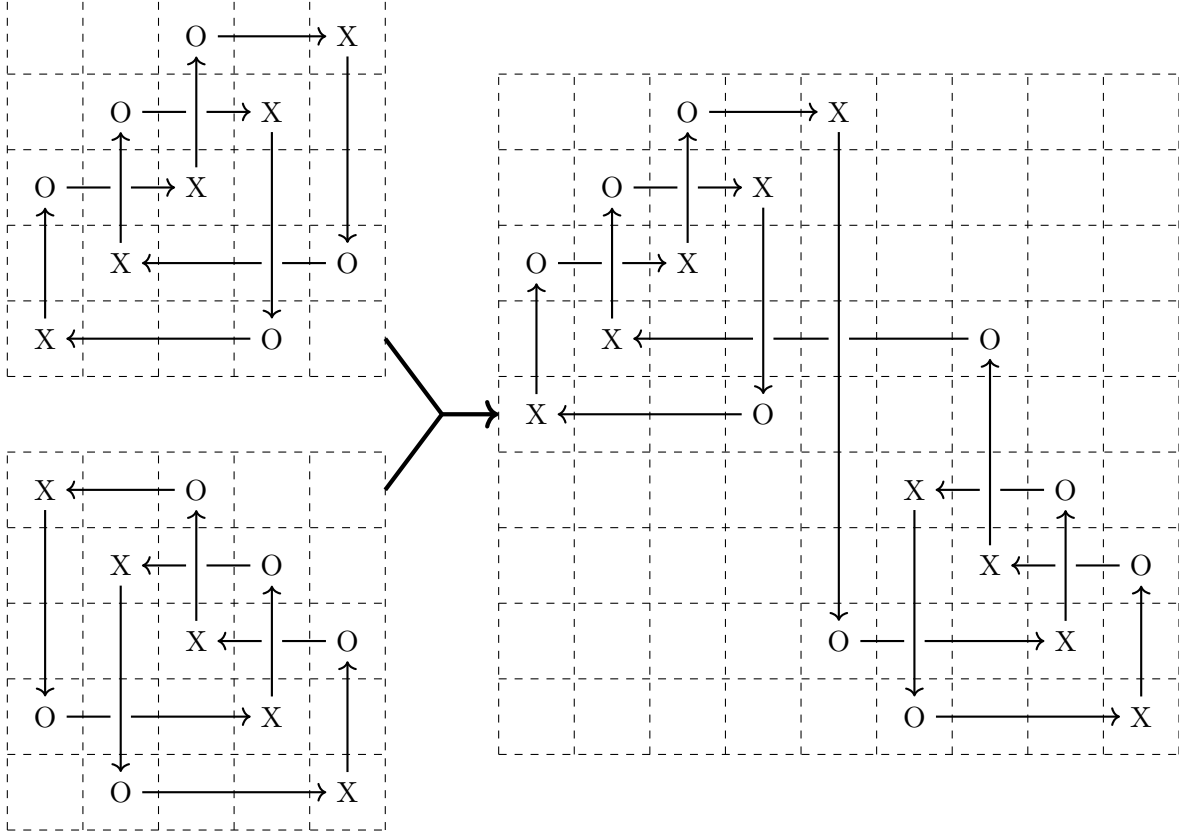


FIGURE 5.2. The concatenation of 3_1 (bottom-left) and 3_1^* (top-left) into $3_1 \# 3_1^*$ (right).

We do the same with the X from column n_1 of g_1 and row 1 of g_2 . The result is a size $n_1 + n_2 - 1$ grid diagram representing the connect sum of the knots contained in grids g_1 and g_2 .

Note that this construction assumes that the grids contain knots. If it is performed with links of more than one component, then only one component in each grid will be connected. Now we use concatenation as described above to provide a lower bound for the number of grid diagrams.

THEOREM 5.1.7. *For any non-trivial knot type K and all $n \geq \alpha(K)$, $\alpha(K) \cdot (n - \alpha(K) + 1)! \leq |\mathcal{G}_{\alpha(K)}(K)| \cdot |\mathcal{G}_{n-\alpha(K)+1}(0_1)| \leq |\mathcal{G}_n(K)|$*

PROOF. There are at least $\alpha(K)$ grid diagrams in $\mathcal{G}_{\alpha(K)}(K)$ by Lemma 5.1.5 and there are at least $(n - \alpha(K) + 1)!$ grid diagrams in $\mathcal{G}_{n-\alpha(K)+1}(0_1)$ by Lemma 5.1.6. Then $\alpha(K) \cdot (n - \alpha(K) + 1)!$ provides a lower bound on $|\mathcal{G}_{\alpha(K)}(K)| \cdot |\mathcal{G}_{n-\alpha(K)+1}(0_1)|$. Let $g_1 \in \mathcal{G}_{\alpha(K)}(K)$ and $g_2 \in \mathcal{G}_{n-\alpha(K)+1}(0_1)$, then the result of concatenating g_1 and g_2 as described above will be a grid representing $K \# 0_1 = K$, hence it is a grid diagram in $\mathcal{G}_n(K)$. There are $|\mathcal{G}_{\alpha(K)}(K)| \cdot |\mathcal{G}_{n-\alpha(K)+1}(0_1)|$ ways to choose g_1 and g_2 , each of which will result in a unique grid, so this provides a lower bound on $|\mathcal{G}_n(K)|$. \square

Upper bounds of $|\mathcal{G}_n(K)|$ are directly related to the FWD conjecture. Note that since $P_n(K) = \frac{|\mathcal{G}_n(K)|}{n!(n-1)!}$, a bound of $|\mathcal{G}_n(K)| \leq f(n) \cdot n!(n-1)!$ such that $f(n) \rightarrow 0$ as $n \rightarrow \infty$ would be equivalent to a proof of the FWD conjecture. In Chapter 6, it is shown that $P_n(K) = O(n^{-1/10})$, which means $|\mathcal{G}_n(K)| = O(n^{-1/10}n!(n-1)!)$. The numerical results in Section 7.3 imply that this is far from a tight upper bound and that $P_n(K)$ is likely to be $O(a^{-n})$ for some $a > 1$.

5.2. Grids and Writhe

It is useful, particularly in the implementation of the Wang-Landau algorithm where energy is at least partially defined by writhe, to know how the Cromwell moves affect the projected writhe of a knot. In most cases, a Cromwell move will change writhe by ± 1 or 0. The exception is that commutations between the first and last columns or rows may change writhe by 2. Moreover, the change in writhe can be calculated in $O(1)$ time, assuming the grid is encoded in an efficient way. These facts will be proven starting with commutations.

LEMMA 5.2.1. *Performing a commutation in a grid diagram between rows or columns i and $i + 1$ for $i = 1, 2, \dots, n - 1$ results in a projected writhe change of ± 1 or 0.*

PROOF. Consider columns i and $i + 1$ with $i < n$. Any crossings that are added or removed as the result of a commutation of columns i and $i + 1$ will only appear in those columns. All other crossings will remain fixed. Consider three cases:

- (1) Both entries in one column are above both entries in the other column (Figure 5.3). In this case the commutation will not add or remove any crossings. Hence the writhe will not change.
- (2) The entries of one column are both between the entries of the other column (Figure 5.4). In this case if the horizontal edges in the rows of the “between” segment are on the same side of the column, (Figure 5.4(a)), then the commutation performs a type II Reidemeister move which does not change the writhe. On the other hand, if the edges are on opposite sides of the column (Figure 5.4(b)), then one crossing will be removed while another crossing with the same contribution to writhe will be simultaneously added, resulting in a writhe change of 0.
- (3) The columns share a row (Figure 5.5). If the vertical edges in these columns are on opposite sides of the shared row (Figure 5.5(b)), then there will be no crossing changes

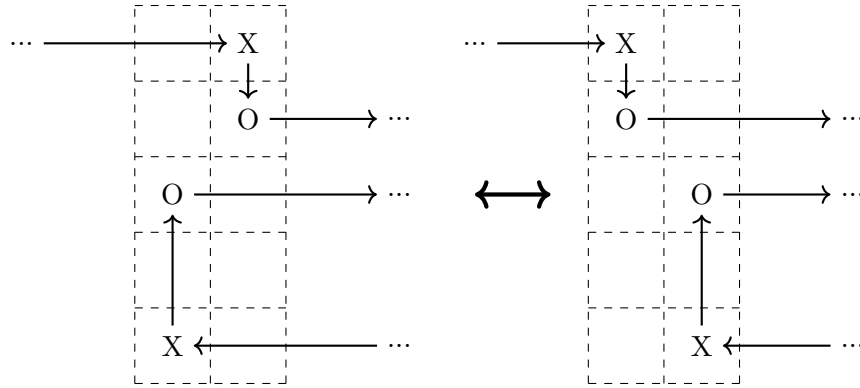


FIGURE 5.3. A commutation which does not change projected writhe.

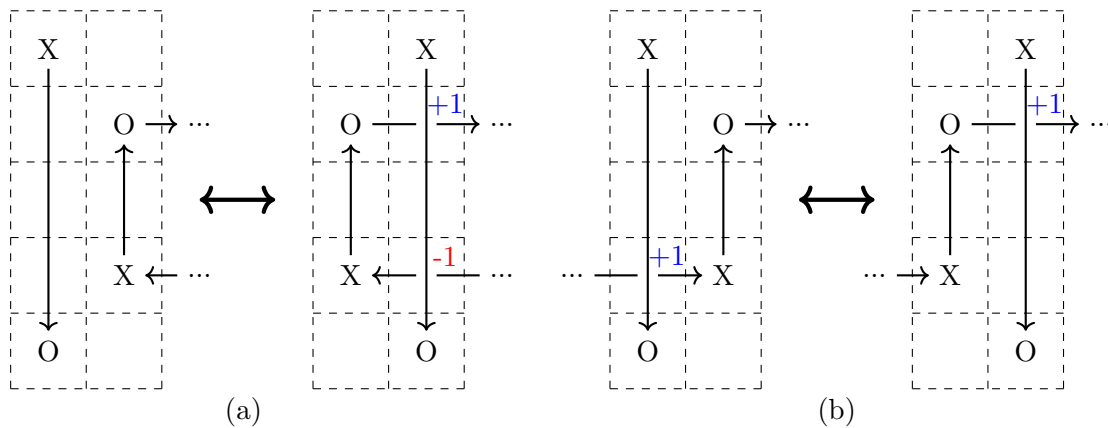


FIGURE 5.4. Commutations which do not change projected writhe, despite adding and removing crossings.

and hence no change in writhe. On the other hand, if the vertical edges are both below or both above the shared row (Figure 5.5(a)), then the horizontal edge coming from the shorter of the two vertical edges will either add or remove a single crossing, i.e. a type I Reidemeister move will be performed resulting in a ± 1 change in writhe. The sign of this change can be predicted by which vertical edge is shorter combined with the directions of all involved edges .

An identical argument proves this result for row commutations. □

Note that this does not account for commuting the first and last rows or columns, which is also a valid Cromwell move. This will be accounted for later. Also, writhe change of interleaved exchanges are not mentioned in Lemma 5.2.1, as this is not a valid Cromwell move.

Now to show the behavior of writhe under stabilizations,

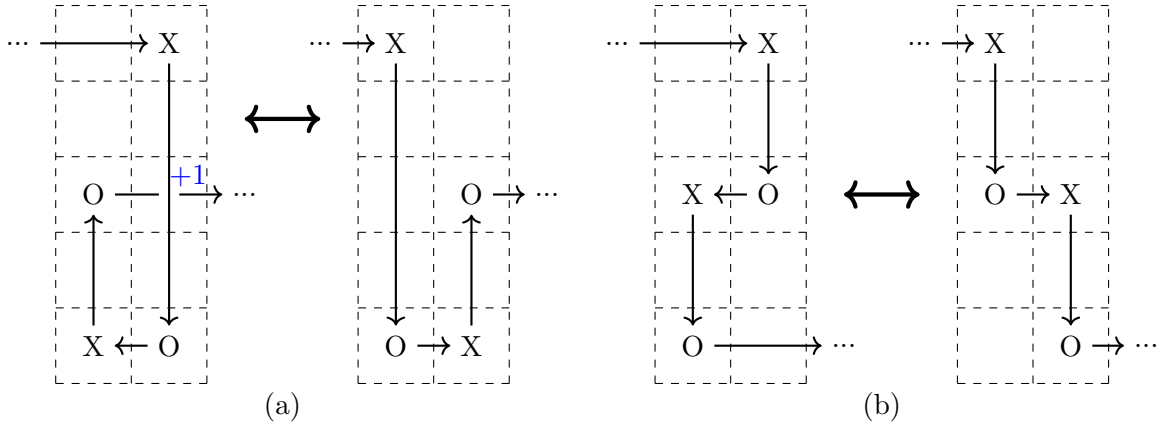


FIGURE 5.5. (a) A writhe changing commutation. (b) A writhe fixing commutation.

LEMMA 5.2.2. *A general stabilization will change the projected writhe of a grid diagram by ± 1 or 0.*

PROOF. Without loss of generality, consider a general stabilization where a row and vertical grid line are selected. There are two main cases:

- (1) The grid line selected is between the entries of the selected row (as in Figure 2.9). In this case, there will be no new crossings introduced, nor will any be removed. Hence the writhe will not change.
- (2) The grid line selected is not between the vertices in the selected row (Figure 5.6). In this case, new crossings may be introduced, but no crossings will be removed. Consider the two horizontal edges resulting from the stabilization, the longer one will occupy all of the columns that the original horizontal edge did as well as several new columns. All of the existing intersections with the original row will exist in this new row. The rest of the columns occupied by this edge will be exactly the columns occupied by the other new row. Hence, any new intersections in these columns will intersect both of these edges. These horizontal edges are antiparallel, so any contribution to writhe from an a vertical edge intersecting one of these edges is immediately canceled by the intersection with the other edge. The one exception is if one of the vertical edges intersecting the longer of the new horizontal edges terminates at the shorter of the new horizontal edges (as is the case in Figure 5.6). In this case, there is a contribution to writhe of ± 1 .

Hence a general stabilization will change the writhe of a grid diagram by ± 1 or 0. □

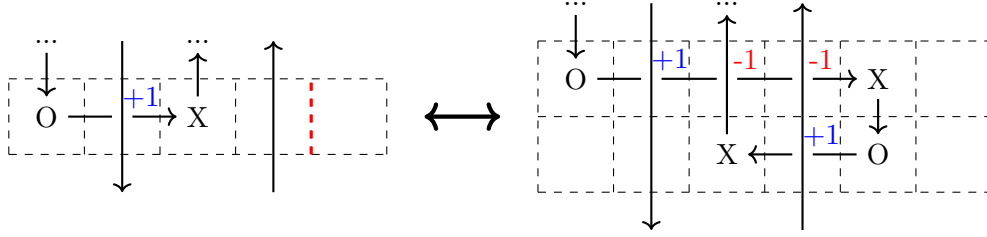


FIGURE 5.6. This stabilization (\rightarrow) changes the writhe by -1 , and the corresponding destabilization (\leftarrow) changes the writhe by $+1$.

This means that the writhe change of a general stabilization depends only on where the new entries are inserted and which direction the edges which terminated in the original row/column. Note that if one restricts to elementary stabilizations, writhe changes of ± 1 and 0 are all still possible. Since destabilizations are the inverse operation of stabilizations, we immediately get the following corollary to Lemma 5.2.2.

COROLLARY 5.2.3. *A general destabilization will result in a writhe change of ± 1 or 0 .*

PROOF. As destabilizations are the inverse operation of a stabilization, any given destabilization will have the exact opposite effect as the corresponding stabilization it is an inverse of. So, a stabilization that changes the writhe by $+1$ will be undone by a destabilization that changes the writhe by -1 . \square

This change in writhe can be determined by examining the directions and lengths of the edges in the destabilizing rows/columns. Now to examine writhe change under cyclic permutations.

LEMMA 5.2.4. *A cyclic permutation by one unit will result in at most a ± 1 change in writhe.*

PROOF. Without loss of generality, consider a cyclic permutation one unit to the right. Consider the entries in the rightmost column. Denote the row index of the topmost entry in this column with N and the row index of the bottommost entry with S . There are now two cases.

- (1) The other vertical edge that terminates in row N is below row N (Figure 5.7). The chain of edges following this edge will eventually return to the bottom of the rightmost edge, meaning there must be an even number of vertical edges from this component which pass completely through row N , half oriented north and half oriented south. The same is true of edges from other components passing through row N . Suppose there are $2m$ vertical edges which pass through row N . Now consider the vertical edges which pass

through the edge in row N before and after the cyclic permutation. The intersecting edges after the cyclic permutation will be the complement of the intersecting edges before the cyclic permutation. So if the edge in row N intersected k north edges and ℓ south edges before the cyclic permutation, then the edge after the cyclic permutation will intersect $m - k$ north edges and $m - \ell$ south edges. Since the direction of the edge in row N will reverse, the contribution to writhe of an intersecting edge of a particular orientation will also change to its opposite. Without loss of generality, suppose the edge in row N was oriented west before the cyclic permutation. Then the contribution of that edge to writhe was $k - \ell$. Then after the cyclic permutation, the edge's contribution to writhe will be $(m - \ell) - (m - k) = k - \ell$. Hence there will be no change in writhe from this edge.

- (2) The other vertical edge terminating in row N is north of row N (Figure 5.8). Then, because the string of edges must eventually reach the rightmost column below row N , there will be an odd number of vertical edges passing through row N . All of these edges will be paired north/south like the previous case except for the extra one which must be oriented in the opposite direction of the vertical edges terminating in row N . There will be a change in writhe of $+1$ due to this edge as it will either be part of a -1 crossing before the cyclic permutation with no corresponding crossing after the cyclic permutation, or be a part of a $+1$ crossing after the cyclic permutation with no corresponding crossing before the cyclic permutation.

We can follow a near identical argument as above to show that the edge in row S will have a change in writhe contribution of either 0 or -1 . No other horizontal edges can gain or lose a crossing in this cyclic permutation, so these are the only possible changes in writhe. Adding the changes in the contributions to writhe of rows N and S give a writhe change of ± 1 or 0 under a cyclic permutation by 1 unit to the right. These arguments can be applied to cyclic permutations of one unit up, down, or left as well. □

We can see that one only needs to look at the two edges before and the two edges after the rightmost edge to know exactly how writhe will change under a cyclic permutation one unit to the right. Now we may combine this result with Lemma 5.2.1 to look how writhe behaves when permuting the first and last rows or columns.

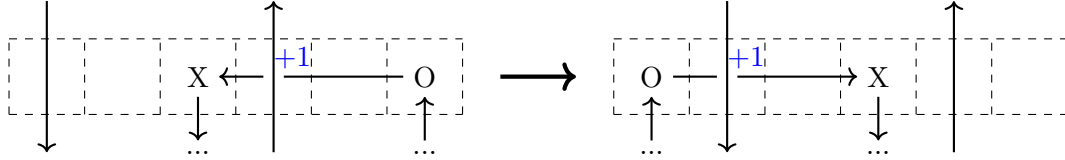


FIGURE 5.7. An example of a cyclic permutation one unit to the right fixing the writhe contribution in the row of the northernmost entry in the rightmost column. This is guaranteed by the other vertical edge terminating in this row being entirely south of the row.

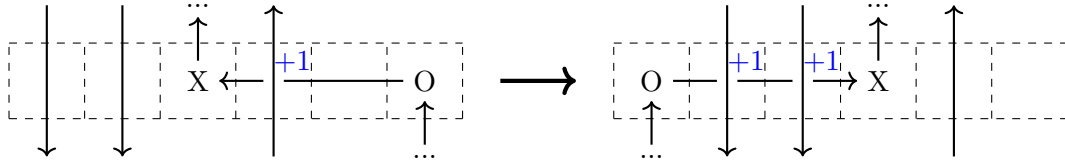


FIGURE 5.8. An example of a cyclic permutation one unit to the right adding one to the writhe contribution in the row of the northernmost entry in the rightmost column. This is guaranteed by the other vertical edge terminating in this row being entirely north of the row.

LEMMA 5.2.5. *A commutation between the first and last rows or columns will change writhe by no more than 2.*

PROOF. Consider that this commutation could also be achieved by cyclically permuting one unit so the columns or rows are directly (as opposed to cyclically) adjacent, then commuting them, then cyclically permuting back. Without loss of generality, consider a commutation between the last column and the first column. Construct this by cyclically permuting the grid diagram one unit to the right, commuting columns 1 and 2, then cyclically permuting one unit to the left.

If the commutation after the first cyclic permutation doesn't change the writhe, then the only writhe change will be from the two cyclic permutations, each of which can change writhe by no more than 1. Hence, in this case, writhe can change by no more than 2.

If the intermediate commutation step does change the writhe, it will change it by ± 1 . Either the topmost or the bottommost entries in the commuting columns must be in the same row by proof of Lemma 5.2.1. Without loss of generality, assume the topmost entries are in the same row. This means that the edge in that row will have no change in its contribution to writhe by under either cyclic permutation by the proof of Lemma 5.2.4. Then in the bottommost rows, the cyclic permutation to the right could only possibly change the writhe by -1 or 0 , and the cyclic permutation to the left could only possibly change the writhe by $+1$ or 0 , also by the proof of

Lemma 5.2.4. So the cyclic permutations combined will change the writhe by ± 1 or 0. Combined with the intermediate commutation, the writhe will change in this process by at most 2. \square

In each case, the change in writhe of a Cromwell move can be fully determined by the sizes and directions of the edges in the rows and columns directly associated with the move, and at most two edges before and after those edges. Assuming $O(1)$ access to these pieces of information, change in writhe can be calculated in $O(1)$ time, meaning it is not a computational hindrance to use writhe as an energy function in a Wang-Landau algorithm using Cromwell moves as transitions, as is done in Section 7.2.2.

The Frisch-Wasserman-Delbrück Conjecture(FWD) for Grid Diagrams

Here a proof of Theorem 2.5.5 is provided. This theorem, restricted to $K = 0_1$, is Frisch-Wassermann-Delbrück conjecture for grid diagrams. By taking $v = c_2(K)$ (see Section 2.3.6.3), we see that Theorem 2.5.5 is a corollary of the following theorem,

THEOREM 6.0.1. *Let g be a grid diagram chosen uniformly from $\mathcal{G}_{n,1}$, the set of $n \times n$ grid diagrams representing knots. Then for any $v \in \mathbb{Z}$, $P[c_2(g) = v] = O(n^{-1/10})$.*

The proof and theorem are based on a recent paper by *Even-Zohar et al.* [EZHLN18], which proved a similar theorem for petal diagrams. Specifically, they used the skein relation

$$(6.1) \quad c_2 \left(\begin{array}{c} \nearrow \searrow \\ \nwarrow \nearrow \end{array} \right) - c_2 \left(\begin{array}{c} \nwarrow \nearrow \\ \nearrow \searrow \end{array} \right) = lk \left(\begin{array}{c} \nearrow \searrow \\ \nearrow \searrow \end{array} \right)$$

to show that, for a uniformly random petal diagram ω with $2n + 1$ petals, $P[c_2(\omega) = v]$ tends to 0 for any value of v as $n \rightarrow \infty$. This was done with applications of Chebyshev's inequality in the form [Ros14]

$$(6.2) \quad P \left[X \leq \frac{E[X]}{2} \right] \leq \frac{4V[X]}{E[X]^2},$$

and Theorem 6.0.2 due to Erdős

THEOREM 6.0.2 ([Erd45]). *Let $a_1, \dots, a_t \in \mathbb{R}$. At most $\binom{t}{\lfloor t/2 \rfloor}$ of the 2^t sums $\{\sum_{i \in I} a_i \mid I \subseteq \{1, \dots, t\}\}$ are contained in any open interval of length $\min_i |a_i|$.*

As noted by [EZHLN18], the conclusion of Theorem 6.0.2 can be restated probabilistically as the probability that the sum over a subset of $\{a_i\}_{i=1}^t$, chosen uniformly at random, is in such an interval is bounded above by $\binom{t}{\lfloor t/2 \rfloor} / 2^t \leq \frac{1}{\sqrt{t}}$.

Petal diagrams are actually a subset of arc diagrams, which themselves are equivalent to grid diagrams, so it stands to reason that this method can be applied to grid diagrams. The core

issue in converting the proof from [EZHLN18] to grid diagrams is that it hinges on “swaps” that correspond to exchanging adjacent rows in grid diagrams. In a petal diagram, those swaps are guaranteed to be crossing changes, whereas an adjacent row exchange in a grid diagram will only result in a crossing change if the rows are interleaved. This is important, as the skein relation in Equation (6.1) only applies when a crossing change is performed. Here, the proof of [EZHLN18] is adapted to grid diagrams, accounting for interleaving.

6.1. Proof of the FWD Conjecture for Grid Diagrams

To prove Theorem 6.0.1, we will need to perform crossing changes and smoothings in grid diagrams. Since it is known that non-interleaved adjacent row exchanges never change the link type, we can say that these are necessarily not topologically equivalent moves to performing a crossing change (see Section 2.3.4). On the other hand, as can be seen in Figure 6.1, the exchange of two adjacent interleaved rows is topologically equivalent to a single crossing change [BCH⁺19]. Additionally, swapping the locations of the O’s in two adjacent rows is equivalent to a diagrammatic smoothing, which can also be seen in Figure 6.1. In order to apply the skein relation in Equation (6.1), we need to know that these operations are equivalent to performing a crossing change and a smoothing to the same crossing in some regular diagram of the link. This is not immediately clear when looking at the row exchange in a grid diagram, so we continue to appeal to the corresponding arc presentation.

Consider looking at an arc presentation from down the z -axis. As described here, this would look like several line segments emanating from a central point, and is not immediately useful, but the conformation can be perturbed slightly into a regular diagram. Given that this is a small perturbation, all of the interleaved pairs of rows (adjacent or not) will necessarily have a crossing associated to them in this diagram. We may now use this regular diagram and these crossings as our reference point for applying Equation (6.1), where an exchange of the interleaved rows corresponds to changing the relevant crossing, and swapping the O’s in those rows corresponds to a diagrammatic smoothing at that same crossing.

The crux of the proof for FWD in grid diagrams will be performing random row exchanges and observing the expected behavior of the Casson invariant, c_2 , as a result of these exchanges. To this end, we need to be able to estimate how many of these exchanges will actually be between

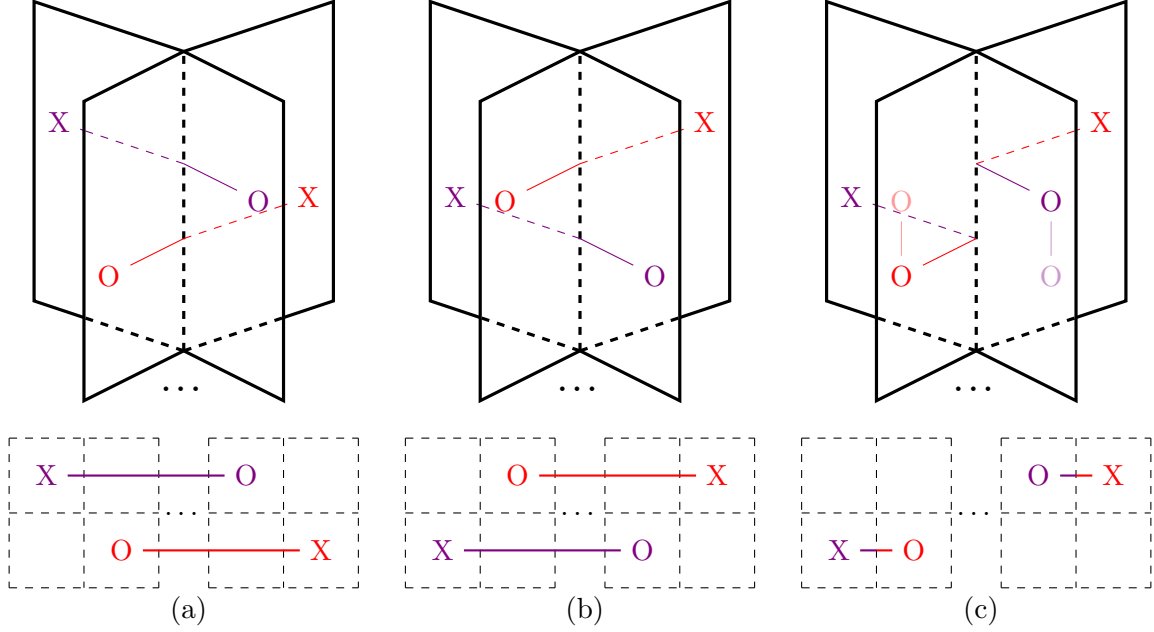


FIGURE 6.1. (a) A pair of interleaved rows in the corresponding arc presentation. (b) After exchanging the interleaved rows we get a crossing change. (c) Exchanging the O's results in a smoothing.

interleaved rows. So we count the number of grid diagrams where a particular pair of rows are interleaved.

LEMMA 6.1.1. *Let $n \geq 4$ and $2 \leq m \leq n - 2$. There are $\frac{n!(n-2)!(n-3)}{3}$ size n grid diagrams of knots with rows i and j are interleaved. There are $\frac{n!(n-2)!}{3}$ size n grid diagrams of 2-component links with rows i and j are interleaved, are of differing components, and the component in row i is size m .*

PROOF. Consider rows i and j in a size n grid diagram. Let x_i and x_j be the column indices of the X's in rows i and j respectively. Similarly, let o_i and o_j be the column indices of the O's in rows i and j . If rows i and j are interleaved, then any horizontal cyclic permutations of the final grid will leave rows i and j interleaved. Hence, we can count the number of conformations where rows i and j are interleaved with $x_i = 1$ and multiply the answer by n .

If row i and row j are interleaved, then by definition either $x_i < x_j < o_i < o_j$ or $x_i < o_j < o_i < x_j$. All instances of the second case can be obtained by swapping x_j and o_j from an instance of the first case, so we will assume we have the first case and multiply the number by two at the end. Now let ℓ be the number of columns separating column x_i and x_j , i.e. $0 \leq \ell = x_j - x_i - 1 \leq n - 4$. Assuming $x_j < o_i$, rows i and j can only be interleaved if $o_i < o_j$. If

we let $1 \leq k \leq n - \ell - 3$, then we can choose $o_i = n - k$ and there are k possible selections for o_j with $o_i < o_j$. This is $\sum_{k=1}^{n-\ell-3} k = \frac{(n-\ell-2)(n-\ell-3)}{2}$ ways to choose o_i and o_j . So there are $2n \sum_{\ell=0}^{n-4} \sum_{k=1}^{n-\ell-3} k = \frac{n(n-1)(n-2)(n-3)}{3} = \frac{n!}{3(n-4)!}$ ways to choose the X's and O's of rows i and j in such a way that they are interleaved.

By following the constructions in Theorems 5.1.2 and 5.1.3, we achieve our counts. Given a particular pair of interleaved rows i and j we count how many grid diagrams of knots can be formed. We can count these grid diagrams by completing the knot in a way similar to the proof of Theorem 5.1.2. There are $n - 2$ choices for the location of the O in column x_i . There are $n - 3$ choices for the location of the X sharing a row with that O. There are $n - 3$ choices for the next O and $n - 4$ choices for the next X. Continuing in this fashion yields $(n - 2)!(n - 3)!$ total ways to complete an $n \times n$ grid diagram of a knot from interleaved rows i and j . Hence the total number of grid diagrams of knots with rows i and j interleaved is

$$(6.3) \quad \frac{n!(n-2)!(n-3)!}{3(n-4)!} = \frac{n!(n-2)!(n-3)}{3}$$

Now, we count the result for two-component links. Assume that rows i and j are interleaved and each from a different component of the link. There are $\frac{n!}{3(n-4)!}$ ways in which rows i and j may be interleaved. Moreover, assume that row i is part of a size m component. Proceeding as before, there are $n - 2$ choices for the O in column x_i . There are $n - 4$ choices for the X sharing a row with that O, accounting for the already placed X's and O's in rows i and j . There are $n - m$ choices for the last O placed in the first component, and $n - m - 1$ choices for the second to last X. The final X in this component must be placed in column o_i to complete the component. The remaining component will then have $(n - m - 1)!(n - m - 2)!$ ways to place its X's and O's by the same reasoning. So the number of two-component links with rows i and j interleaved and of differing components, with the component in row i occupying m rows is

$$(6.4) \quad \frac{n!}{3(n-4)!} \frac{(n-2)!}{(n-m-1)!} \frac{(n-4)!}{(n-m-2)!} (n-m-1)!(n-m-2)!$$

which reduces to

$$(6.5) \quad \frac{n!(n-2)!}{3}$$

□

Since our strategy for proving FWD in grids is to use Equation (6.1), we will need a grasp on the behavior of linking number in random grid diagrams in order to work with the right-hand side of the equation. We will use a strategy of exchanging a random subset of adjacent rows to determine the behavior of linking number. As linking number will only change from the exchange of adjacent interleaved rows from differing components, we will need to estimate how many such pairs there are.

LEMMA 6.1.2. *Let g be an $n \times n$ grid of a 2-component link with components of size m and $n - m$ where $m \geq 3$ and $n \geq 8$. Then the probability that less than $\frac{m(n-m)}{6n}$ pairs of rows $2i - 1$ and $2i$, for $1 \leq i \leq \lfloor n/2 \rfloor$, are interleaved and of differing components is $O\left(\frac{n^3}{m^2(n-m)^2}\right)$.*

PROOF. Let Z denote the number of pairs of rows that satisfy the condition of the lemma, and let $Z_i = 1$ if rows $2i - 1$ and $2i$ satisfy the condition, and 0 otherwise. Hence $Z = \sum_{i=1}^{\lfloor n/2 \rfloor} Z_i$.

From the proof of Theorem 5.1.3, we know that the number of size n grids of 2-component links with a size m component in row $2i$ is $\frac{n!(n-1)!}{n-m}$. This means that the number of links with a size $n - m$ component in row $2i$ is $\frac{n!(n-1)!}{m}$. Then the number of $n \times n$ grid diagrams of 2-component links with components of size m and $n - m$ is $\frac{n!(n-1)!}{n-m} + \frac{n!(n-1)!}{m} = \frac{n!n!}{m(n-m)}$. The expected value for Z_i is then the number of 2-component links with components of size m and $n - m$ with rows $2i - 1$ and $2i$ interleaved and of differing components (Lemma 6.1.1) divided by the number of 2-component links with components of size m and $n - m$,

$$(6.6) \quad E[Z_i] = \frac{2n!(n-2)!m(n-m)}{3n!n!} = \frac{2m(n-m)}{3n(n-1)}.$$

Then we get the expected value of Z ,

$$(6.7) \quad \frac{m(n-m)}{3n} \leq \lfloor n/2 \rfloor \frac{2m(n-m)}{3n(n-1)} = \sum_{i=0}^{\lfloor n/2 \rfloor} E[Z_i] = E[Z],$$

which yields variance

$$(6.8) \quad V[Z_i] = E[Z_i^2] - E[Z_i]^2 = \frac{2m(n-m)}{3n(n-1)} - \left(\frac{2m(n-m)}{3n(n-1)}\right)^2 \leq \frac{2m(n-m)}{3n(n-1)}$$

Now consider $E[Z_i Z_j]$ for $i \neq j$. This is the probability that rows $2i - 1$ and $2i$ are interleaved and of differing components, while rows $2j - 1$ and $2j$ are also interleaved and of differing components. First, construct rows $2i - 1$ and $2i$ to be interleaving. The proof of Lemma 6.1.1 establishes that

there are $\frac{n!}{3^{(n-4)!}}$ ways to do this. Now we wish to construct rows $2j - 1$ and $2j$ such that they are interleaving. We are only interested in an upper bound for $E[Z_i Z_j]$, so we will consider all $\frac{n!}{3^{(n-4)!}}$ interleaved constructions of rows $2j - 1$ and $2j$, although some of these will not be compatible with the entries in rows $2i - 1$ and $2i$. Completing the construction of the rest of the grid will be easier if we assume that the entries selected in rows $2i - 1$, $2i$, $2j - 1$, and $2j$ are all in different columns. Note that each construction of a pair of interleaved rows can be cyclically permuted to $n - 1$ other pairs of interleaved rows. If we divide all of these constructions for rows $2j - 1$ and $2j$ into classes of size n determined by this cyclic permutation, then we can note that 4 elements in each class will have the X in row $2j - 1$ in the same column as an entry in row $2i - 1$ or $2i$. Considering all 4 entries in rows $2j - 1$ and $2j$ gives us at most 16 elements of each class that share a column with an entry in row $2i - 1$ or $2i$. Hence the probability that any selected pair of interleaved rows $2j - 1$ and $2j$ share a column with row $2i - 1$ or $2i$ is bounded above by $16/n$. Hence, we will assume that the entries selected in rows $2i - 1$, $2i$, $2j - 1$, and $2j$ are all in different columns, with a probability bounded by $16/n$ that this is not the case.

To complete the construction, we will need to decide which rows from $2i - 1$, $2i$, $2j - 1$, and $2j$ are in which component. There are 4 ways to make this decision, but without loss of generality, let us assume that rows $2i$ and $2j$ are in the component of size m . We will start the construction by placing an O in the column containing the X in row $2i$, but before placing any X's or O's, we note that at some point in constructing this component, we must place an X in the column containing the O in row $2j$. There will be $m - 2$ X's placed to create this component, and the last one must be in the column containing the O in row $2i$. Hence, there are $m - 3$ choices for which X will connect to row $2j$. Once this choice is made, we place an O in the column shared with the X in row $2i$. There are $n - 4$ ways to make this choice. Now there are $n - 8$ choices for where to place the next X followed by $n - 5$ ways to place the next O. The argument continues as we have seen, eventually yielding $4(m - 3) \frac{(n-4)!}{(n-m-2)!} \frac{(n-8)!}{(n-m-4)!} (n - m - 2)!(n - m - 3)!$ ways to complete the link given rows $2i - 1$, $2i$, $2j - 1$, and $2j$.

Hence we get

$$(6.9) \quad E[Z_i Z_j] \leq \frac{(4(m - 3)(n - 4)!(n - 8)!(n - m - 3) + 16/n)n!n!(n - m)m}{9n!n!(n - 4)!(n - 4)!}$$

$$(6.10) \quad \leq \frac{4m^2(n - m)^2}{9(n - 7)^4} + O(n^{-1})$$

Now we may bound covariance,

$$(6.11) \quad \text{COV}[Z_i, Z_j] = E[Z_i Z_j] - E[Z_i]E[Z_j]$$

$$(6.12) \quad \leq \frac{4m^2(n-m)^2}{9(n-7)^4} + O(n^{-1}) - \frac{4m^2(n-m)^2}{9n^2(n-1)^2}$$

$$(6.13) \quad = O(n^{-1}),$$

and the variance of Z ,

$$(6.14) \quad V[Z] = \sum_{i=1}^{\lfloor n/2 \rfloor} V[Z_i] + \sum_{i \neq j} \text{COV}[Z_i, Z_j] \leq \lfloor n/2 \rfloor \frac{2m(n-m)}{3n(n-1)} + 4\lfloor n/2 \rfloor^2 O(n^{-1})$$

$$(6.15) \quad = O(n).$$

Finally, we apply Chebyshev's inequality (as in Equation (6.2)):

$$(6.16) \quad P \left[Z \leq \frac{m(n-m)}{6n} \right] \leq P \left[Z \leq \frac{E[Z]}{2} \right] \leq \frac{4V[Z]}{E[Z]^2}$$

$$(6.17) \quad \leq 4 \frac{O(n)}{\left(\frac{m(n-m)}{3n} \right)^2}$$

$$(6.18) \quad = O \left(\frac{n^3}{m^2(n-m)^2} \right)$$

□

Now we will combine Lemma 6.1.2 with Theorem 6.0.2 to get a result about the expected linking number.

THEOREM 6.1.3. *Let g be a random size n grid diagram of a 2-component link with components of size m and $n-m$, with $m, n \in \mathbb{N}$, $m \geq 3$, $n \geq 8$, and $v \in \mathbb{Z}$. Then $P[\text{lk}(g) = v] \leq \sqrt{\frac{6n}{m(n-m)}} + O\left(\frac{n^3}{m^2(n-m)^2}\right)$.*

PROOF. Let g be a random 2-component $n \times n$ grid diagram where one component occupies m rows, and the other component occupies $n-m$ rows. Consider the operation of exchanging rows $2i-1$ and $2i$ and call it σ_i . Now define g' to be the grid obtained by performing a subset of $\{\sigma_i\}_{i=1}^{\lfloor n/2 \rfloor}$ chosen uniformly at random from the $2^{\lfloor n/2 \rfloor}$ possible subsets. Note that if g is chosen uniformly at random, then g' is also a uniformly random grid from the set of $n \times n$ grid diagrams of 2-component links with components of size m and $n-m$.

Each exchange that occurs between interleaved rows containing different components will change the linking number by ± 1 . So, if there are t such pairs of rows, then by Theorem 6.0.2, the probability that the change in linking number is in an interval $(v - \text{lk}(g) - 1, v - \text{lk}(g) + 1)$ is bounded above by $\frac{1}{\sqrt{t}}$. Hence $P[\text{lk}(g') = v \mid t] = P[\text{lk}(g') - \text{lk}(g) = v - \text{lk}(g) \mid t] \leq \frac{1}{\sqrt{t}}$.

Lemma 6.1.2 shows that the probability that less than $\frac{m(n-m)}{6n}$ of the pairs are interleaved and between separate components is $O\left(\frac{n^3}{m^2(n-m)^2}\right)$. So,

$$(6.19) \quad P[\text{lk}(g') = v] \leq \sqrt{\frac{6n}{m(n-m)}} + O\left(\frac{n^3}{m^2(n-m)^2}\right).$$

□

COROLLARY 6.1.4. *Let g be a random $n \times n$ grid diagram of a 2-component link with components of size m and $n - m$ where, for a given j , rows $2j - 1$ and $2j$ are of differing components, not interleaved, and share no columns, and let $v \in \mathbb{Z}$. Then*

$$(6.20) \quad P[\text{lk}(g) = v] = O\left(n^{5/2}m^{-3/2}(n-m)^{-3/2} + n^5m^{-3}(n-m)^{-3}\right).$$

PROOF. Let A be the set of grids representing 2-component links with components of sizes m and $n - m$. Let B be the set of all grids in A with linking number v . Let C be the set of all grids in A where rows $2j - 1$ and $2j$ satisfy the conditions stated. Then, the probability we wish to bound is equivalent to $|B \cap C|/|C|$. If we note that the bound provided by Theorem 6.1.3 is for $\frac{|B|}{|A|}$, then we can say

$$(6.21) \quad \frac{|B \cap C|}{|C|} \leq \frac{|B|}{|C|} = \frac{|B|}{|A|} \cdot \frac{|A|}{|C|} \leq \left(\sqrt{\frac{6n}{m(n-m)}} + O\left(\frac{n^3}{m^2(n-m)^2}\right) \right) \cdot \frac{|A|}{|C|}.$$

It has already been shown (in the proof of Lemma 6.1.2) that $|A| = \frac{n!n!}{m(n-m)}$. There is a bijection between grids in A where rows $2j - 1$ and $2j$ are interleaved and grids where those rows are not interleaved and do not share a column. This bijection can be constructed by swapping the location of the O's in rows $2j$ and $2j - 1$. Therefore, Lemma 6.1.1 gives $|C| = \frac{n!(n-2)!}{3}$. So

$$(6.22) \quad \frac{|B \cap C|}{|C|} \leq \left(\sqrt{\frac{6n}{m(n-m)}} + O\left(\frac{n^3}{m^2(n-m)^2}\right) \right) \cdot \frac{3n!n!}{m(n-m)n!(n-2)!}$$

$$(6.23) \quad = O\left(n^{5/2}m^{-3/2}(n-m)^{-3/2} + n^5m^{-3}(n-m)^{-3}\right).$$

□

We note that the bounds given depend on m . It will be helpful to bound m both above and below by linear expressions of n , i.e. we want $m = \Theta(n)$ (Section 2.2). With $m = \Theta(n)$, we can treat all terms of m or $n - m$ as though they are some constant multiple of n in the limit. The following lemma shows that most of the 2-component grid diagrams that we will get from our smoothings will have $n/4 \leq m \leq 3n/4$, i.e. $m = \Theta(n)$,

LEMMA 6.1.5. *Let g be a random $n \times n$ grid representing a knot, and let $D \leq n/2$ be an integer. If rows $2i - 1$ and $2i$ are interleaved, then let m_i be the size of the component in row $2i - 1$ after swapping the O's in these rows, and let $m_i = 0$ if they are not interleaved. Then, the following event holds with probability at most $O(D^{-1} + n^{-1})$:*

$$(6.24) \quad Z = |\{i \in \{1, 2, \dots, D\} \mid n/4 \leq m_i \leq 3n/4\}| < D/12$$

PROOF. Assume rows $2i - 1$ and $2i$ of g are interleaved. By Lemma 6.1.1 this is true with probability $\frac{n!(n-2)!(n-3)}{3n!(n-1)!} = \frac{n-3}{3(n-1)}$. If we place X's and O's as in the proof of Lemma 6.1.1 to complete the knot, then m_i will be 1 plus the number of X's placed when the X is placed in the same column as the O in row $2i$. There are $n - 3$ possible points at which this selection can be made, each with equal probability. So each value $m_i = 2, \dots, n - 2$ has probability $\frac{1}{n-3}$.

Let $Z_i = 1$ if $m_i \in [n/4, 3n/4]$ and 0 otherwise, thus $Z = \sum_{i=1}^D Z_i$. The interval $[n/4, 3n/4]$ contains between $(n - 1)/2$ and $(n + 2)/2$ integers. So

$$(6.25) \quad \frac{1}{6} = \frac{n-3}{3(n-1)} \cdot \frac{(n-1)}{2(n-3)} \leq E[Z_i].$$

Which means that $\frac{D}{6} \leq E[Z]$. Note that for any random variable Z_i which only takes the values 1 or 0, we get

$$(6.26) \quad V[Z_i] = E[Z_i^2] - E[Z_i]^2 = E[Z_i] - E[Z_i]^2 \leq \frac{1}{4}.$$

Now consider $E[Z_i Z_j]$, which is equal to the probability that both m_i and m_j fall in the interval $[n/4, 3n/4]$. Suppose rows $2i - 1$ and $2i$ are interleaved, rows $2j - 1$ and $2j$ are interleaved, and that they share no column. As shown in the proof of Lemma 6.1.2, we may overestimate the number of ways to interleave both pairs of rows by $\frac{n!n!}{9(n-4)!(n-4)!}$ and that the proportion of these selections of rows where there are multiple entries in one column is $O(n^{-1})$. There are $(n - 4)!(n - 5)!$ ways to complete the knot, so the probability of getting a knot where the desired rows are both interleaved

is bounded above by

$$(6.27) \quad \frac{n!n!(n-4)!(n-5)!}{9(n-4)!(n-4)!n!(n-1)!} = \frac{n}{9(n-4)}$$

for which a proportion of $O(n^{-1})$ have columns with entries in two of rows $2i-1$, $2i$, $2j-1$, and $2j$.

Now we assume rows $2i-1$ and $2i$ are interleaved, rows $2j-1$ and $2j$ are interleaved, and that their entries share no column. We need the probability that a grid with these rows will have $m_i, m_j \in [n/4, 3n/4]$. We will constructively explore this probability. Starting with the column of the X in row $2i-1$ we will place O's and X's as in previous proofs. There will be $n-4$ X's placed in this fashion, the last of which must connect to the O in row $2i-1$. This means that there are $n-5$ points at which the X may be placed that will connect to the O in row $2i$. If this selection is made in the t_i th position, then m_i will be t_i+1 , t_i+2 , or t_i+3 , depending on whether rows $2j-1$ and/or $2j$ were connected before or after this X is placed. This means we can guarantee that m_i is in the interval $[n/4, 3n/4]$ if $t_i \in [n/4-1, 3n/4-3]$ which contains between $(n-5)/2$ and $(n-2)/2$ integers.

Now choose $t_{j_1}, t_{j_2} \in \{1, 2, \dots, n-6\}$ to be locations within the remaining $n-6$ choices for the X's. Here t_{j_1} will be the position of the X that connects to row $2j-1$ and t_{j_2} will be the position of the X that connects to row $2j$. The distance $t_{j_1} - t_{j_2} \pmod{n-6}$ will be a value between m_j-1 and m_j-4 . Note that all values $t_{j_1} - t_{j_2} \pmod{n-6} \in \{1, 2, \dots, n-7\}$ are equally likely. Now we want $t_{j_1} - t_{j_2} \pmod{n-6} \in [n/4-1, 3n/4-4]$ which contains between $(n-7)/2$ and $(n-4)/2$ integers.

So we have

$$(6.28) \quad E[Z_i Z_j] \leq \frac{n}{9(n-4)} \cdot \left(\frac{n-2}{2(n-5)} \cdot \frac{n-4}{2(n-7)} + O(n^{-1}) \right)$$

$$(6.29) \quad = \frac{n(n-2)}{36(n-5)(n-7)} + O(n^{-1}),$$

then we get

$$(6.30) \quad \text{Cov}[Z_i, Z_j] \leq \frac{n(n-2)}{36(n-5)(n-7)} + O(n^{-1}) - \left(\frac{1}{6} \right)^2$$

$$(6.31) \quad = O(n^{-1}).$$

This leads us to

$$(6.32) \quad V[Z] \leq \frac{D}{4} + D^2 \cdot O(n^{-1})$$

So by Chebyshev's inequality,

$$(6.33) \quad P \left[Z \leq \frac{D}{12} \right] \leq P \left[Z \leq \frac{E[Z]}{2} \right] \leq \frac{4V[Z]}{E[Z]^2}$$

$$(6.34) \quad \leq \frac{4 \left(\frac{D}{4} + D^2 \cdot O(n^{-1}) \right)}{D^2/36}$$

$$(6.35) \quad = O(D^{-1} + n^{-1})$$

□

Let g_i denote the link that results from swapping the O's in rows $2i$ and $2i - 1$ of a 1-component grid diagram, g (the operation from Figure 6.1 (b) to (c)). Then g_i is the 2-component link represented on the right-hand side of Equation (6.1). In order to prove Theorem 6.0.1, we will show that $|\text{lk}(g_i)|$ is “large” with a certain amount of consistency.

LEMMA 6.1.6. *Let g be grid diagram selected uniformly from $\mathcal{G}_{n,1}$ and let $d \leq n/16$. Then the probability that less than d pairs of rows $2i - 1, 2i$ for $1 \leq i \leq 8d$ are interleaved with $|\text{lk}(g_i)| \geq 2d^2$ is $O(d^{-1} + d^2n^{-1/2} + n^{-1})$.*

PROOF. We assume that at least $2d$ of these pairs of rows are interleaved with components of g_i between size $n/4$ and $3n/4$. By Lemma 6.1.5, with $8d = D$, the probability that this is not the case is $O(d^{-1} + n^{-1})$. Now, from Corollary 6.1.4, we see that when $m \in [n/4, 3n/4]$, the probability of g_i having any given linking number given component sizes m and $n - m$ is bounded by

$$(6.36) \quad O \left(n^{5/2} m^{-3/2} (n - m)^{-3/2} + n^5 m^{-3} (n - m)^{-3} \right) = O \left(n^{5/2} n^{-3/2} n^{-3/2} + n^5 n^{-3} n^{-3} \right)$$

$$(6.37) \quad = O(n^{-1/2})$$

Therefore, $P [|\text{lk}(g_i)| < 2d^2] \leq 4d^2 P [|\text{lk}(g_i)| = v] = O(d^2 n^{-1/2})$. Now by Markov's inequality [Ros14], the probability that more than d of these $2d$ links have linking number less than $2d^2$ is bounded above by $2O(d^2 n^{-1/2}) = O(d^2 n^{-1/2})$. So by taking the union bound with $O(d^{-1} + n^{-1})$, we get the desired result. □

Now we may put it all together to prove the main result:

PROOF OF THEOREM 6.0.1. Let g be a grid diagram selected uniformly at random from $\mathcal{G}_{n,1}$ and let $d = \sqrt[5]{n}$. Note that $\sqrt[5]{n} \leq n/16$ for sufficiently large n , so d satisfies the hypothesis of Lemma 6.1.6. Denote an exchange between rows $2i - 1$ and $2i$ by σ_i . We modify g by taking a random subset exchanges picked uniformly from all 2^{8d} subsets of $\{\sigma_i\}_{i=1}^{8d}$. The resulting grid, denoted g'' , will also be uniformly random in $\mathcal{G}_{n,1}$.

Consider an exchange σ_i “big” if rows $2i - 1$ and $2i$ are interleaved and $|\text{lk}(g_i)| \geq 2d^2$. By Lemma 6.1.6, we will only have less than d big swaps with probability bounded by $O(d^{-1} + d^2 n^{-1/2} + n^{-1}) = O(n^{-1/10})$. So, we assume that there are at least d big swaps.

Let g' be the intermediate grid diagram obtained by performing the selected “non-big” exchanges on g . Denote the result of swapping the O’s in row $2i - 1$ and $2i$ of g' by g'_i if these rows are interleaved. Each interleaved exchange performs a crossing change which will change the linking number of any other swap by ± 1 or 0 . So we can see that $2d^2 - 7d \leq |\text{lk}(g_i)| - 7d \leq |\text{lk}(g'_i)|$ for the big swaps. When $7 \leq d$, we get $d^2 \leq |\text{lk}(g'_i)|$.

By iterating on the skein relation, $c_2 \left(\begin{array}{c} \nearrow \searrow \\ \nwarrow \nearrow \end{array} \right) - c_2 \left(\begin{array}{c} \nwarrow \nearrow \\ \nearrow \searrow \end{array} \right) = \text{lk} \left(\begin{array}{c} \nearrow \searrow \\ \nearrow \searrow \end{array} \right)$, we get

$$(6.38) \quad c_2(g'') = c_2(g') + \sum_{i=1}^d X_i \varepsilon(g', \sigma_i) \text{lk}(g'_i) + \sum_{1 \leq i < j \leq d} X_i X_j \delta(g', \tau_i, \tau_j)$$

where $X_i = 1$ if swap i was chosen, and 0 otherwise, $\varepsilon(g', \sigma_i) = \pm 1$ depending on if the exchange changes a crossing from $\begin{array}{c} \nearrow \searrow \\ \nwarrow \nearrow \end{array}$ to $\begin{array}{c} \nwarrow \nearrow \\ \nearrow \searrow \end{array}$ or vice versa, and $\delta(g', \tau_i, \tau_j) \leq 1$ is a correction term for the effect that each exchange has on the linking numbers associated to the subsequent exchanges. Applying Theorem 6.0.2 to the first sum shows that that it falls in any interval $(v - d^2/2, v + d^2/2)$ with probability smaller than $\frac{1}{\sqrt{d}}$. The magnitude of the second sum is bounded above by $d^2/2$, so v is still attained with probability at most $\frac{1}{\sqrt{d}}$. Then the probability that $c_2(g'')$ attains a value of v is

$$(6.39) \quad P[c_2(g'') = v] = O(d^{-1/2}) + O(n^{-1/10}) = O(n^{-1/10})$$

□

This means that $P_n(K) = O(n^{-1/10})$ for any knot type K , i.e. Theorem 2.5.5 is a corollary to Theorem 6.0.1. In terms of enumeration, this is equivalent to $|\mathcal{G}_n(K)| = O(n!(n-1)!n^{-1/10})$. In all other proven forms of the FWD conjecture, with exception to petal diagrams, knotting probability has been shown to converge to 1 at an exponential rate, i.e. $P_n(0_1) = O(a^{-n})$ for some

$a > 1$ [SW88, DPS94, Dia95, Cha17]. Knotting probability in the petal model is conjectured to also converge exponentially [EZHLN18]. We conjecture here, based on numerical evidence in Section 7.3.1, that $P_n(K) = O(a^{-n})$ for grid diagrams as well.

Random Grid Diagrams

There are several ways to generate random grid diagrams. Each has its benefits and drawbacks.

7.1. Uniformly Random $n \times n$ Grid Diagrams

The proofs of Theorems 5.1.1 and 5.1.2 provide constructive ways to generate elements of \mathcal{G}_n and $\mathcal{G}_{n,1}$ uniformly at random. Likewise, the proofs of Theorems 5.1.3 and 5.1.4 provide a couple ways to generate elements of $\mathcal{G}_{n,c}$. Following the proof of Theorem 5.1.3 will not quite generate elements uniformly, but Theorem 5.1.4 tells us that selecting derangements with c cycles to select the O's will provide a uniformly random element of $\mathcal{G}_{n,c}$.

This is useful if we want to numerically understand some behavior of grids in general, such as how the length of the chain inside the grid varies with the size of the grid. One can simply generate a large ensemble of $n \times n$ grid diagrams uniformly at random and measure the desired quantity and analyze the statistics of those measurements, i.e. a Monte Carlo simulation.

Of particular interest is that this method can theoretically be used to obtain numerical data to estimate the rate at which $P_n(K) \rightarrow 0$ (Theorem 2.5.5). Specifically, one can uniformly generate a large number of grid diagrams from $\mathcal{G}_{n,1}$, then identify the knot types and calculate the proportion of the samples which are of that knot type as an estimate of $\frac{|\mathcal{G}_n(K)|}{n!(n-1)!}$, and consequently $|\mathcal{G}_n(K)|$. Repeating this for larger and larger n gives a sense of the trend of $P_n(K)$.

This proves to be inefficient, as computing the link type of a diagram is NP in the crossing number [HLP99]. In particular, knot polynomials (Section 2.3.6.3) are a common way to identify knots and links, but the computational complexity of calculating them via skein relations is exponential in the crossing number. Also, since $P_n(K) \rightarrow 0$ as $n \rightarrow \infty$, each knot type grows exceedingly rare as grid size increases, which means the number of samples required to see even one grid diagram of a particular knot type will grow prohibitively large. Based on a simple preliminary simulation of this type, such sampling appears to become computationally infeasible at around $n = 20$. For comparison, in the time that over 10^6 samples were obtained and identified for $n = 15$, only 378 samples were identified at $n = 20$. In general this type of Monte Carlo simulation is useful

when considering easily calculated properties for grid diagrams of all knot or link types, but is not scalable for examining specific knot types.

7.2. Markov Chain Algorithms for Grid Diagrams

This section will lay out the groundwork for two Markov chain algorithms for grid diagrams. The first is an algorithm designed to sample from a canonical-like distribution of grid diagrams with fixed knot type. The second is an implementation of the Wang-Landau algorithm applied to grid diagrams. As we will see, the Wang-Landau algorithm is generally more useful for examining the questions laid out in the introduction.

To start, let's clearly define the states and transitions of the chain. The state space will be some $\Omega \subseteq \mathcal{G}(L)$ for a link type L . The transitions will be defined by the Cromwell moves: stabilization, destabilization, and commutation. Since cyclic permutations can be constructed by a composition of the other moves, they may be omitted from the list of transitions. See Section 7.2.3 for a discussion about the pros and cons of including cyclic permutations. Also of note, we will use general stabilizations and destabilizations as opposed to traditional stabilizations and destabilizations. Discussion of this decision can be found in Section 7.2.4

Both of the algorithms presented here are Metropolis-Hastings Markov chains (Section 2.4.2), i.e. the transitions are chosen and then accepted or rejected with some probability. So, we need a method to choose the transitions before they are accepted or rejected. Both the Wang-Landau and canonical-like algorithms will choose the transitions in the same way but will use different values for the acceptance probability, P_{accept} .

ALGORITHM 7.2.1 (General Grid Diagram Markov Chain).

- (1) *Let g be the current grid diagram of link type L .*
- (2) *Choose, uniformly at random, the type of move: stabilization, destabilization, or commutation.*
 - (a) *If the chosen move is a stabilization,*
 - (i) *choose a row or column uniformly at random.*
 - (ii) *Then choose a grid line perpendicular to the chosen row/column.*
 - (iii) *Finally, choose if the topmost/leftmost inserted vertex will be an X or an O .*
 - (iv) *The stabilization is defined by adding in vertices in the order chosen in the chosen row/column at the chosen grid line.*

- (b) *If the chosen move is a destabilization,*
 - (i) *choose a row or column uniformly at random.*
 - (ii) *If the two entries in that row or column are adjacent, then the destabilization is defined by removing those two entries. Otherwise it is an invalid move.*
- (c) *If the chosen move is a commutation,*
 - (i) *choose a row or column uniformly at random.*
 - (ii) *The commutation is defined by exchanging that row or column with the next one, cyclically, to the right or below it. If the two rows/columns are interleaved, then this is an invalid move.*
- (3) *If the chosen move is valid, then let g' be the grid obtained by performing the chosen move.*
- (4) *With probability $P_{\text{accept}}(g \rightarrow g')$, transition to g' . Otherwise stay in state g (with probability $1 - P_{\text{accept}}(g \rightarrow g')$).*

Note that, by Theorem 2.3.4, Algorithm 7.2.1 is necessarily ergodic if $\Omega = \mathcal{G}(L)$. Also, by Theorem 2.3.5, Algorithm 7.2.1 remains ergodic for $L = 0_1$ if $\Omega = \bigcup_{n=2}^M \mathcal{G}_n(0_1)$ for any $M > 2$, i.e. the set of all grid diagrams of the unknot with grid size $\leq M$. This second case does not necessarily hold for other knots and links.

To complete the algorithm, a distribution π must be chosen and corresponding acceptance probabilities that satisfy detailed balance must be selected. Recall (from Section 2.4) that the detailed balance equation for a Metropolis-Hastings Markov chain is,

$$(7.1) \quad \pi(g)P_{\text{choose}}(g \rightarrow g')P_{\text{accept}}(g \rightarrow g') = \pi(g')P_{\text{choose}}(g' \rightarrow g)P_{\text{accept}}(g' \rightarrow g)$$

where $P_{\text{choose}}(g \rightarrow g')$ is the probability of choosing *any* transition from state g to g' . Assuming there is a transition between g and g' , it will be helpful to rewrite this as

$$(7.2) \quad \frac{P_{\text{accept}}(g \rightarrow g')}{P_{\text{accept}}(g' \rightarrow g)} = \frac{\pi(g')}{\pi(g)} \cdot \frac{P_{\text{choose}}(g' \rightarrow g)}{P_{\text{choose}}(g \rightarrow g')}.$$

If there is only one transition from g to g' , then $P_{\text{choose}}(g \rightarrow g')$ can be replaced with the probability of choosing that specific transition. However, grids often have multiple possible transitions between them. As an extreme case, consider the “stair” unknots described in the proof of Lemma 5.1.6. Using the general stabilizations and destabilizations as chosen in Algorithm 1, there are $2n$

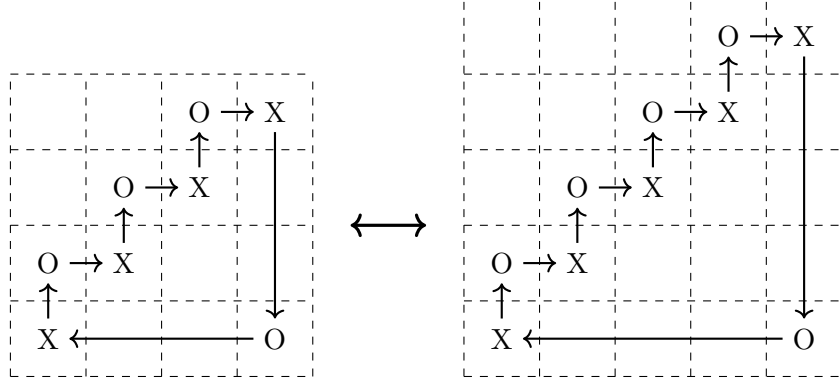


FIGURE 7.1. $n \times n$ and $(n+1) \times (n+1)$ stair unknots. The number of stabilizations and destabilizations between them depends on the precise way stabilizations and destabilizations are defined.

stabilizations and $2n$ destabilizations that will transition between an $n \times n$ stair unknot and an $(n+1) \times (n+1)$ stair unknot (figure 7.1).

This is particularly important to note when solving for the P_{accept} values from detailed balance. In particular, the ratio $\frac{P_{\text{choose}}(g' \rightarrow g)}{P_{\text{choose}}(g \rightarrow g')}$ should be computable without too many details about g and g' (to keep the time complexity of calculating P_{accept} at $O(1)$). Ideally, the number of transitions from g to g' are always in one-to-one correspondence with transitions from g' to g as they are in the previous stair unknot example.

For an example of how this may fail to occur, consider choosing destabilizations by choosing a vertex instead of a row or column. The vertex would then be able to be destabilized if it is adjacent to another vertex. In the case of the stair unknots, there would now be $2(n+1) - 1$ destabilizations from the size $n+1$ stair knot to the size n stair knot, as compared to $2n$ stabilizations in the other direction. So, it seems there is a 1-to- $\frac{2(n+1)-1}{2n}$ correspondence of stabilizations and destabilizations, but this is only in the specific case of stair unknots. To contrast, there would be a 1-to-2 correspondence between the grids in Figure 2.9 ($n = 4$). Thus, this hypothetical move selection would require all possible transitions between two grids to be calculated every time a stabilization or destabilization is selected just to calculate P_{accept} .

To address this, the following theorem shows that the way stabilizations and destabilizations are chosen in Algorithm 7.2.1 is a 1-to-1 correspondence.

THEOREM 7.2.2. *Consider two grid diagrams g and g' such that g' can be obtained by a general stabilization of g . The number of general stabilizations transforming g into g' is equal to the number of general destabilizations transforming g' to g , as selected in step 2 of Algorithm 7.2.1.*

PROOF. Without loss of generality, we will consider general stabilizations that insert a vertically adjacent X/O pair by selecting a row and a vertical grid line. Each statement has an analogous statement by swapping the words row and column, as well as horizontal and vertical. Let $\{\sigma_i\}_{i=1}^m$ be the set of general stabilizations that transform g into g' . Specifically, let σ_i be the stabilization that inserts an X/O pair into row r_i at the vertical grid line c_i . This means that there is a possible destabilization in g' at column c_i . Let this destabilization be σ_i^{-1} . Now we want to show that the map $\sigma_i \rightarrow \sigma_i^{-1}$ is a bijection of stabilizations and destabilizations between g and g' .

Let $\sigma_i^{-1} = \sigma_j^{-1}$. Since σ_i^{-1} is defined to be the destabilization of column c_i , then $\sigma_i^{-1} = \sigma_j^{-1}$ implies $c_i = c_j$. This means that σ_i and σ_j must both insert at vertical grid line c_i . Now, assume the row of insertion of σ_i is different from that of σ_j , i.e. $r_i \neq r_j$. Then the result of stabilization σ_i has entries in column c_i and rows r_i and r_{i+1} . However, the result of stabilization σ_j will have entries in column $c_j = c_i$ and rows r_j and r_{j+1} . This means that the resulting column c_i will have entries in different rows after each of these stabilizations, hence the grid diagrams resulting from each of these stabilizations will be distinct. This is a contradiction, hence $\sigma_i = \sigma_j$, and the mapping $\sigma_i \rightarrow \sigma_i^{-1}$ is injective.

Now we wish to show that $\{\sigma_i^{-1}\}_{i=1}^m$ represents all possible general destabilizations which transform g' into g . Let σ' be a general destabilization of column c in g' transforming it into g . Then let r and $r + 1$ be the rows that contain the entries in column c . Then, for some i , there is a stabilization σ_i in row $r_i = r$ and vertical grid line $c_i = c$ that will transform g into g' . Hence $\sigma' = \sigma_i^{-1}$, i.e. the mapping $\sigma_i \rightarrow \sigma_i^{-1}$ is surjective. Thus $\sigma_i \rightarrow \sigma_i^{-1}$ is a bijection, and there are the same number of general stabilizations from g to g' as general destabilizations from g' to g . \square

It is important that we don't overlook this same consideration for commutations.

THEOREM 7.2.3. *Given two $n \times n$ grids g and g' , the number of commutations that transform g into g' is equal to the number of commutations that transform g' into g .*

PROOF. Denote a row commutation between rows i and $i + 1 \pmod{n}$ of g by σ_i and a commutation of the same rows of g' by σ'_i . Note that if σ_i transforms g into g' , then σ'_i transforms g' into g . The mapping $\sigma_i \rightarrow \sigma'_i$ is a bijection between row commutations transforming g into g' and row commutations transforming g' into g . An equivalent mapping can be made for column commutations. \square

So, we have a one-to-one correspondence of transitions between all pairs of grid diagrams g and g' in $\mathcal{G}(L)$. Since P_{choose} is determined entirely from Algorithm 7.2.1, we can rewrite Equation (7.2) in more precise terms. First, assuming the current state has grid size n , then the probability of choosing a specific

- stabilization is $\frac{1}{3} \cdot \frac{1}{2n} \cdot \frac{1}{n+1} \cdot \frac{1}{2} = \frac{1}{12n(n+1)}$,
- destabilization is $\frac{1}{3} \cdot \frac{1}{2n} = \frac{1}{6n}$, and
- commutation is $\frac{1}{3} \cdot \frac{1}{2n} = \frac{1}{6n}$.

Now let m be the number of transitions from g to g' . If $m = 0$, then detailed balance is satisfied, as it will reduce to $0 = 0$. If $m > 0$, then we know there are also m transitions from g' to g , per Theorems 7.2.2 and 7.2.3. So, if the transition from g to g' is a commutation with $|g| = |g'| = n$, then Equation (7.2) becomes

$$(7.3) \quad \frac{P_{\text{accept}}(g \rightarrow g')}{P_{\text{accept}}(g' \rightarrow g)} = \frac{\pi(g')}{\pi(g)} \cdot \frac{6nm}{6nm}$$

$$(7.4) \quad = \frac{\pi(g')}{\pi(g)}.$$

If $g \rightarrow g'$ is a stabilization with $|g| = n$, then we get

$$(7.5) \quad \frac{P_{\text{accept}}(g \rightarrow g')}{P_{\text{accept}}(g' \rightarrow g)} = \frac{\pi(g')}{\pi(g)} \cdot \frac{12n(n+1)m}{6(n+1)m}$$

$$(7.6) \quad = \frac{\pi(g')}{\pi(g)} \cdot 2n.$$

Finally, if $g \rightarrow g'$ is a destabilization with $|g| = n$, we get

$$(7.7) \quad \frac{P_{\text{accept}}(g \rightarrow g')}{P_{\text{accept}}(g' \rightarrow g)} = \frac{\pi(g')}{\pi(g)} \cdot \frac{6nm}{12(n-1)nm}$$

$$(7.8) \quad = \frac{\pi(g')}{\pi(g)} \cdot \frac{1}{2(n-1)}.$$

So with $|g| = n$, we use

$$(7.9) \quad P_{\text{accept}}(g \rightarrow g') = \min \left\{ 1, \frac{\pi(g')}{\pi(g)} \right\}$$

for commutations,

$$(7.10) \quad P_{\text{accept}}(g \rightarrow g') = \min \left\{ 1, \frac{\pi(g')}{\pi(g)} \cdot 2n \right\}$$

for stabilizations, and

$$(7.11) \quad P_{\text{accept}}(g \rightarrow g') = \min \left\{ 1, \frac{\pi(g')}{\pi(g)} \cdot \frac{1}{2(n-1)} \right\}$$

for destabilizations.

7.2.1. A Markov Chain Algorithm with a Canonical-Like Posterior Distribution.

We need only to choose a valid posterior distribution π , and we may use Algorithm 7.2.1 with the acceptance probabilities as calculated from equations (7.9), (7.10), and (7.11). This version of the algorithm may be used for Monte Carlo sampling and uses a distribution based on the canonical distribution, popular in physics. This decision was made to imitate the distribution of the BFACF algorithm (Section 2.4.4). Specifically, use

$$(7.12) \quad \pi(g) = \frac{z^{|g|}}{\Xi(z)|g|!(|g|-1)!}$$

with

$$(7.13) \quad \Xi(z) = \sum_{n=0}^{\infty} \frac{z^n |\mathcal{G}_n(K)|}{n!(n-1)!}.$$

Let $P_{\text{accept}}(+0)$, $P_{\text{accept}}(-1)$, and $P_{\text{accept}}(+1)$ be the probabilities of accepting a commutation, destabilization, or stabilization, respectively. If the current state is an $n \times n$ grid diagram, then combining the distribution in Equation 7.12 with Equations (7.9), (7.11), and (7.10), we get

$$(7.14) \quad P_{\text{accept}}(+0) = 1$$

$$(7.15) \quad P_{\text{accept}}(-1) = \min \left\{ 1, \frac{2z}{n+1} \right\}$$

$$(7.16) \quad P_{\text{accept}}(+1) = \min \left\{ 1, \frac{z^{-1}n}{2} \right\}$$

This is only valid if $\Xi(z)$ converges.

PROPOSITION 7.2.4. *If $0 < z < 1$, then $\Xi(z)$ converges.*

PROOF. Apply the root test to the series combined with the fact that $\frac{|\mathcal{G}_n(K)|}{n!(n-1)!} \leq 1$:

$$(7.17) \quad \lim_{n \rightarrow \infty} \left| \frac{z^n |\mathcal{G}_n(K)|}{n!(n-1)!} \right| \leq \lim_{n \rightarrow \infty} (z^n)^{1/n} = z.$$

This means $\Xi(z)$ converges when $z < 1$. □

It is unclear whether or not $\Xi(z)$ converges for any values $z \geq 1$. This depends entirely on the behavior of $\frac{|\mathcal{G}_n(K)|}{n!(n-1)!} = P_n(K)$. From Theorem 6.0.1, we can say that $P_n(K) \leq Cn^{-1/10}$ in the limit, but this doesn't change the ultimate rate of convergence of $\Xi(z)$. For $\Xi(z)$ to converge for $z > 1$, then we must have $P_n(K) = O(a^n)$ for some a , in which case $\Xi(z)$ will converge for $z < a^{-1}$. Preliminary runs seem to indicate that this algorithm converges for z values larger than 1, which is the first indicator that $P_n(K) = O(a^n)$. On the other hand, if $P_n(K)$ decays sufficiently faster than exponential, i.e. $(P_n(K))^{1/n} \rightarrow 0$, then $\Xi(z)$ will converge for $z \in (0, \infty)$. The estimated decay of $P_n(K)$ is examined in Section 7.3.1 using the Wang-Landau algorithm as described in Section 7.2.2, and is found to likely be exponential or faster.

7.2.2. Wang-Landau and Grid Diagrams. Recall from Section 2.4.3 that the posterior distribution π of a Wang-Landau algorithm is defined by weights W_{E_i} meant to estimate the density of some energy function. In particular, if $E(g)$ is some energy function defined for a grid diagram g , then $\frac{\pi(g)}{\pi(g')} \approx \frac{W_{E(g')}}{W_{E(g)}}$. So Algorithm 7.2.1 can be run as a Wang-Landau algorithm with acceptance probabilities derived from Equations (7.9), (7.10), and (7.11). Namely, if a transition $g \rightarrow g'$ is a commutation, then

$$(7.18) \quad P_{\text{accept}}(g \rightarrow g') = \min \left\{ 1, \frac{W_{E(g)}}{W_{E(g')}} \right\}.$$

If $g \rightarrow g'$ is a stabilization,

$$(7.19) \quad P_{\text{accept}}(g \rightarrow g') = \min \left\{ 1, \frac{W_{E(g)}}{W_{E(g')}} \cdot 2|g| \right\}.$$

Finally, if $g \rightarrow g'$ is a destabilization,

$$(7.20) \quad P_{\text{accept}}(g \rightarrow g') = \min \left\{ 1, \frac{W_{E(g)}}{W_{E(g')}} \cdot \frac{1}{2(|g| - 1)} \right\}.$$

It would seem that the only remaining step is to choose an appropriate energy function E . However, the specific state space needs to be addressed. If we let $\Omega = \mathcal{G}(K)$, then we have infinitely many states to explore, and grid size will tend to grow without bound. So, instead we use $\Omega = \bigcup_{n=2}^M \mathcal{G}_n(K)$ for some $M > 2$. As previously mentioned, the Markov chain with this state space is ergodic if $K = 0_1$, but this is not necessarily the case for other knot types. For other knot types, it is sufficient to say that there is an N such that $\bigcup_{n=2}^N \mathcal{G}_n(K) \subset \Omega_0$, where $\Omega_0 \subset \Omega$ is the ergodicity class explored by the algorithm. In this way, the weights can be considered accurate

for $n \leq N$. For $n > N$, the weights may be inaccurate, as not every state can be reached. It is, however, difficult to know what the relationship between N and M is, but the data in Section 7.3.2 seems to imply that for $M = 100$, it is possible that $N \approx 70$ is sufficient.

The only thing that remains is to choose an energy function E . The first obvious candidate is $E(g) = |g|$. Using this means that our Wang-Landau weights will be able to estimate the growth of $|\mathcal{G}_n(K)|$. This means that we can make inferences about $|\mathcal{G}_n(K)|$ directly from the trained Wang-Landau weights. Then, if we want to do Monte Carlo sampling of a particular knot with uniform sampling from within various grid sizes, we can use the Wang-Landau weights to generate these samples.

For exploring questions of writhe, we may choose $E(g) = w(g)$. But then we must consider that these weights will represent all grids of knot type K with size up to M . So if we use the trained weights with $E(g) = w(g)$, then we will be sampling uniformly from classes with constant writhe across all grid sizes. These classes will each be very much non-uniform in the grid sizes represented, leaning very heavily towards the largest grid sizes. This may or may not be very useful, but it does add complications that can be rectified by including grid size in the energy.

That is, we can let $E(g) = (|g|, w(g))$. In this case, using the weights for Monte Carlo sampling will result in sampling every grid size/writhe pair uniformly. This may not be desirable, but if we look at the weights themselves, they will provide a picture of how writhe is distributed across each grid size. If we restrict to just looking at the weights of some grid size n , then we can find a weighted average for the mean writhe of the grid diagrams of that size directly from the Wang-Landau weights (see Section 7.3.2).

7.2.3. Cyclic Permutations in Grid Diagram Markov Chains. Cyclic permutations are notably absent from Algorithm 7.2.1. The reason for this is efficiency. Generally, adding more transitions between distant states of a Markov chain is desirable as it will generally shorten the convergence rate of the Markov chain. Performing more than one cyclic permutation does not likely achieve this, however. Consider the following sequence of Cromwell moves performed on a grid diagram of size 5 or larger:

- (1) Cyclically permute 2 units to the right and 1 unit down.
- (2) Commute columns 3 and 4.
- (3) Cyclically permute 1 unit to the right and 1 unit down.

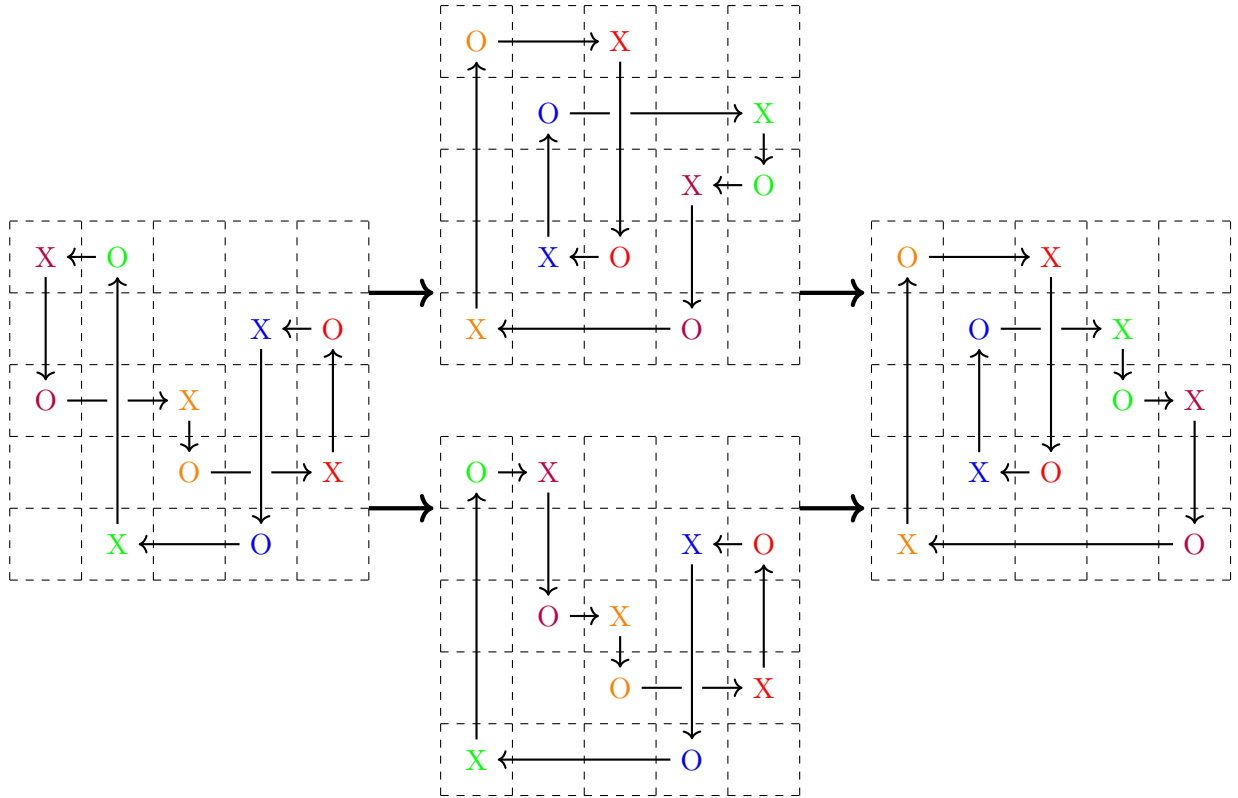


FIGURE 7.2. Following the top path, the grid diagram on the left is cyclically permuted three units to the right and two units down followed by commuting columns 4 and 5. Following the bottom path, columns 1 and 2 are commuted followed by cyclically permuting three units to the right and two units down. Any commutation or column n and $n + 1 \pmod{5}$ in the left grid diagram followed by cyclically permuting three units to the right and two units down is equivalent to performing the cyclic permutation first and then commuting columns $n + 3 \pmod{5}$ and $n + 4 \pmod{5}$. Color added to aid in tracking the transformations.

This is the same as the sequence

- (1) Cyclically permute 3 units to the right and 2 units down.
- (2) Commute columns 4 and 5.

or

- (1) Commute columns 1 and 2.
- (2) Cyclically permute 3 units to the right and 2 units down.

The latter two cases are demonstrated in Figure 7.2. Note that, because the commutation in the first sequence was valid, i.e. the commuted columns are not interleaved, then the commutations in the other sequences must also be valid. In general, cyclic permutations will translate the locations

of other valid Cromwell moves. This can be described as cyclic permutations being in some way commutative with the other Cromwell moves. The notable exception being destabilizations and stabilizations may become valid or invalid if entries in the first and last column (or row) share a row (column).

Suppose we change Algorithm 7.2.1 by giving each Cromwell move, including cyclic permutation, a $1/4$ probability of being chosen. This means that approximately $1/4$ of our moves will be cyclic permutations, but many of these will be essentially redundant, as they could have all been performed at once, then the other Cromwell moves could have been performed, with some possible exceptions for a few stabilizations and destabilizations. So, the effective mixing of this algorithm is not increased by the presence of cyclic permutations. In fact it may be reduced.

The argument here hinges on performing Translations too often. Suppose, instead, we modify Algorithm 7.2.1 so that we choose cyclic permutations with, say, $1/t$ probability and the other three moves with $(1-t)/3$ probability each where t is the number of Markov steps between samples. Then we expect to take approximately 1 cyclic permutation when generating each sample. We are no longer wasting time performing extra unnecessary cyclic permutations, but still gain the benefit of cyclically permuting at least once (which would require multiple other moves to do). This could be beneficial, but has not been tested.

Another consideration is the computational complexity of performing the moves. As implemented, the time complexity of performing a commutation is $O(1)$, while stabilizations and destabilizations are $O(n)$. Translations are also $O(n)$, so performing many of these could potentially slow down real-time performance of the algorithm.

Also, if the Wang-Landau energy includes writhe, then we need to be able to calculate the change in writhe from the current conformation to a proposed next conformation. The time complexity of this, as implemented, for commutations, stabilizations, and destabilizations is $O(1)$ (see Section 5.2). Calculating the writhe change of cyclically permuting a grid by one unit can be calculated in $O(1)$ time by the proof of Lemma 5.2.4. However, attempting to include larger cyclic permutations with this method would require $O(n)$ time to iterate the calculation for each unit that the grid diagram is being shifted.

7.2.4. Stabilizations and Destabilizations in Grid Diagram Markov Chains. For stabilizations and destabilizations, there is the question of whether to use traditional stabilizations and

destabilizations, or to use the generalized versions. The time complexity of the implementations are equivalent at $O(n)$ for each, and calculating writhe changes are $O(1)$ for each. If we note that regular stabilizations are a subset of general stabilizations, then we see that general stabilizations will add transitions between more states.

The question is, does this actually help us traverse the chain faster. In contrast to cyclic permutations, which are essentially commutative with the other operations, performing a stabilization or destabilization will change the grid dramatically enough that it will add or remove other possible Cromwell moves. This would likely help to randomize the conformations faster, i.e. improve convergence of the Markov chain to the posterior distribution. As of now, no direct comparison has been made.

7.3. Numerical Results for Grid Diagrams

7.3.1. Decay of $P_n(K)$. Wang-Landau weights were trained for grid diagrams of prime knots with crossing number at most 9 where energy $E(g) = |g|$. An initial weight modification value was chosen as $\ln(f) = 1$ which was updated according to $\ln(f)/2$ until a final modification value of $\ln(f) = 10^{-5}$ was attained. The grid size for these runs was bounded at 500, so the algorithm was unable to explore grid sizes larger than this. Let W_n be the weight associated to $|g| = n$. In this way, these weights estimate the ratio $\frac{|\mathcal{G}_n(K)|}{|\mathcal{G}_m(K)|} \approx \frac{W_n}{W_m}$.

There are many ways to use these weights to interpret $|\mathcal{G}_n(K)|$. The primary question of $|\mathcal{G}_n(K)|$ is how it grows, i.e. $\frac{|\mathcal{G}_{n+1}(K)|}{|\mathcal{G}_n(K)|}$. However, since $|\mathcal{G}_n(K)|$ is already known to be at least factorial in growth (Theorem 5.1.7) this ratio can be difficult to interpret. Instead, consider

$$(7.21) \quad \frac{P_{n+1}(K)}{P_n(K)} = \frac{n!(n-1)!|\mathcal{G}_{n+1}(K)|}{n!(n+1)!|\mathcal{G}_n(K)|} \approx \frac{W_{n+1}}{n(n+1)W_n}.$$

Plots for these ratios can be found in Figures 7.3, 7.4, and 7.5. The error for $\frac{W_{n+1}}{W_n}$ is calculated using Proportion (2.25). This error is then propagated to the ratio of knotting probabilities by

$$(7.22) \quad \sigma\left(\frac{P_{n+1}(K)}{P_n(K)}\right) = \frac{W_{n+1}}{n(n+1)W_n} \cdot \sigma\left(\ln\left(\frac{W_{n+1}}{W_n}\right)\right) \sim \frac{W_{n+1}}{n(n+1)W_n} \cdot \sqrt{\frac{W_{n+1} \cdot \ln(f)}{W_n}}.$$

It is worth noting that the error in (2.25) is only proportional, and the error bars in the figures are likely much larger than the actual error.

To interpret these results, consider the decay of $P_n(K)$. Theorem 6.0.1 shows that $P_n(K)$ goes to 0 at least as fast as $n^{-1/10}$. However, the decay is likely much faster than this. Consider the

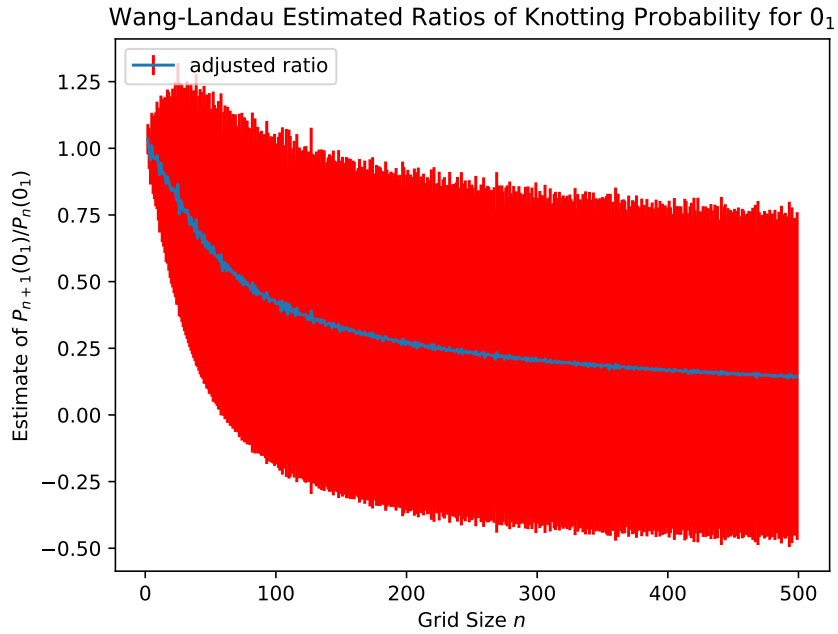


FIGURE 7.3. Ratios of consecutive knotting probabilities for 0_1 . Error bars are propagated by Equation (7.22).

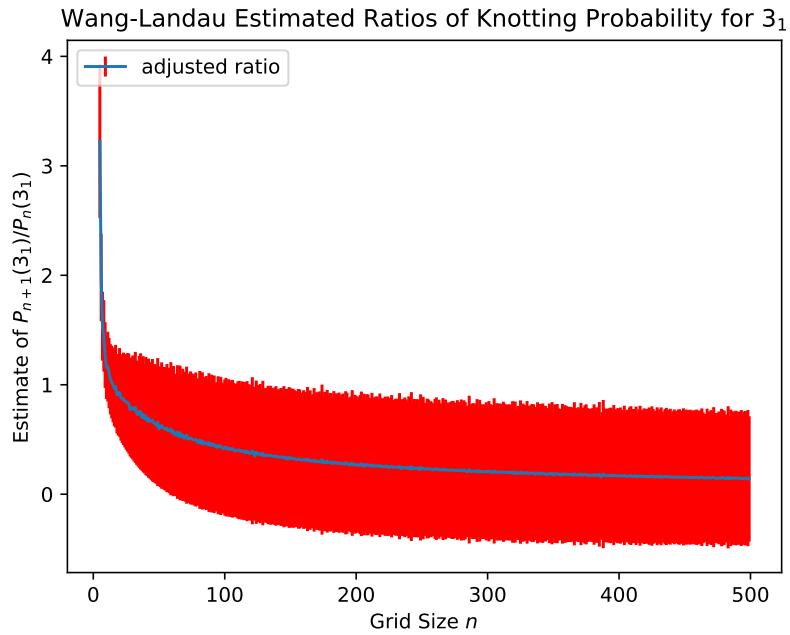


FIGURE 7.4. Ratios of consecutive knotting probabilities for 3_1 . Error bars are propagated by Equation (7.22).

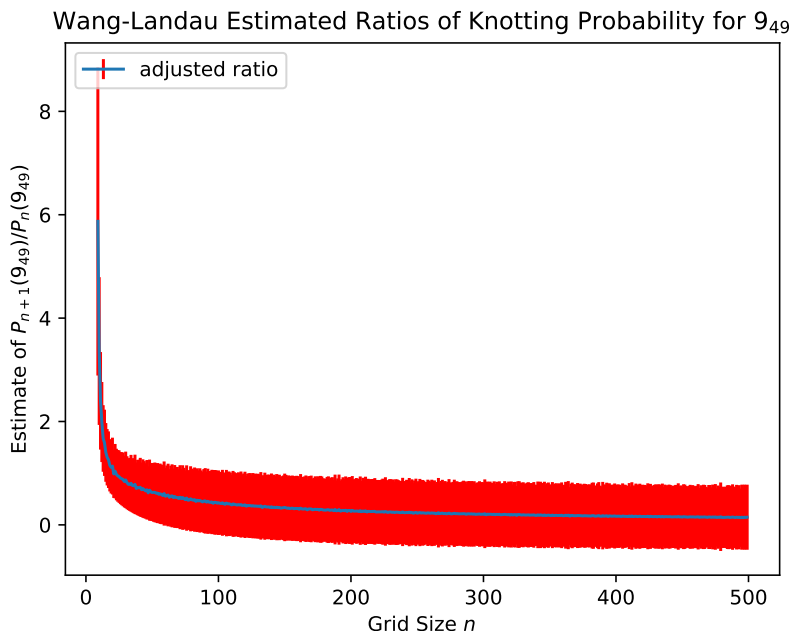


FIGURE 7.5. Ratios of consecutive knotting probabilities for 9_{49} . Error bars are propagated by Equation (7.22).

case where $P_n(K) \rightarrow 0$ exponentially. This would mean that the consecutive ratios $\frac{P_{n+1}(K)}{P_n(K)} \rightarrow \ell$ as $n \rightarrow \infty$ for some $0 < \ell < 1$. From the estimated values of $\frac{P_{n+1}(K)}{P_n(K)}$, this may be the case, as the values go below 1 and continue to decrease.

It is unclear, however, if there is a value ℓ that serves as an asymptote for any of these graphs. It is possible that $\frac{P_{n+1}(K)}{P_n(K)} \rightarrow 0$, in which case $P_n(K)$ decays faster than exponential. In any case, the data is enough to conjecture that the decay is at least exponential.

7.3.2. Mean Writhe. As mentioned in Section 2.5, the original reason that grids were explored in this work was to examine the behavior of writhe in grid diagrams. To this end Wang-Landau weights were trained for grid diagrams of knots with crossing number at most 9 where energy $E(g) = (|g|, w(g))$ with a final modification value of $\ln(f) = 10^{-5}$. The grid size for these runs was bounded at 100, so the algorithm was unable to explore grid sizes larger than this. If $W_{i,j}$ is the Wang-Landau weight associated to the energy $E(g) = (i, j)$, then the weights obtained from these runs can be used to directly estimate the mean writhe of size n grid diagrams of fixed knot type K by

$$(7.23) \quad \frac{\sum_{g \in \mathcal{G}_n(K)} w(g)}{|\mathcal{G}_n(K)|} \approx \frac{\sum_{j \in \mathbb{Z}} W_{n,j} \cdot j}{\sum_{j \in \mathbb{Z}} W_{n,j}}$$

where $W_{n,j} = 0$ if there are no grids of size n with writhe j . The error of this calculation can be measured directly for achiral knots, as the value on the left-hand side of Equation (7.23) is exactly 0 for these knots. For the unknot (Figure 7.6), all mean estimates are within 0.026 of 0. The largest distance from 0 of mean estimates for achiral knots was about 0.306, which occurred at $n = 97$ for the 8_{17} link (Figure 7.7).

For $n < 70$ the errors of each achiral knot are comparable to 0_1 . For n larger than 70, there is a trend for the mean writhes to veer away from 0, as can be seen in Figure 7.7. This is not seen for the unknot, which is likely explained by Theorem 2.3.5, which proves that the Markov chain restricted to $n \leq 100$ remains ergodic for the unknot. For other knots, it is likely that small grid sizes are explored sufficiently, but for grid sizes near the boundary of $n = 100$, the state space may not be sufficient for satisfactory exploration.

A similar pattern is seen in the graphs of the estimated mean writhes of the chiral knots as well. The chiral knots all follow a pattern which varies in a similar way to the achiral knots. For each of the chiral knots, the mean writhe for $20 < n < 70$ varied on an order similar to the unknot, but around a value distinct from 0. For $n > 70$, the mean writhes vary in a way similar to the achiral knots, likely due to error from lack of ergodicity. Figure 7.8 shows the estimated mean writhe for the 9_{47} knot.

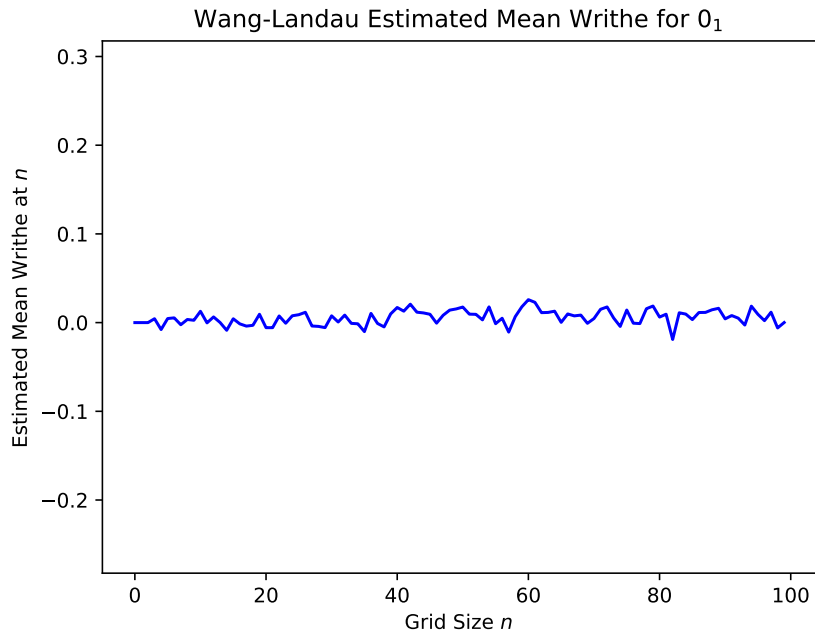


FIGURE 7.6. Estimated mean writhes of size n grid diagrams for 0_1 .

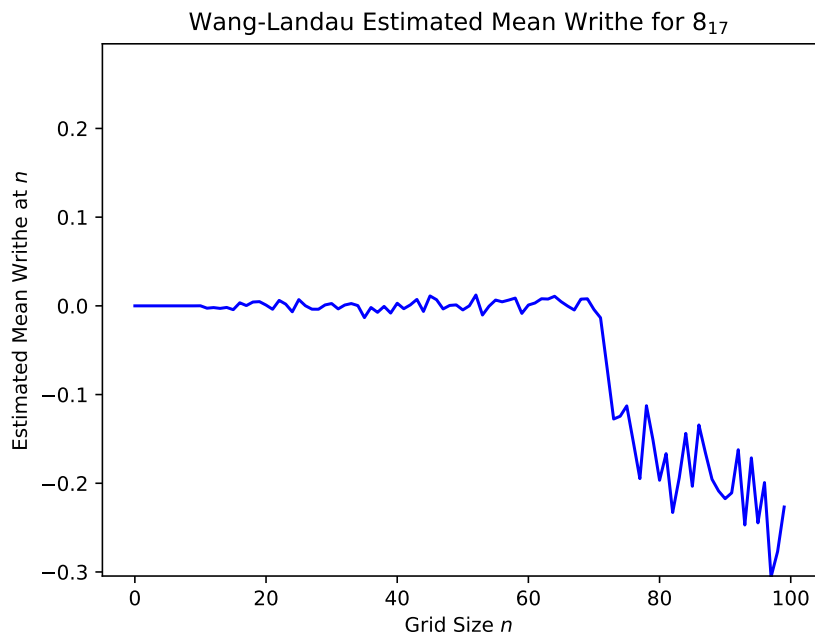


FIGURE 7.7. Estimated mean writhes of size n grid diagrams for 8_{17} .

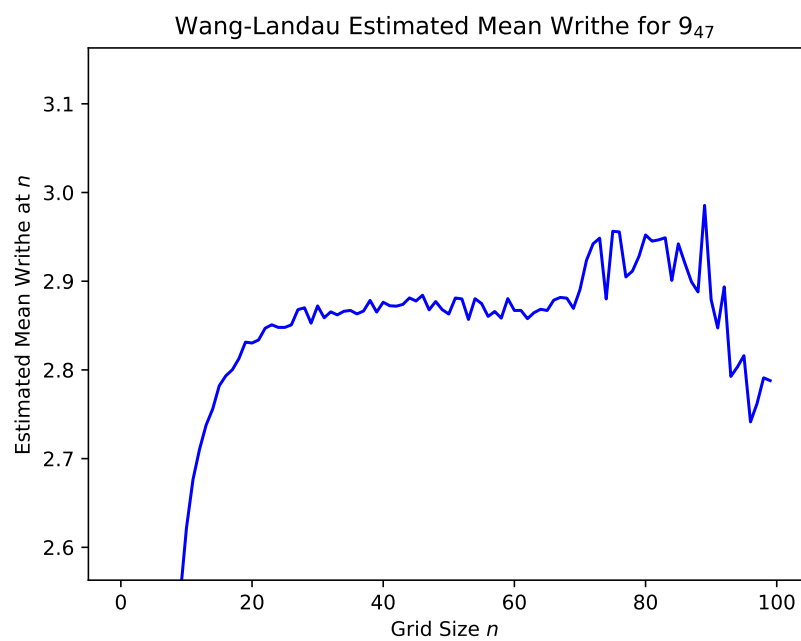


FIGURE 7.8. Estimated mean writhes of size n grid diagrams for 9_{47} .

CHAPTER 8

Conclusion

The work presented here, as much research does, creates as many new questions as it answers. Chapter 3 provides a way to establish a canonical isotopy class for links. This method, assuming Conjectures 2.5.4 and 2.5.3 both hold, fully distinguishes unoriented link isotopy classes. The primary drawback is that it doesn't always completely distinguish choices of orientation. The next steps to continue the work of Chapter 3 are to extend the table to larger crossing numbers and more components, as well as finding a stronger indicator of orientation than linking number.

Future work extending the canonical link isotopy class table could make good use of Wang-Landau for lattice links as described in Chapter 4 by defining energy of a c -component lattice link ω as $(|\omega|, s_1(\omega), \dots, s_c(\omega))$ or using c separate energies defined by $(|\omega|, s_i(\omega))$ with $1 \leq i \leq c$. The mean writhes can then be calculated from the Wang-Landau weights by a weighted estimate as is done for grid diagrams in Section 7.3.2. This would allow for a simultaneous estimate of the mean writhes for all lengths up to some maximum length, which would be very difficult to do with BFACF sampling.

Chapter 5 provided formulas for calculating the total number of $n \times n$ grid diagrams, as well as the proportion of those that represent c -component links for all possible values of c . For $|\mathcal{G}_n(K)|$ a lower bound was provided, but a better lower bound may yet exist and is left for future work. For upper bounds of $|\mathcal{G}_n(K)|$, the proof of FWD for grid diagrams in Chapter 6 provided $O(n^{-1/10}n!(n-1)!)$ as an upper bound that appears to be loose according to the numerical data shown in Section 7.3.1. Hence, a better upper bound for $|\mathcal{G}_n(K)|$ remains to be proven through some other method.

Chapter 7 presents several methods for exploring random knots in grid diagrams. Direct uniform sampling can be performed quickly in a way that it cannot for lattice links, however if interpreting the results requires identification of the link, then it is recommended to use Wang-Landau (Section 7.2.2) if possible. The canonical-like algorithm that is presented in Section 7.2.1 is deprecated by Wang-Landau with energy = grid size.

The use of Wang-Landau in exploring traits of knots and links has a future with much potential. If one wishes to perform Monte Carlo sampling, then a distribution can be selected by transforming a set of trained Wang-Landau weights, which is a potential that is not explored in this work. Wang-Landau could also be implemented for other knot presentations such as braids or any other presentation that can be finitely encoded and with a set of transformations which form an ergodic Markov chain.

Another possible use of Wang-Landau is as a link identification tool. Consider a coarse (large f) Wang-Landau weight training starting with a grid diagram g containing an unknown knot with energy defined as $(|g|, w(g))$. The set of energy values is an invariant of the knot, hence can be used to distinguish knot types. For example, 3_1 can attain $(5, 3)$ and 3_1^* can attain $(5, -3)$, but not vice versa. Expanding this concept to other definitions of energy could further distinguish link types if grid size and writhe are not sufficient. Additionally, this method could be applied to any other link representation where Wang-Landau can be implemented for fixed link type, such as lattice links.

APPENDIX A

Index of Notation

- $c_2(L)$ The coefficient of t^2 in the Alexander-Conway polynomial, also known as the Casson invariant, page 20
- $\chi(C)$ The sign associated to an oriented crossing C , page 8
- $\mathcal{C}_{i,j}(D)$ The set of crossings between component i and j in a regular diagram D , page 7
- $E(\omega)$ The Wang-Landau energy of state ω , page 30
- \mathcal{E} The set of all valid Wang-Landau energy values for the given state space, page 30
- E_i The i th indexed energy in \mathcal{E} , page 30
- \mathcal{G} The set of all grid diagrams, page 11
- $\mathcal{G}(L)$ The set of all grids which represent link type L , page 11
- \mathcal{G}_n The set of all $n \times n$ grid diagrams, page 11
- $\mathcal{G}_{n,c}$ The set of all $n \times n$ grid diagrams representing some link with c components, page 11
- $\mathcal{G}_n(L)$ The set of all $n \times n$ grids representing link type L , page 11
- $\text{lk}(L)$ Linking number of 2-component link L , page 18
- $\text{lk}_{i,j}(L)$ The linking number between the i th and j th components of L , page 19
- μ_{E_i} The number of states in a state space Ω with energy value E_i , page 30
- $!n$ The number of derangements of n objects, page 4
- Ω The state space of a Markov chain, page 26
- $\Omega(g(n))$ A function is $\Omega(g(n))$ if it is bounded below by $c \cdot g(n)$ for sufficiently large n , page 5
- $O(g(n))$ A function is $O(g(n))$ if it is bounded above by $c \cdot g(n)$ for sufficiently large n , page 5
- $\Theta(g(n))$ A function is $\Theta(g(n))$ if it is bounded below and above by constant multiples of $g(n)$ for sufficiently large n , page 5
- $P_{\text{accept}}(\omega \rightarrow \omega')$ The probability that a chosen transition is performed in a Metropolis-Hastings Markov chain, page 29
- $P_{\text{choose}}(\omega \rightarrow \omega')$ The probability that a transition is chosen in a Metropolis-Hastings Markov chain, page 29

- $\pi(\omega)$ The posterior distribution of a Markov chain, i.e. $\pi(\omega) = \lim P^t(\omega_0 \rightarrow \omega)$, page 27
- $P(\omega \rightarrow \omega')$ Probability of transitioning to state ω' from state ω , page 26
- $P^t(\omega \rightarrow \omega')$ Probability of being at state ω' after taking t steps from state ω , page 27
- $s_i(\omega)$ The self-writhe of component i of a link represented by ω . Whether writhe here means space writhe or projected writhe depends on what kind of link representation ω is, page 21
- S_n The set of permutations on n objects, page 4
- $\mathcal{S}_n(L)$ Average of sum of self-writhe for all length n conformations of L in the simple cubic lattice, page 37
- $\mathcal{S}_n(L, i)$ Average of self-writhe for component i in all length n conformations of L in the simple cubic lattice, page 37
- $w(\omega)$ The total writhe of link ω . Whether writhe here means space writhe or projected writhe depends on what kind of link representation ω is, page 21
- z_0 The critical value for the fugacity parameter of BFACF. It is approximately .2134, page 34
- $\mathcal{Z}_n(L)$ The set of all length n simple cubic lattice conformations of link type L , page 37

APPENDIX B

Link Nomenclature Data

TABLE B.1. Mean self-writhe of minimum step prime 2-component links with 9 or fewer crossings. Numbers based on all conformations found as described in Section 3.4. All data is for the canonical link isotopy class shown in Appendix C.

Link	$\mathcal{S}_{\min}(L)$	$\mathcal{S}_{\min}(L, 1)$	$\mathcal{S}_{\min}(L, 2)$	Link	$\mathcal{S}_{\min}(L)$	$\mathcal{S}_{\min}(L, 1)$	$\mathcal{S}_{\min}(L, 2)$
0_1^2	0.0	0.0	0.0	2_1^2	0.0	0.0	0.0
4_1^2	0.8125	0.4063	0.4063	5_1^2	1.3492	0.6746	0.6746
6_1^2	1.65	0.825	0.825	6_2^2	0.0	0.0	0.0
6_3^2	1.9438	0.9719	0.9719	7_1^2	2.1636	1.0818	1.0818
7_2^2	0.7	0.35	0.35	7_3^2	2.4903	2.4427	0.0476
7_4^2	4.2553	4.1811	0.0743	7_5^2	2.3625	2.7563	-0.3937
7_6^2	1.4375	1.4375	0.0	7_7^2	3.5368	3.5368	0.0
7_8^2	3.0479	3.0479	0.0	8_1^2	2.597	1.2985	1.2985
8_2^2	0.8123	0.4062	0.4062	8_3^2	2.7172	1.3586	1.3586
8_4^2	0.8164	0.4082	0.4082	8_5^2	1.1765	0.5883	0.5883
8_6^2	3.1666	1.5833	1.5833	8_7^2	2.7215	1.3607	1.3607
8_8^2	0.0	0.0	0.0	8_9^2	0.9355	0.6021	0.3333
8_{10}^2	0.9525	0.7288	0.2236	8_{11}^2	4.6944	4.6667	0.0278
8_{12}^2	2.0538	2.2909	-0.237	8_{13}^2	2.1324	2.1324	0.0
8_{14}^2	3.0967	3.0967	0.0	8_{15}^2	0.2157	0.0	0.2157
8_{16}^2	0.5	0.5	0.0	9_1^2	2.8941	1.447	1.447
9_2^2	0.1111	0.0556	0.0556	9_3^2	3.3805	1.6903	1.6903
9_4^2	3.0645	1.5323	1.5323	9_5^2	1.3981	0.6991	0.6991
9_6^2	1.4	0.7	0.7	9_7^2	1.3925	0.6963	0.6963
9_8^2	1.7545	0.8773	0.8773	9_9^2	0.25	0.125	0.125
9_{10}^2	3.7033	1.8517	1.8517	9_{11}^2	3.2995	1.6625	1.6369

Link	$\mathcal{S}_{\min}(L)$	$\mathcal{S}_{\min}(L, 1)$	$\mathcal{S}_{\min}(L, 2)$	Link	$\mathcal{S}_{\min}(L)$	$\mathcal{S}_{\min}(L, 1)$	$\mathcal{S}_{\min}(L, 2)$
9_{12}^2	0.6007	0.3003	0.3003	9_{13}^2	7.2952	6.8843	0.4109
9_{14}^2	5.2603	5.4536	-0.1933	9_{15}^2	5.416	5.1609	0.255
9_{16}^2	3.75	3.85	-0.1	9_{17}^2	3.475	4.0375	-0.5625
9_{18}^2	5.4567	5.3384	0.1183	9_{19}^2	5.0661	4.2521	0.814
9_{20}^2	1.5936	2.4532	-0.8596	9_{21}^2	3.5098	4.1327	-0.6229
9_{22}^2	3.3149	3.3409	-0.026	9_{23}^2	0.2848	0.1424	0.1424
9_{24}^2	3.4834	1.7417	1.7417	9_{25}^2	1.2996	1.0981	0.2014
9_{26}^2	1.4789	1.1295	0.3494	9_{27}^2	5.2194	5.1917	0.0278
9_{28}^2	1.6508	1.6825	-0.0317	9_{29}^2	5.3492	5.7828	-0.4336
9_{30}^2	5.3474	4.9738	0.3736	9_{31}^2	4.2443	4.2443	0.0
9_{32}^2	2.7083	2.7083	0.0	9_{33}^2	2.75	2.75	0.0
9_{34}^2	0.5544	0.8803	-0.3259	9_{35}^2	2.227	2.0239	0.2032
9_{36}^2	0.2631	0.2631	0.0	9_{37}^2	1.275	1.275	0.0
9_{38}^2	1.5682	1.5682	0.0	9_{39}^2	3.4055	3.3163	0.0892
9_{40}^2	1.6981	2.1969	-0.4988	9_{41}^2	1.4257	1.0832	0.3425
9_{42}^2	0.9931	1.0069	-0.0139	9_{43}^2	6.2	6.2	0.0
9_{44}^2	5.9718	5.9718	0.0	9_{45}^2	4.6428	4.6396	0.0032
9_{46}^2	4.2077	4.2077	0.0	9_{47}^2	4.5319	4.535	-0.003
9_{48}^2	4.8315	4.7893	0.0422	9_{49}^2	3.9829	3.6718	0.3111
9_{50}^2	2.5914	2.9207	-0.3294	9_{51}^2	2.7063	2.7204	-0.0141
9_{52}^2	3.8318	3.8318	0.0	9_{53}^2	2.0343	1.0172	1.0172
9_{54}^2	1.3141	0.6571	0.6571	9_{55}^2	6.0315	6.0381	-0.0066
9_{56}^2	4.8282	4.8282	0.0	9_{57}^2	0.4678	0.882	-0.4142
9_{58}^2	1.9706	1.3676	0.6029	9_{59}^2	6.2428	6.2428	0.0
9_{60}^2	4.5041	4.5041	0.0	9_{61}^2	0.0	1.0	-1.0

TABLE B.2. Table containing 95% confidence intervals for $\mathcal{S}_n(L++)$, the mean sum of self-writes for the canonical links as seen in Appendix C, for lengths $n = 76, 100, 150, 200, 250,$ and 300 based on BFACF simulations. Confidence intervals do not vary widely for different lengths. This supports the hypothesis that mean writhe is well-behaved as length increases. Additionally, only achiral links have confidence intervals that include 0.

L	$\mathcal{S}_{76}(L++)$	$\mathcal{S}_{100}(L++)$	$\mathcal{S}_{150}(L++)$	$\mathcal{S}_{200}(L++)$	$\mathcal{S}_{250}(L++)$	$\mathcal{S}_{300}(L++)$
2_1^2	[-0.013 0.007]	[-0.031 0.037]	[-0.039 0.103]	[-0.037 0.102]	[-0.212 0.255]	[-0.192 0.511]
4_1^2	[0.894 0.921]	[0.889 0.897]	[0.79 0.949]	[0.755 0.877]	[0.764 0.889]	[0.779 0.977]
5_1^2	[1.455 1.48]	[1.465 1.468]	[1.41 1.532]	[1.401 1.607]	[1.399 1.575]	[1.295 1.565]
6_1^2	[1.724 1.747]	[1.711 1.719]	[1.679 1.699]	[1.624 1.692]	[1.563 1.728]	[1.606 1.848]
6_2^2	[-0.01 0.013]	[-0.005 0.007]	[-0.025 0.015]	[-0.156 0.042]	[-0.048 0.068]	[-0.044 0.11]
6_3^2	[2.042 2.065]	[2.064 2.068]	[2.039 2.147]	[1.957 2.225]	[1.978 2.205]	[1.939 2.24]
7_1^2	[2.284 2.305]	[2.287 2.291]	[2.271 2.289]	[2.188 2.364]	[2.204 2.351]	[2.218 2.347]
7_2^2	[0.569 0.59]	[0.571 0.578]	[0.576 0.601]	[0.413 0.788]	[0.569 0.668]	[0.579 0.711]
7_3^2	[2.641 2.661]	[2.665 2.672]	[2.67 2.695]	[2.667 2.728]	[2.631 2.702]	[2.599 2.782]
7_4^2	[4.306 4.327]	[4.325 4.334]	[4.313 4.331]	[4.292 4.348]	[4.277 4.332]	[4.283 4.377]
7_5^2	[2.517 2.538]	[2.541 2.544]	[2.531 2.552]	[2.532 2.602]	[2.522 2.591]	[2.495 2.63]
7_6^2	[1.428 1.449]	[1.419 1.428]	[1.404 1.432]	[1.411 1.445]	[1.379 1.434]	[1.379 1.511]
7_7^2	[3.532 3.555]	[3.535 3.54]	[3.464 3.563]	[3.51 3.592]	[3.442 3.557]	[3.492 3.672]
7_8^2	[3.214 3.237]	[3.25 3.259]	[3.25 3.3]	[3.248 3.324]	[3.234 3.315]	[3.213 3.328]
8_1^2	[2.579 2.599]	[2.545 2.547]	[2.486 2.505]	[2.443 2.477]	[2.396 2.465]	[2.361 2.543]
8_2^2	[0.802 0.822]	[0.798 0.814]	[0.769 0.791]	[0.761 0.79]	[0.72 0.816]	[0.702 0.884]
8_3^2	[2.884 2.903]	[2.885 2.895]	[2.872 2.909]	[2.861 2.907]	[2.838 2.894]	[2.828 2.952]
8_4^2	[0.905 0.924]	[0.914 0.917]	[0.89 0.912]	[0.868 0.94]	[0.828 0.894]	[0.843 0.965]
8_5^2	[1.164 1.172]	[1.172 1.174]	[1.18 1.192]	[1.171 1.22]	[1.133 1.2]	[1.149 1.234]
8_6^2	[3.234 3.253]	[3.269 3.271]	[3.289 3.306]	[3.29 3.33]	[3.259 3.352]	[3.288 3.373]
8_7^2	[2.841 2.86]	[2.862 2.874]	[2.853 2.869]	[2.829 2.864]	[2.82 2.884]	[2.787 2.872]
8_8^2	[-0.014 0.005]	[-0.002 0.002]	[-0.009 0.006]	[-0.002 0.033]	[-0.029 0.063]	[-0.041 0.043]
8_9^2	[0.846 0.865]	[0.84 0.842]	[0.809 0.854]	[0.777 0.92]	[0.772 0.827]	[0.788 0.849]
8_{10}^2	[0.911 0.93]	[0.926 0.928]	[0.915 0.927]	[0.893 0.927]	[0.885 0.948]	[0.831 0.954]
8_{11}^2	[4.937 4.956]	[4.968 4.976]	[4.966 4.988]	[4.944 4.98]	[4.969 5.025]	[4.915 4.978]
8_{12}^2	[1.907 1.925]	[1.905 1.913]	[1.897 1.929]	[1.904 1.932]	[1.857 1.949]	[1.87 1.931]
8_{13}^2	[1.963 1.982]	[1.946 1.949]	[1.928 1.951]	[1.945 2.0]	[1.939 2.003]	[1.881 2.05]

L	$\mathcal{S}_{76}(L++)$	$\mathcal{S}_{100}(L++)$	$\mathcal{S}_{150}(L++)$	$\mathcal{S}_{200}(L++)$	$\mathcal{S}_{250}(L++)$	$\mathcal{S}_{300}(L++)$
8_{14}^2	[3.111 3.13]	[3.127 3.13]	[3.13 3.145]	[3.13 3.185]	[3.09 3.18]	[3.076 3.197]
8_{15}^2	[0.059 0.08]	[0.054 0.057]	[0.025 0.052]	[0.029 0.056]	[0.022 0.059]	[0.029 0.076]
8_{16}^2	[0.234 0.254]	[0.22 0.229]	[0.205 0.218]	[0.188 0.219]	[0.17 0.226]	[0.171 0.239]
9_1^2	[3.104 3.122]	[3.099 3.11]	[3.071 3.086]	[3.001 3.069]	[2.959 3.135]	[2.983 3.12]
9_2^2	[0.24 0.257]	[0.232 0.234]	[0.192 0.213]	[0.188 0.235]	[0.152 0.213]	[0.164 0.231]
9_3^2	[3.457 3.474]	[3.491 3.494]	[3.485 3.505]	[3.473 3.506]	[3.486 3.541]	[3.444 3.511]
9_4^2	[3.13 3.138]	[3.133 3.135]	[3.101 3.113]	[3.074 3.111]	[3.043 3.097]	[2.972 3.055]
9_5^2	[1.387 1.405]	[1.402 1.405]	[1.391 1.422]	[1.359 1.462]	[1.379 1.439]	[1.364 1.425]
9_6^2	[1.361 1.378]	[1.367 1.369]	[1.354 1.366]	[1.347 1.37]	[1.32 1.374]	[1.312 1.373]
9_7^2	[1.486 1.503]	[1.498 1.5]	[1.474 1.505]	[1.475 1.511]	[1.469 1.523]	[1.463 1.542]
9_8^2	[1.741 1.759]	[1.769 1.771]	[1.784 1.8]	[1.781 1.831]	[1.769 1.892]	[1.81 1.888]
9_9^2	[0.301 0.319]	[0.32 0.323]	[0.308 0.319]	[0.279 0.324]	[0.276 0.329]	[0.244 0.402]
9_{10}^2	[3.813 3.83]	[3.86 3.863]	[3.89 3.906]	[3.861 3.932]	[3.925 3.988]	[3.765 4.09]
9_{11}^2	[3.423 3.44]	[3.456 3.459]	[3.455 3.47]	[3.432 3.53]	[3.453 3.506]	[3.406 3.483]
9_{12}^2	[0.599 0.616]	[0.597 0.6]	[0.589 0.601]	[0.591 0.616]	[0.561 0.615]	[0.536 0.691]
9_{13}^2	[7.128 7.145]	[7.128 7.131]	[7.087 7.109]	[7.056 7.092]	[7.046 7.1]	[7.031 7.092]
9_{14}^2	[5.364 5.381]	[5.368 5.37]	[5.341 5.372]	[5.336 5.36]	[5.315 5.369]	[5.29 5.351]
9_{15}^2	[5.4 5.417]	[5.411 5.413]	[5.405 5.417]	[5.399 5.415]	[5.382 5.442]	[5.163 5.593]
9_{16}^2	[3.659 3.676]	[3.645 3.647]	[3.644 3.66]	[3.635 3.67]	[3.646 3.699]	[3.631 3.692]
9_{17}^2	[3.746 3.763]	[3.766 3.769]	[3.779 3.795]	[3.784 3.809]	[3.779 3.833]	[3.785 3.845]
9_{18}^2	[5.506 5.523]	[5.526 5.528]	[5.521 5.536]	[5.527 5.562]	[5.52 5.574]	[5.514 5.575]
9_{19}^2	[5.132 5.149]	[5.137 5.139]	[5.113 5.124]	[5.089 5.106]	[5.058 5.119]	[5.045 5.106]
9_{20}^2	[1.723 1.74]	[1.733 1.736]	[1.748 1.76]	[1.746 1.769]	[1.74 1.801]	[1.676 1.905]
9_{21}^2	[3.435 3.452]	[3.444 3.447]	[3.43 3.442]	[3.434 3.456]	[3.433 3.493]	[3.396 3.505]
9_{22}^2	[3.399 3.416]	[3.431 3.433]	[3.425 3.436]	[3.396 3.493]	[3.396 3.45]	[3.39 3.45]
9_{23}^2	[0.287 0.304]	[0.276 0.279]	[0.248 0.263]	[0.236 0.271]	[0.223 0.277]	[0.247 0.381]
9_{24}^2	[3.427 3.444]	[3.47 3.473]	[3.476 3.491]	[3.457 3.482]	[3.458 3.512]	[3.45 3.516]
9_{25}^2	[1.437 1.455]	[1.481 1.483]	[1.486 1.516]	[1.472 1.507]	[1.456 1.516]	[1.456 1.534]
9_{26}^2	[1.513 1.53]	[1.557 1.559]	[1.553 1.575]	[1.552 1.576]	[1.551 1.604]	[1.566 1.627]
9_{27}^2	[5.541 5.558]	[5.592 5.594]	[5.594 5.612]	[5.586 5.628]	[5.571 5.633]	[5.596 5.665]
9_{28}^2	[1.308 1.325]	[1.296 1.298]	[1.275 1.287]	[1.263 1.283]	[1.215 1.269]	[1.233 1.293]
9_{29}^2	[5.402 5.419]	[5.407 5.409]	[5.4 5.412]	[5.392 5.42]	[5.387 5.446]	[5.34 5.415]

L	$\mathcal{S}_{76}(L++)$	$\mathcal{S}_{100}(L++)$	$\mathcal{S}_{150}(L++)$	$\mathcal{S}_{200}(L++)$	$\mathcal{S}_{250}(L++)$	$\mathcal{S}_{300}(L++)$
9_{30}^2	[5.432 5.449]	[5.46 5.463]	[5.449 5.486]	[5.447 5.507]	[5.438 5.496]	[5.441 5.502]
9_{31}^2	[4.252 4.269]	[4.232 4.235]	[4.199 4.213]	[4.183 4.213]	[4.184 4.237]	[4.129 4.226]
9_{32}^2	[2.568 2.585]	[2.529 2.532]	[2.508 2.522]	[2.474 2.597]	[2.49 2.543]	[2.483 2.544]
9_{33}^2	[2.618 2.635]	[2.659 2.662]	[2.677 2.695]	[2.673 2.703]	[2.657 2.716]	[2.65 2.71]
9_{34}^2	[0.584 0.601]	[0.594 0.597]	[0.6 0.613]	[0.571 0.614]	[0.559 0.642]	[0.587 0.647]
9_{35}^2	[2.243 2.259]	[2.243 2.245]	[2.215 2.226]	[2.173 2.217]	[2.148 2.317]	[2.183 2.243]
9_{36}^2	[0.29 0.308]	[0.289 0.292]	[0.264 0.29]	[0.239 0.26]	[0.247 0.3]	[0.142 0.239]
9_{37}^2	[1.418 1.435]	[1.407 1.41]	[1.395 1.422]	[1.363 1.405]	[1.381 1.434]	[1.368 1.437]
9_{38}^2	[1.442 1.459]	[1.482 1.484]	[1.48 1.507]	[1.479 1.509]	[1.438 1.491]	[1.472 1.532]
9_{39}^2	[3.402 3.419]	[3.411 3.414]	[3.406 3.417]	[3.388 3.416]	[3.383 3.435]	[3.373 3.44]
9_{40}^2	[1.742 1.759]	[1.754 1.756]	[1.764 1.778]	[1.752 1.795]	[1.764 1.818]	[1.714 1.827]
9_{41}^2	[1.401 1.418]	[1.415 1.418]	[1.404 1.423]	[1.36 1.419]	[1.404 1.462]	[1.392 1.452]
9_{42}^2	[0.615 0.632]	[0.597 0.599]	[0.591 0.604]	[0.574 0.633]	[0.576 0.634]	[0.565 0.626]
9_{43}^2	[6.319 6.339]	[6.3 6.303]	[6.257 6.29]	[6.236 6.318]	[6.192 6.295]	[6.243 6.318]
9_{44}^2	[6.046 6.066]	[6.07 6.072]	[6.07 6.082]	[6.003 6.134]	[6.01 6.106]	[5.968 6.055]
9_{45}^2	[4.633 4.652]	[4.63 4.633]	[4.626 4.641]	[4.63 4.706]	[4.629 4.685]	[4.58 4.666]
9_{46}^2	[4.3 4.319]	[4.342 4.345]	[4.368 4.398]	[4.362 4.4]	[4.339 4.393]	[4.374 4.462]
9_{47}^2	[4.556 4.576]	[4.581 4.584]	[4.573 4.595]	[4.595 4.634]	[4.562 4.631]	[4.569 4.679]
9_{48}^2	[4.838 4.856]	[4.83 4.833]	[4.81 4.825]	[4.745 4.84]	[4.806 4.861]	[4.787 4.862]
9_{49}^2	[4.075 4.096]	[4.094 4.097]	[4.091 4.115]	[4.083 4.166]	[4.058 4.13]	[4.061 4.182]
9_{50}^2	[2.52 2.54]	[2.547 2.55]	[2.557 2.57]	[2.539 2.576]	[2.561 2.616]	[2.433 2.585]
9_{51}^2	[2.657 2.676]	[2.663 2.666]	[2.648 2.663]	[2.646 2.673]	[2.617 2.687]	[2.614 2.691]
9_{52}^2	[4.088 4.107]	[4.126 4.129]	[4.136 4.148]	[4.12 4.151]	[4.114 4.182]	[4.051 4.136]
9_{53}^2	[2.132 2.152]	[2.141 2.143]	[2.12 2.152]	[2.132 2.16]	[2.086 2.189]	[2.143 2.223]
9_{54}^2	[1.351 1.37]	[1.369 1.372]	[1.371 1.385]	[1.348 1.401]	[1.291 1.388]	[1.329 1.45]
9_{55}^2	[6.1 6.119]	[6.14 6.142]	[6.147 6.167]	[6.099 6.15]	[6.121 6.177]	[6.036 6.137]
9_{56}^2	[4.759 4.778]	[4.741 4.744]	[4.72 4.732]	[4.696 4.744]	[4.692 4.747]	[4.7 4.761]
9_{57}^2	[0.617 0.637]	[0.603 0.606]	[0.584 0.596]	[0.563 0.593]	[0.526 0.659]	[0.579 0.7]
9_{58}^2	[2.12 2.138]	[2.165 2.169]	[2.169 2.209]	[2.171 2.193]	[2.152 2.207]	[2.114 2.218]
9_{59}^2	[6.428 6.447]	[6.459 6.461]	[6.464 6.478]	[6.438 6.503]	[6.433 6.488]	[6.407 6.511]
9_{60}^2	[4.345 4.363]	[4.356 4.359]	[4.359 4.373]	[4.326 4.397]	[4.25 4.384]	[4.324 4.41]
9_{61}^2	[-0.0 0.02]	[-0.002 0.001]	[-0.006 0.009]	[-0.024 0.014]	[-0.012 0.044]	[0.009 0.104]

TABLE B.3. Table containing 95% confidence intervals for $\mathcal{S}_n(L++, 1)$, the mean self-writhe of component 1 for the canonical links as seen in Appendix C, for lengths $n = 76, 100, 150, 200, 250$, and 300 based on BFACF simulations. As before, confidence intervals do not vary widely for different lengths, thus supporting the hypothesis that mean component writhe is well-behaved as length increases.

L	$\mathcal{S}_{76}(L++, 1)$	$\mathcal{S}_{100}(L++, 1)$	$\mathcal{S}_{150}(L++, 1)$	$\mathcal{S}_{200}(L++, 1)$	$\mathcal{S}_{250}(L++, 1)$	$\mathcal{S}_{300}(L++, 1)$
2_1^2	[-0.006 0.008]	[-0.009 0.04]	[-0.032 0.067]	[-0.054 0.043]	[-0.138 0.176]	[-0.202 0.308]
4_1^2	[0.444 0.465]	[0.443 0.449]	[0.377 0.493]	[0.391 0.481]	[0.38 0.469]	[0.334 0.476]
5_1^2	[0.724 0.747]	[0.732 0.735]	[0.695 0.794]	[0.685 0.844]	[0.66 0.793]	[0.641 0.836]
6_1^2	[0.863 0.883]	[0.854 0.861]	[0.837 0.852]	[0.812 0.862]	[0.755 0.875]	[0.793 0.971]
6_2^2	[-0.01 0.012]	[-0.004 0.006]	[-0.018 0.014]	[-0.144 0.014]	[-0.025 0.061]	[-0.042 0.072]
6_3^2	[1.019 1.046]	[1.031 1.035]	[0.999 1.097]	[0.979 1.207]	[0.98 1.166]	[0.944 1.175]
7_1^2	[1.135 1.158]	[1.141 1.146]	[1.127 1.142]	[1.027 1.167]	[1.106 1.219]	[1.062 1.161]
7_2^2	[0.271 0.297]	[0.284 0.29]	[0.274 0.295]	[0.211 0.509]	[0.273 0.351]	[0.274 0.376]
7_3^2	[1.309 1.35]	[1.328 1.336]	[1.327 1.351]	[1.318 1.373]	[1.302 1.363]	[1.235 1.384]
7_4^2	[3.989 4.008]	[4.01 4.018]	[4.007 4.023]	[3.992 4.04]	[3.989 4.038]	[3.978 4.059]
7_5^2	[2.824 2.843]	[2.85 2.853]	[2.838 2.856]	[2.843 2.904]	[2.824 2.883]	[2.797 2.915]
7_6^2	[1.404 1.422]	[1.389 1.397]	[1.375 1.399]	[1.381 1.41]	[1.357 1.404]	[1.323 1.433]
7_7^2	[3.489 3.509]	[3.485 3.489]	[3.421 3.504]	[3.458 3.527]	[3.419 3.515]	[3.447 3.603]
7_8^2	[3.293 3.313]	[3.318 3.326]	[3.314 3.356]	[3.304 3.368]	[3.31 3.379]	[3.298 3.396]
8_1^2	[1.293 1.313]	[1.272 1.274]	[1.244 1.259]	[1.225 1.251]	[1.174 1.226]	[1.169 1.303]
8_2^2	[0.395 0.423]	[0.396 0.412]	[0.38 0.398]	[0.373 0.396]	[0.348 0.42]	[0.331 0.468]
8_3^2	[1.431 1.461]	[1.442 1.454]	[1.429 1.462]	[1.435 1.474]	[1.412 1.457]	[1.401 1.499]
8_4^2	[0.445 0.469]	[0.457 0.46]	[0.443 0.462]	[0.417 0.476]	[0.421 0.473]	[0.406 0.497]
8_5^2	[0.576 0.589]	[0.584 0.587]	[0.585 0.596]	[0.575 0.618]	[0.547 0.602]	[0.554 0.623]
8_6^2	[1.552 1.643]	[1.633 1.637]	[1.638 1.656]	[1.632 1.671]	[1.591 1.675]	[1.64 1.714]
8_7^2	[1.39 1.431]	[1.422 1.435]	[1.423 1.438]	[1.415 1.445]	[1.412 1.465]	[1.389 1.456]
8_8^2	[-0.028 0.011]	[-0.002 0.003]	[-0.004 0.01]	[0.006 0.035]	[-0.03 0.044]	[-0.029 0.037]
8_9^2	[0.512 0.53]	[0.519 0.521]	[0.508 0.548]	[0.471 0.599]	[0.486 0.534]	[0.5 0.554]
8_{10}^2	[0.623 0.641]	[0.628 0.63]	[0.612 0.623]	[0.594 0.625]	[0.589 0.644]	[0.567 0.676]
8_{11}^2	[4.431 4.456]	[4.45 4.457]	[4.441 4.462]	[4.423 4.455]	[4.444 4.492]	[4.397 4.451]
8_{12}^2	[2.409 2.433]	[2.424 2.431]	[2.416 2.444]	[2.422 2.447]	[2.363 2.445]	[2.406 2.46]
8_{13}^2	[1.955 1.972]	[1.925 1.927]	[1.906 1.926]	[1.917 1.965]	[1.911 1.967]	[1.836 1.98]
8_{14}^2	[3.186 3.203]	[3.194 3.196]	[3.181 3.195]	[3.17 3.218]	[3.159 3.238]	[3.133 3.236]

L	$\mathcal{S}_{76}(L++, 1)$	$\mathcal{S}_{100}(L++, 1)$	$\mathcal{S}_{150}(L++, 1)$	$\mathcal{S}_{200}(L++, 1)$	$\mathcal{S}_{250}(L++, 1)$	$\mathcal{S}_{300}(L++, 1)$
8_{15}^2	[0.051 0.061]	[0.052 0.053]	[0.038 0.052]	[0.034 0.048]	[0.037 0.055]	[0.039 0.06]
8_{16}^2	[0.161 0.18]	[0.155 0.162]	[0.143 0.154]	[0.132 0.16]	[0.107 0.156]	[0.118 0.179]
9_1^2	[1.547 1.57]	[1.545 1.556]	[1.534 1.547]	[1.504 1.559]	[1.489 1.632]	[1.474 1.58]
9_2^2	[0.117 0.143]	[0.115 0.118]	[0.093 0.111]	[0.082 0.12]	[0.07 0.119]	[0.055 0.108]
9_3^2	[1.711 1.742]	[1.745 1.751]	[1.732 1.754]	[1.727 1.758]	[1.737 1.785]	[1.701 1.757]
9_4^2	[1.563 1.573]	[1.566 1.571]	[1.549 1.559]	[1.535 1.565]	[1.509 1.552]	[1.47 1.533]
9_5^2	[0.681 0.705]	[0.7 0.703]	[0.687 0.715]	[0.666 0.751]	[0.687 0.734]	[0.675 0.723]
9_6^2	[0.674 0.704]	[0.682 0.685]	[0.674 0.685]	[0.673 0.692]	[0.649 0.692]	[0.645 0.693]
9_7^2	[0.74 0.765]	[0.748 0.751]	[0.729 0.757]	[0.73 0.76]	[0.719 0.762]	[0.724 0.786]
9_8^2	[0.852 0.887]	[0.884 0.888]	[0.891 0.907]	[0.865 0.912]	[0.865 0.974]	[0.885 0.952]
9_9^2	[0.15 0.178]	[0.159 0.163]	[0.153 0.164]	[0.133 0.17]	[0.129 0.172]	[0.089 0.212]
9_{10}^2	[1.87 1.925]	[1.925 1.931]	[1.941 1.961]	[1.897 1.973]	[1.945 2.006]	[1.845 2.146]
9_{11}^2	[1.693 1.728]	[1.728 1.734]	[1.721 1.737]	[1.708 1.798]	[1.715 1.761]	[1.692 1.756]
9_{12}^2	[0.29 0.321]	[0.296 0.299]	[0.289 0.3]	[0.306 0.337]	[0.272 0.319]	[0.22 0.349]
9_{13}^2	[6.757 6.774]	[6.775 6.777]	[6.755 6.775]	[6.737 6.769]	[6.734 6.783]	[6.714 6.768]
9_{14}^2	[5.636 5.653]	[5.674 5.676]	[5.663 5.692]	[5.657 5.679]	[5.628 5.677]	[5.617 5.671]
9_{15}^2	[5.068 5.085]	[5.087 5.089]	[5.095 5.106]	[5.102 5.116]	[5.089 5.143]	[4.938 5.317]
9_{16}^2	[3.936 3.953]	[3.94 3.942]	[3.946 3.96]	[3.947 3.978]	[3.954 4.003]	[3.939 3.993]
9_{17}^2	[4.11 4.127]	[4.11 4.112]	[4.101 4.116]	[4.092 4.115]	[4.094 4.143]	[4.094 4.149]
9_{18}^2	[5.233 5.25]	[5.227 5.229]	[5.21 5.223]	[5.21 5.241]	[5.202 5.251]	[5.204 5.259]
9_{19}^2	[4.426 4.444]	[4.43 4.432]	[4.411 4.421]	[4.395 4.408]	[4.37 4.422]	[4.37 4.421]
9_{20}^2	[2.421 2.438]	[2.429 2.431]	[2.446 2.456]	[2.447 2.467]	[2.434 2.485]	[2.362 2.552]
9_{21}^2	[3.574 3.594]	[3.581 3.584]	[3.574 3.584]	[3.576 3.595]	[3.564 3.615]	[3.539 3.63]
9_{22}^2	[3.276 3.296]	[3.297 3.299]	[3.289 3.299]	[3.267 3.352]	[3.264 3.31]	[3.264 3.315]
9_{23}^2	[0.132 0.154]	[0.137 0.141]	[0.125 0.139]	[0.105 0.134]	[0.107 0.15]	[0.108 0.214]
9_{24}^2	[1.71 1.766]	[1.732 1.736]	[1.73 1.745]	[1.718 1.74]	[1.718 1.764]	[1.726 1.781]
9_{25}^2	[0.924 0.946]	[0.952 0.955]	[0.957 0.985]	[0.947 0.979]	[0.936 0.99]	[0.916 0.986]
9_{26}^2	[1.032 1.052]	[1.048 1.051]	[1.036 1.056]	[1.027 1.049]	[1.011 1.059]	[1.037 1.091]
9_{27}^2	[4.855 4.881]	[4.876 4.879]	[4.859 4.878]	[4.847 4.887]	[4.833 4.888]	[4.852 4.913]
9_{28}^2	[1.991 2.015]	[2.015 2.018]	[2.009 2.02]	[1.993 2.012]	[1.958 2.007]	[1.976 2.031]
9_{29}^2	[5.735 5.751]	[5.735 5.738]	[5.711 5.721]	[5.695 5.721]	[5.692 5.745]	[5.633 5.701]
9_{30}^2	[5.117 5.134]	[5.153 5.155]	[5.157 5.191]	[5.149 5.203]	[5.148 5.2]	[5.15 5.204]

L	$\mathcal{S}_{76}(L++, 1)$	$\mathcal{S}_{100}(L++, 1)$	$\mathcal{S}_{150}(L++, 1)$	$\mathcal{S}_{200}(L++, 1)$	$\mathcal{S}_{250}(L++, 1)$	$\mathcal{S}_{300}(L++, 1)$
9_{31}^2	[4.227 4.243]	[4.181 4.184]	[4.149 4.161]	[4.134 4.161]	[4.139 4.186]	[4.091 4.177]
9_{32}^2	[2.566 2.582]	[2.513 2.515]	[2.486 2.498]	[2.452 2.561]	[2.466 2.513]	[2.469 2.524]
9_{33}^2	[2.635 2.651]	[2.698 2.701]	[2.716 2.732]	[2.715 2.741]	[2.691 2.744]	[2.689 2.742]
9_{34}^2	[0.97 0.991]	[0.962 0.964]	[0.955 0.966]	[0.936 0.972]	[0.928 0.998]	[0.951 1.001]
9_{35}^2	[1.834 1.85]	[1.829 1.832]	[1.81 1.82]	[1.768 1.805]	[1.758 1.898]	[1.777 1.827]
9_{36}^2	[0.224 0.241]	[0.204 0.207]	[0.198 0.221]	[0.188 0.207]	[0.192 0.238]	[0.12 0.205]
9_{37}^2	[1.422 1.437]	[1.398 1.4]	[1.383 1.406]	[1.356 1.393]	[1.363 1.409]	[1.354 1.415]
9_{38}^2	[1.43 1.445]	[1.473 1.475]	[1.479 1.502]	[1.478 1.504]	[1.445 1.492]	[1.481 1.534]
9_{39}^2	[3.367 3.383]	[3.4 3.402]	[3.409 3.419]	[3.391 3.415]	[3.395 3.44]	[3.379 3.436]
9_{40}^2	[2.203 2.219]	[2.293 2.296]	[2.377 2.389]	[2.398 2.434]	[2.417 2.461]	[2.34 2.433]
9_{41}^2	[1.143 1.16]	[1.206 1.208]	[1.227 1.242]	[1.218 1.266]	[1.243 1.29]	[1.235 1.282]
9_{42}^2	[0.761 0.776]	[0.781 0.783]	[0.804 0.815]	[0.792 0.842]	[0.801 0.85]	[0.804 0.855]
9_{43}^2	[6.276 6.293]	[6.257 6.26]	[6.224 6.253]	[6.188 6.26]	[6.164 6.254]	[6.2 6.266]
9_{44}^2	[6.127 6.144]	[6.146 6.148]	[6.14 6.151]	[6.082 6.198]	[6.071 6.156]	[6.056 6.134]
9_{45}^2	[4.571 4.588]	[4.573 4.575]	[4.579 4.593]	[4.591 4.66]	[4.586 4.634]	[4.534 4.61]
9_{46}^2	[4.373 4.39]	[4.41 4.412]	[4.431 4.458]	[4.43 4.464]	[4.412 4.461]	[4.443 4.521]
9_{47}^2	[4.611 4.629]	[4.629 4.631]	[4.618 4.637]	[4.638 4.672]	[4.609 4.669]	[4.599 4.696]
9_{48}^2	[4.759 4.776]	[4.758 4.761]	[4.745 4.758]	[4.682 4.766]	[4.735 4.784]	[4.719 4.786]
9_{49}^2	[3.8 3.818]	[3.816 3.819]	[3.807 3.827]	[3.8 3.869]	[3.769 3.829]	[3.759 3.86]
9_{50}^2	[2.952 2.97]	[2.972 2.975]	[2.976 2.986]	[2.949 2.98]	[2.984 3.03]	[2.882 3.008]
9_{51}^2	[2.945 2.964]	[2.989 2.991]	[3.006 3.018]	[3.008 3.03]	[3.001 3.058]	[2.985 3.047]
9_{52}^2	[3.704 3.722]	[3.757 3.759]	[3.771 3.782]	[3.762 3.788]	[3.759 3.815]	[3.677 3.747]
9_{53}^2	[1.061 1.076]	[1.07 1.072]	[1.057 1.08]	[1.07 1.09]	[1.024 1.096]	[1.07 1.128]
9_{54}^2	[0.669 0.713]	[0.684 0.686]	[0.68 0.693]	[0.681 0.723]	[0.657 0.732]	[0.65 0.741]
9_{55}^2	[6.159 6.176]	[6.196 6.198]	[6.2 6.218]	[6.157 6.202]	[6.172 6.221]	[6.104 6.194]
9_{56}^2	[4.702 4.719]	[4.687 4.69]	[4.67 4.681]	[4.65 4.692]	[4.651 4.699]	[4.658 4.712]
9_{57}^2	[0.988 1.005]	[0.961 0.964]	[0.926 0.936]	[0.897 0.922]	[0.841 0.95]	[0.869 0.969]
9_{58}^2	[1.711 1.731]	[1.792 1.795]	[1.821 1.856]	[1.84 1.859]	[1.819 1.865]	[1.8 1.89]
9_{59}^2	[6.404 6.421]	[6.43 6.432]	[6.431 6.444]	[6.413 6.471]	[6.397 6.446]	[6.368 6.461]
9_{60}^2	[4.378 4.395]	[4.396 4.398]	[4.402 4.415]	[4.379 4.442]	[4.313 4.432]	[4.403 4.481]
9_{61}^2	[0.937 0.951]	[0.924 0.926]	[0.907 0.918]	[0.886 0.913]	[0.894 0.934]	[0.892 0.959]

TABLE B.4. Table containing 95% confidence intervals for $\mathcal{S}_n(L++, 2)$, the mean self-writhe of component 2 for the canonical links as seen in Appendix C, for lengths $n = 76, 100, 150, 200, 250$, and 300 based on BFACF simulations. Again, confidence intervals do not vary widely for different lengths.

L	$\mathcal{S}_{76}(L++, 2)$	$\mathcal{S}_{100}(L++, 2)$	$\mathcal{S}_{150}(L++, 2)$	$\mathcal{S}_{200}(L++, 2)$	$\mathcal{S}_{250}(L++, 2)$	$\mathcal{S}_{300}(L++, 2)$
2_1^2	[-0.011 0.003]	[-0.037 0.011]	[-0.036 0.066]	[-0.106 0.087]	[-0.173 0.178]	[-0.12 0.334]
4_1^2	[0.443 0.464]	[0.444 0.45]	[0.376 0.493]	[0.336 0.424]	[0.357 0.447]	[0.401 0.544]
5_1^2	[0.72 0.743]	[0.732 0.735]	[0.678 0.775]	[0.657 0.822]	[0.692 0.829]	[0.59 0.792]
6_1^2	[0.853 0.873]	[0.854 0.861]	[0.837 0.853]	[0.795 0.847]	[0.771 0.89]	[0.756 0.934]
6_2^2	[-0.01 0.011]	[-0.005 0.005]	[-0.019 0.013]	[-0.067 0.083]	[-0.051 0.035]	[-0.038 0.074]
6_3^2	[1.008 1.034]	[1.031 1.035]	[0.997 1.094]	[0.892 1.105]	[0.93 1.107]	[0.915 1.145]
7_1^2	[1.137 1.16]	[1.143 1.148]	[1.137 1.152]	[1.109 1.249]	[1.059 1.171]	[1.121 1.221]
7_2^2	[0.283 0.308]	[0.284 0.29]	[0.293 0.314]	[0.093 0.389]	[0.268 0.345]	[0.269 0.37]
7_3^2	[1.301 1.342]	[1.333 1.341]	[1.331 1.356]	[1.324 1.38]	[1.304 1.364]	[1.306 1.456]
7_4^2	[0.311 0.324]	[0.312 0.318]	[0.303 0.313]	[0.289 0.319]	[0.276 0.307]	[0.286 0.337]
7_5^2	[-0.313 -0.299]	[-0.31 -0.308]	[-0.311 -0.3]	[-0.326 -0.286]	[-0.316 -0.278]	[-0.329 -0.258]
7_6^2	[0.02 0.031]	[0.028 0.033]	[0.023 0.039]	[0.023 0.042]	[0.011 0.042]	[0.032 0.102]
7_7^2	[0.038 0.051]	[0.05 0.052]	[0.024 0.078]	[0.036 0.081]	[0.001 0.065]	[0.009 0.105]
7_8^2	[-0.084 -0.072]	[-0.07 -0.065]	[-0.074 -0.047]	[-0.07 -0.03]	[-0.091 -0.05]	[-0.106 -0.047]
8_1^2	[1.277 1.296]	[1.272 1.274]	[1.236 1.252]	[1.209 1.235]	[1.204 1.257]	[1.148 1.284]
8_2^2	[0.388 0.418]	[0.394 0.41]	[0.382 0.4]	[0.379 0.403]	[0.347 0.421]	[0.325 0.463]
8_3^2	[1.433 1.463]	[1.436 1.448]	[1.428 1.461]	[1.41 1.449]	[1.409 1.454]	[1.39 1.489]
8_4^2	[0.444 0.47]	[0.456 0.458]	[0.439 0.458]	[0.429 0.486]	[0.389 0.439]	[0.406 0.499]
8_5^2	[0.579 0.592]	[0.586 0.589]	[0.589 0.601]	[0.578 0.62]	[0.564 0.619]	[0.569 0.637]
8_6^2	[1.601 1.693]	[1.633 1.637]	[1.641 1.659]	[1.639 1.678]	[1.63 1.715]	[1.616 1.692]
8_7^2	[1.42 1.46]	[1.432 1.445]	[1.423 1.438]	[1.402 1.431]	[1.388 1.44]	[1.373 1.441]
8_8^2	[-0.015 0.023]	[-0.002 0.002]	[-0.012 0.003]	[-0.02 0.01]	[-0.026 0.046]	[-0.036 0.03]
8_9^2	[0.328 0.341]	[0.321 0.322]	[0.291 0.315]	[0.276 0.35]	[0.276 0.304]	[0.276 0.306]
8_{10}^2	[0.283 0.295]	[0.297 0.299]	[0.3 0.306]	[0.291 0.309]	[0.284 0.316]	[0.24 0.301]
8_{11}^2	[0.492 0.513]	[0.516 0.522]	[0.518 0.533]	[0.512 0.534]	[0.513 0.545]	[0.505 0.541]
8_{12}^2	[-0.516 -0.494]	[-0.522 -0.516]	[-0.528 -0.507]	[-0.526 -0.508]	[-0.529 -0.474]	[-0.551 -0.515]
8_{13}^2	[0.005 0.014]	[0.021 0.023]	[0.018 0.029]	[0.018 0.046]	[0.016 0.048]	[0.015 0.101]
8_{14}^2	[-0.079 -0.069]	[-0.067 -0.066]	[-0.055 -0.046]	[-0.051 -0.022]	[-0.087 -0.04]	[-0.079 -0.017]

L	$\mathcal{S}_{76}(L++, 2)$	$\mathcal{S}_{100}(L++, 2)$	$\mathcal{S}_{150}(L++, 2)$	$\mathcal{S}_{200}(L++, 2)$	$\mathcal{S}_{250}(L++, 2)$	$\mathcal{S}_{300}(L++, 2)$
8_{15}^2	[0.004 0.023]	[0.002 0.004]	[-0.018 0.005]	[-0.01 0.014]	[-0.021 0.011]	[-0.013 0.023]
8_{16}^2	[0.069 0.078]	[0.064 0.068]	[0.06 0.066]	[0.05 0.065]	[0.054 0.08]	[0.04 0.073]
9_1^2	[1.542 1.566]	[1.548 1.56]	[1.531 1.544]	[1.476 1.531]	[1.414 1.56]	[1.472 1.578]
9_2^2	[0.106 0.132]	[0.115 0.118]	[0.092 0.11]	[0.091 0.13]	[0.064 0.113]	[0.09 0.142]
9_3^2	[1.724 1.754]	[1.742 1.747]	[1.741 1.763]	[1.731 1.762]	[1.729 1.776]	[1.72 1.776]
9_4^2	[1.561 1.572]	[1.563 1.568]	[1.547 1.558]	[1.527 1.558]	[1.518 1.561]	[1.48 1.544]
9_5^2	[0.691 0.715]	[0.7 0.703]	[0.691 0.72]	[0.659 0.745]	[0.675 0.722]	[0.672 0.719]
9_6^2	[0.666 0.696]	[0.683 0.686]	[0.676 0.686]	[0.666 0.685]	[0.656 0.699]	[0.65 0.698]
9_7^2	[0.729 0.755]	[0.748 0.751]	[0.733 0.761]	[0.733 0.763]	[0.734 0.777]	[0.717 0.778]
9_8^2	[0.863 0.898]	[0.882 0.886]	[0.885 0.901]	[0.894 0.941]	[0.857 0.966]	[0.896 0.963]
9_9^2	[0.132 0.16]	[0.159 0.162]	[0.15 0.161]	[0.131 0.169]	[0.13 0.174]	[0.111 0.234]
9_{10}^2	[1.897 1.952]	[1.93 1.937]	[1.937 1.957]	[1.923 1.999]	[1.95 2.012]	[1.783 2.08]
9_{11}^2	[1.703 1.738]	[1.724 1.729]	[1.725 1.741]	[1.683 1.774]	[1.719 1.765]	[1.689 1.752]
9_{12}^2	[0.286 0.318]	[0.299 0.303]	[0.294 0.306]	[0.277 0.308]	[0.269 0.315]	[0.266 0.392]
9_{13}^2	[0.365 0.376]	[0.352 0.354]	[0.328 0.339]	[0.312 0.329]	[0.301 0.327]	[0.306 0.335]
9_{14}^2	[-0.277 -0.266]	[-0.307 -0.305]	[-0.329 -0.313]	[-0.326 -0.314]	[-0.324 -0.297]	[-0.338 -0.309]
9_{15}^2	[0.326 0.338]	[0.323 0.324]	[0.308 0.314]	[0.294 0.302]	[0.281 0.31]	[0.146 0.355]
9_{16}^2	[-0.283 -0.272]	[-0.296 -0.294]	[-0.305 -0.297]	[-0.319 -0.302]	[-0.319 -0.293]	[-0.319 -0.29]
9_{17}^2	[-0.37 -0.359]	[-0.344 -0.343]	[-0.325 -0.317]	[-0.313 -0.301]	[-0.325 -0.299]	[-0.321 -0.292]
9_{18}^2	[0.267 0.278]	[0.298 0.3]	[0.308 0.316]	[0.31 0.328]	[0.307 0.333]	[0.298 0.327]
9_{19}^2	[0.698 0.713]	[0.706 0.708]	[0.699 0.706]	[0.691 0.701]	[0.674 0.711]	[0.662 0.699]
9_{20}^2	[-0.705 -0.691]	[-0.697 -0.695]	[-0.701 -0.693]	[-0.706 -0.692]	[-0.708 -0.67]	[-0.738 -0.595]
9_{21}^2	[-0.149 -0.131]	[-0.138 -0.136]	[-0.146 -0.139]	[-0.148 -0.133]	[-0.146 -0.108]	[-0.168 -0.101]
9_{22}^2	[0.113 0.131]	[0.133 0.135]	[0.133 0.141]	[0.105 0.165]	[0.119 0.153]	[0.112 0.149]
9_{23}^2	[0.141 0.164]	[0.137 0.14]	[0.117 0.131]	[0.119 0.148]	[0.1 0.143]	[0.099 0.205]
9_{24}^2	[1.67 1.726]	[1.735 1.739]	[1.738 1.753]	[1.73 1.751]	[1.722 1.767]	[1.702 1.757]
9_{25}^2	[0.502 0.52]	[0.528 0.53]	[0.52 0.539]	[0.517 0.537]	[0.506 0.54]	[0.522 0.565]
9_{26}^2	[0.471 0.487]	[0.507 0.509]	[0.511 0.525]	[0.518 0.533]	[0.528 0.558]	[0.516 0.55]
9_{27}^2	[0.67 0.693]	[0.714 0.717]	[0.728 0.742]	[0.726 0.755]	[0.722 0.761]	[0.726 0.769]
9_{28}^2	[-0.697 -0.675]	[-0.721 -0.718]	[-0.738 -0.729]	[-0.736 -0.722]	[-0.757 -0.723]	[-0.76 -0.722]
9_{29}^2	[-0.338 -0.327]	[-0.329 -0.328]	[-0.313 -0.307]	[-0.309 -0.295]	[-0.316 -0.287]	[-0.308 -0.272]
9_{30}^2	[0.309 0.32]	[0.306 0.308]	[0.284 0.303]	[0.286 0.316]	[0.279 0.307]	[0.28 0.309]

L	$\mathcal{S}_{76}(L++, 2)$	$\mathcal{S}_{100}(L++, 2)$	$\mathcal{S}_{150}(L++, 2)$	$\mathcal{S}_{200}(L++, 2)$	$\mathcal{S}_{250}(L++, 2)$	$\mathcal{S}_{300}(L++, 2)$
9_{31}^2	[0.022 0.03]	[0.05 0.052]	[0.048 0.055]	[0.043 0.058]	[0.035 0.061]	[0.02 0.066]
9_{32}^2	[-0.001 0.006]	[0.016 0.017]	[0.02 0.026]	[-0.0 0.058]	[0.014 0.04]	[0.003 0.032]
9_{33}^2	[-0.02 -0.013]	[-0.04 -0.039]	[-0.043 -0.034]	[-0.047 -0.033]	[-0.046 -0.017]	[-0.05 -0.021]
9_{34}^2	[-0.397 -0.379]	[-0.368 -0.366]	[-0.358 -0.35]	[-0.375 -0.348]	[-0.388 -0.337]	[-0.377 -0.341]
9_{35}^2	[0.402 0.416]	[0.413 0.415]	[0.402 0.409]	[0.394 0.422]	[0.354 0.455]	[0.392 0.429]
9_{36}^2	[0.062 0.071]	[0.084 0.086]	[0.061 0.074]	[0.047 0.057]	[0.045 0.071]	[0.005 0.052]
9_{37}^2	[-0.007 0.001]	[0.008 0.01]	[0.007 0.021]	[-0.001 0.02]	[0.008 0.035]	[0.001 0.035]
9_{38}^2	[0.01 0.017]	[0.009 0.01]	[-0.004 0.009]	[-0.004 0.011]	[-0.017 0.009]	[-0.02 0.01]
9_{39}^2	[0.029 0.041]	[0.011 0.013]	[-0.006 0.001]	[-0.01 0.008]	[-0.024 0.008]	[-0.021 0.019]
9_{40}^2	[-0.467 -0.455]	[-0.541 -0.539]	[-0.617 -0.608]	[-0.656 -0.629]	[-0.665 -0.631]	[-0.651 -0.582]
9_{41}^2	[0.25 0.266]	[0.208 0.21]	[0.172 0.186]	[0.127 0.169]	[0.146 0.186]	[0.142 0.184]
9_{42}^2	[-0.151 -0.139]	[-0.185 -0.183]	[-0.215 -0.207]	[-0.232 -0.195]	[-0.238 -0.203]	[-0.252 -0.216]
9_{43}^2	[0.039 0.049]	[0.043 0.044]	[0.027 0.044]	[0.033 0.073]	[0.009 0.059]	[0.029 0.066]
9_{44}^2	[-0.084 -0.075]	[-0.076 -0.075]	[-0.072 -0.067]	[-0.101 -0.043]	[-0.077 -0.034]	[-0.103 -0.065]
9_{45}^2	[0.059 0.068]	[0.056 0.058]	[0.044 0.051]	[0.025 0.06]	[0.034 0.06]	[0.032 0.07]
9_{46}^2	[-0.076 -0.068]	[-0.068 -0.067]	[-0.069 -0.055]	[-0.074 -0.057]	[-0.082 -0.058]	[-0.083 -0.044]
9_{47}^2	[-0.059 -0.05]	[-0.048 -0.047]	[-0.049 -0.038]	[-0.05 -0.032]	[-0.059 -0.026]	[-0.05 0.002]
9_{48}^2	[0.075 0.084]	[0.072 0.073]	[0.063 0.069]	[0.047 0.089]	[0.062 0.086]	[0.056 0.089]
9_{49}^2	[0.27 0.282]	[0.277 0.279]	[0.28 0.293]	[0.266 0.314]	[0.274 0.315]	[0.277 0.347]
9_{50}^2	[-0.437 -0.424]	[-0.425 -0.424]	[-0.421 -0.414]	[-0.418 -0.397]	[-0.434 -0.402]	[-0.48 -0.393]
9_{51}^2	[-0.295 -0.28]	[-0.327 -0.325]	[-0.362 -0.352]	[-0.368 -0.352]	[-0.398 -0.356]	[-0.387 -0.34]
9_{52}^2	[0.378 0.392]	[0.369 0.371]	[0.361 0.369]	[0.351 0.37]	[0.341 0.382]	[0.357 0.407]
9_{53}^2	[1.067 1.081]	[1.07 1.072]	[1.056 1.079]	[1.056 1.076]	[1.041 1.114]	[1.055 1.113]
9_{54}^2	[0.647 0.692]	[0.684 0.687]	[0.685 0.698]	[0.651 0.693]	[0.608 0.683]	[0.648 0.739]
9_{55}^2	[-0.062 -0.053]	[-0.056 -0.055]	[-0.056 -0.047]	[-0.067 -0.044]	[-0.061 -0.035]	[-0.086 -0.039]
9_{56}^2	[0.054 0.062]	[0.053 0.054]	[0.048 0.053]	[0.038 0.06]	[0.032 0.057]	[0.032 0.06]
9_{57}^2	[-0.376 -0.362]	[-0.359 -0.357]	[-0.345 -0.337]	[-0.341 -0.323]	[-0.343 -0.262]	[-0.316 -0.244]
9_{58}^2	[0.4 0.416]	[0.372 0.375]	[0.338 0.363]	[0.326 0.339]	[0.322 0.353]	[0.292 0.35]
9_{59}^2	[0.02 0.028]	[0.028 0.029]	[0.031 0.037]	[0.014 0.043]	[0.027 0.051]	[0.021 0.068]
9_{60}^2	[-0.036 -0.028]	[-0.04 -0.039]	[-0.046 -0.039]	[-0.065 -0.034]	[-0.086 -0.026]	[-0.094 -0.056]
9_{61}^2	[-0.941 -0.927]	[-0.926 -0.924]	[-0.917 -0.906]	[-0.918 -0.891]	[-0.918 -0.878]	[-0.903 -0.835]

TABLE B.5. Columns 2, 3, and 4 show confidence intervals for the average of the sum of self-writhes ($\mathcal{S}_{200}(L++)$), and self-writhes of components 1 and 2 ($\mathcal{S}_{200}(L++, 1)$ and $\mathcal{S}_{200}(L++, 2)$) for length 200 links in \mathbb{Z}^3 . For each 2-component link indicated in column 1, the average is taken over an ensemble of statistically independent length 200 lattice links of type L as described in Chapter 3. Combined with the linking number (column 7), these confidence intervals are used to determine which diagram appears as $L++$ in Appendix C with ambiguities for 9_5^2 , 9_{34}^2 , 9_{35}^2 , 9_{39}^2 , and 9_{41}^2 . The Rolfsen diagram's designation in our nomenclature (as described in 2.3.8) is presented in column 5 [Rol76]. Column 6 lists which isotopy class is represented by default in KnotPlot [Hyp]. Note that the KnotPlot conformations are reflections of the Rolfsen Table. Symmetry groups (column 8) are taken from the work of *Henry & Weeks*, *Berglund et al.*, and from SnapPy [HW92, BCC⁺12, CDGW].

L	$\mathcal{S}_{200}(L++)$	$\mathcal{S}_{200}(L++, 1)$	$\mathcal{S}_{200}(L++, 2)$	Rolfsen	KP	lk(L)	Sym
0_1^2	[- -]	[- -]	[- -]	0_1^2	0_1^{2++}	0	Γ_2
2_1^2	[-0.037 0.102]	[-0.054 0.043]	[-0.106 0.087]	2_1^2	2_1^{2++}	1	$\Sigma_{8,2}$
4_1^2	[0.755 0.877]	[0.391 0.481]	[0.336 0.424]	4_1^{2*}	4_1^{2+-}	2	$\Sigma_{4,1}$
5_1^2	[1.401 1.607]	[0.685 0.844]	[0.657 0.822]	5_1^{2*}	5_1^{2++}	0	$\Sigma_{8,1}$
6_1^2	[1.624 1.692]	[0.812 0.862]	[0.795 0.847]	6_1^{2*}	6_1^{2++}	3	$\Sigma_{4,1}$
6_2^2	[-0.156 0.042]	[-0.144 0.014]	[-0.067 0.083]	6_2^2	6_2^{2++}	3	$\Sigma_{8,2}$
6_3^2	[1.957 2.225]	[0.979 1.207]	[0.892 1.105]	6_3^{2*}	6_3^{2+-}	2	$\Sigma_{4,1}$
7_1^2	[2.188 2.364]	[1.027 1.167]	[1.109 1.249]	7_1^{2*}	7_1^{2++}	1	$\Sigma_{4,1}$
7_2^2	[0.413 0.788]	[0.211 0.509]	[0.093 0.389]	7_2^{2*}	7_2^{2+-}	1	$\Sigma_{4,1}$
7_3^2	[2.667 2.728]	[1.318 1.373]	[1.324 1.38]	7_3^{2*}	7_3^{2++}	0	$\Sigma_{8,1}$
7_4^2	[4.292 4.348]	[3.992 4.04]	[0.289 0.319]	7_4^2	7_4^{2++}	0	$\Sigma_{4,2}$
7_5^2	[2.532 2.602]	[2.843 2.904]	[-0.326 - 0.286]	7_5^{2*}	$\tau 7_5^{2++}$	2	$\Sigma_{2,1}$
7_6^2	[1.411 1.445]	[1.381 1.41]	[0.023 0.042]	7_6^{2*}	$\tau 7_6^{2++}$	0	$\Sigma_{4,2}$
7_7^2	[3.51 3.592]	[3.458 3.527]	[0.036 0.081]	7_7^2	7_7^{2++}	2	$\Sigma_{2,1}$
7_8^2	[3.248 3.324]	[3.304 3.368]	[-0.07 - 0.03]	7_8^{2*}	$\tau 7_8^{2++}$	0	$\Sigma_{4,2}$
8_1^2	[2.443 2.477]	[1.225 1.251]	[1.209 1.235]	8_1^{2*}	8_1^{2+-}	4	$\Sigma_{4,1}$
8_2^2	[0.761 0.79]	[0.373 0.396]	[0.379 0.403]	8_2^2	8_2^{2++}	4	$\Sigma_{4,1}$
8_3^2	[2.861 2.907]	[1.435 1.474]	[1.41 1.449]	8_3^{2*}	8_3^{2++}	3	$\Sigma_{4,1}$
8_4^2	[0.868 0.94]	[0.417 0.476]	[0.429 0.486]	8_4^{2*}	8_4^{2+-}	4	$\Sigma_{4,1}$
8_5^2	[1.171 1.22]	[0.575 0.618]	[0.578 0.62]	8_5^{2*}	8_5^{2++}	3	$\Sigma_{4,1}$
8_6^2	[3.29 3.33]	[1.632 1.671]	[1.639 1.678]	8_6^{2*}	8_6^{2++}	2	$\Sigma_{4,1}$

L	$\mathcal{S}_{200}(L++)$	$\mathcal{S}_{200}(L++, 1)$	$\mathcal{S}_{200}(L++, 2)$	Rolfesen	KP	lk(L)	Sym
8_7^2	[2.829 2.864]	[1.415 1.445]	[1.402 1.431]	8_7^{2*}	8_7^2+-	1	$\Sigma_{4,1}$
8_8^2	[-0.002 0.033]	[0.006 0.035]	[-0.02 0.01]	8_8^2	8_8^2++	1	$\Sigma_{8,2}$
8_9^2	[0.777 0.92]	[0.471 0.599]	[0.276 0.35]	8_9^2	$\tau 8_9^{2*}++$	2	$\Sigma_{2,1}$
8_{10}^2	[0.893 0.927]	[0.594 0.625]	[0.291 0.309]	8_{10}^2	$8_{10}^{2*}++$	0	$\Sigma_{4,2}$
8_{11}^2	[4.944 4.98]	[4.423 4.455]	[0.512 0.534]	8_{11}^2	$8_{11}^{2*}++$	2	$\Sigma_{2,1}$
8_{12}^2	[1.904 1.932]	[2.422 2.447]	[-0.526 -0.508]	8_{12}^{2*}	8_{12}^2++	0	$\Sigma_{4,2}$
8_{13}^2	[1.945 2.0]	[1.917 1.965]	[0.018 0.046]	8_{13}^{2*}	8_{13}^2++	0	$\Sigma_{4,2}$
8_{14}^2	[3.13 3.185]	[3.17 3.218]	[-0.051 -0.022]	8_{14}^2	$8_{14}^{2*}++$	2	$\Sigma_{2,1}$
8_{15}^2	[0.029 0.056]	[0.034 0.048]	[-0.01 0.014]	8_{15}^2	$\tau 8_{15}^{2*}++$	0	$\Sigma_{4,2}$
8_{16}^2	[0.188 0.219]	[0.132 0.16]	[0.05 0.065]	8_{16}^2	$8_{16}^{2*}++$	2	$\Sigma_{2,1}$
9_1^2	[3.001 3.069]	[1.504 1.559]	[1.476 1.531]	9_1^{2*}	9_1^2+-	2	$\Sigma_{4,1}$
9_2^2	[0.188 0.235]	[0.082 0.12]	[0.091 0.13]	9_2^2	$9_2^{2*}+-$	2	$\Sigma_{4,1}$
9_3^2	[3.473 3.506]	[1.727 1.758]	[1.731 1.762]	9_3^{2*}	9_3^2+-	1	$\Sigma_{4,1}$
9_4^2	[3.074 3.111]	[1.535 1.565]	[1.527 1.558]	9_4^{2*}	9_4^2++	0	$\Sigma_{8,1}$
9_5^2	[1.359 1.462]	[0.666 0.751]	[0.659 0.745]	9_5^2	$9_5^{2*}++$	0	$\Sigma_{4,1}$
9_6^2	[1.347 1.37]	[0.673 0.692]	[0.666 0.685]	9_6^{2*}	9_6^2+-	2	$\Sigma_{4,1}$
9_7^2	[1.475 1.511]	[0.73 0.76]	[0.733 0.763]	9_7^{2*}	9_7^2+-	2	$\Sigma_{4,1}$
9_8^2	[1.781 1.831]	[0.865 0.912]	[0.894 0.941]	9_8^{2*}	9_8^2+-	1	$\Sigma_{4,1}$
9_9^2	[0.279 0.324]	[0.133 0.17]	[0.131 0.169]	9_9^{2*}	9_9^2++	0	$\Sigma_{8,1}$
9_{10}^2	[3.861 3.932]	[1.897 1.973]	[1.923 1.999]	9_{10}^{2*}	9_{10}^2++	0	$\Sigma_{8,1}$
9_{11}^2	[3.432 3.53]	[1.708 1.798]	[1.683 1.774]	9_{11}^{2*}	9_{11}^2+-	1	$\Sigma_{4,1}$
9_{12}^2	[0.591 0.616]	[0.306 0.337]	[0.277 0.308]	9_{12}^2	$9_{12}^{2*}++$	1	$\Sigma_{4,1}$
9_{13}^2	[7.056 7.092]	[6.737 6.769]	[0.312 0.329]	9_{13}^2	$9_{13}^{2*}++$	0	$\Sigma_{4,2}$
9_{14}^2	[5.336 5.36]	[5.657 5.679]	[-0.326 -0.314]	9_{14}^{2*}	$\tau 9_{14}^2++$	2	$\Sigma_{2,1}$
9_{15}^2	[5.399 5.415]	[5.102 5.116]	[0.294 0.302]	9_{15}^2	$\tau 9_{15}^{2*}++$	0	$\Sigma_{4,2}$
9_{16}^2	[3.635 3.67]	[3.947 3.978]	[-0.319 -0.302]	9_{16}^{2*}	$\tau 9_{16}^2++$	2	$\Sigma_{2,1}$
9_{17}^2	[3.784 3.809]	[4.092 4.115]	[-0.313 -0.301]	9_{17}^{2*}	$\tau 9_{17}^2++$	2	$\Sigma_{2,1}$
9_{18}^2	[5.527 5.562]	[5.21 5.241]	[0.31 0.328]	9_{18}^2	$\tau 9_{18}^{2*}++$	0	$\Sigma_{4,2}$
9_{19}^2	[5.089 5.106]	[4.395 4.408]	[0.691 0.701]	9_{19}^2	$\tau 9_{19}^{2*}++$	1	$\Sigma_{2,1}$

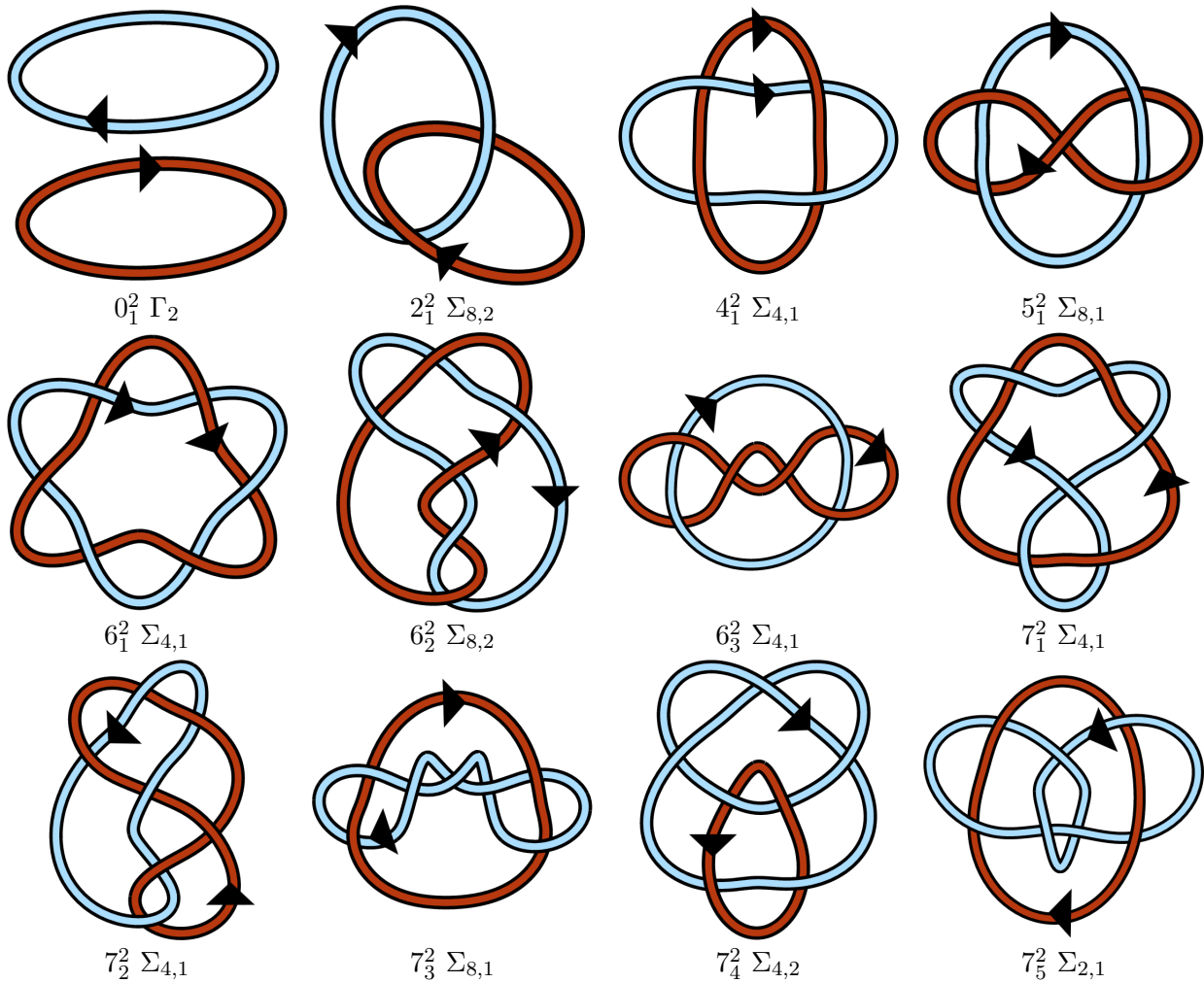
L	$\mathcal{S}_{200}(L++)$	$\mathcal{S}_{200}(L++, 1)$	$\mathcal{S}_{200}(L++, 2)$	Rolfesen	KP	lk(L)	Sym
9_{20}^2	[1.746 1.769]	[2.447 2.467]	[-0.706 - 0.692]	$9_{20}^2 *$	$\tau 9_{20}^2 ++$	3	$\Sigma_{2,1}$
9_{21}^2	[3.434 3.456]	[3.576 3.595]	[-0.148 - 0.133]	9_{21}^2	$\tau 9_{21}^2 *++$	1	$\Sigma_{2,1}$
9_{22}^2	[3.396 3.493]	[3.267 3.352]	[0.105 0.165]	$9_{22}^2 *$	$\tau 9_{22}^2 +-$	3	$\Sigma_{2,1}$
9_{23}^2	[0.236 0.271]	[0.105 0.134]	[0.119 0.148]	9_{23}^2	$9_{23}^2 *++$	2	$\Sigma_{4,1}$
9_{24}^2	[3.457 3.482]	[1.718 1.74]	[1.73 1.751]	$9_{24}^2 *$	$9_{24}^2 ++$	3	$\Sigma_{4,1}$
9_{25}^2	[1.472 1.507]	[0.947 0.979]	[0.517 0.537]	9_{25}^2	$9_{25}^2 *++$	0	$\Sigma_{4,2}$
9_{26}^2	[1.552 1.576]	[1.027 1.049]	[0.518 0.533]	9_{26}^2	$9_{26}^2 *++$	2	$\Sigma_{2,1}$
9_{27}^2	[5.586 5.628]	[4.847 4.887]	[0.726 0.755]	9_{27}^2	$9_{27}^2 *++$	0	$\Sigma_{4,2}$
9_{28}^2	[1.263 1.283]	[1.993 2.012]	[-0.736 - 0.722]	$9_{28}^2 *$	$9_{28}^2 ++$	2	$\Sigma_{2,1}$
9_{29}^2	[5.392 5.42]	[5.695 5.721]	[-0.309 - 0.295]	$9_{29}^2 *$	$9_{29}^2 +-$	2	$\Sigma_{2,1}$
9_{30}^2	[5.447 5.507]	[5.149 5.203]	[0.286 0.316]	9_{30}^2	$9_{30}^2 *+-$	2	$\Sigma_{2,1}$
9_{31}^2	[4.183 4.213]	[4.134 4.161]	[0.043 0.058]	$9_{31}^2 *$	$9_{31}^2 ++$	0	$\Sigma_{4,2}$
9_{32}^2	[2.474 2.597]	[2.452 2.561]	[-0.0 0.058]	$9_{32}^2 *$	$9_{32}^2 ++$	0	$\Sigma_{4,2}$
9_{33}^2	[2.673 2.703]	[2.715 2.741]	[-0.047 - 0.033]	9_{33}^2	$9_{33}^2 *++$	0	$\Sigma_{4,2}$
9_{34}^2	[0.571 0.614]	[0.936 0.972]	[-0.375 - 0.348]	9_{34}^2	$9_{34}^2 *++$	1	{e}
9_{35}^2	[2.173 2.217]	[1.768 1.805]	[0.394 0.422]	$9_{35}^2 *$	$9_{35}^2 ++$	1	{e}
9_{36}^2	[0.239 0.26]	[0.188 0.207]	[0.047 0.057]	$9_{36}^2 *$	$9_{36}^2 ++$	0	$\Sigma_{4,2}$
9_{37}^2	[1.363 1.405]	[1.356 1.393]	[-0.001 0.02]	$9_{37}^2 *$	$9_{37}^2 ++$	0	$\Sigma_{4,2}$
9_{38}^2	[1.479 1.509]	[1.478 1.504]	[-0.004 0.011]	9_{38}^2	$9_{38}^2 *+-$	2	$\Sigma_{2,1}$
9_{39}^2	[3.388 3.416]	[3.391 3.415]	[-0.01 0.008]	9_{39}^2	$9_{39}^2 *++$	1	{e}
9_{40}^2	[1.752 1.795]	[2.398 2.434]	[-0.656 - 0.629]	9_{40}^2	$9_{40}^2 *++$	3	$\Sigma_{2,1}$
9_{41}^2	[1.36 1.419]	[1.218 1.266]	[0.127 0.169]	9_{41}^2	$9_{41}^2 *++$	0	$\Sigma_{2,1}$
9_{42}^2	[0.574 0.633]	[0.792 0.842]	[-0.232 - 0.195]	9_{42}^2	$9_{42}^2 *+-$	1	$\Sigma_{2,1}$
9_{43}^2	[6.236 6.318]	[6.188 6.26]	[0.033 0.073]	9_{43}^2	$9_{43}^2 *+-$	2	$\Sigma_{2,1}$
9_{44}^2	[6.003 6.134]	[6.082 6.198]	[-0.101 - 0.043]	$9_{44}^2 *$	$9_{44}^2 ++$	0	$\Sigma_{4,2}$
9_{45}^2	[4.63 4.706]	[4.591 4.66]	[0.025 0.06]	9_{45}^2	$\tau 9_{45}^2 *++$	2	$\Sigma_{2,1}$
9_{46}^2	[4.362 4.4]	[4.43 4.464]	[-0.074 - 0.057]	$9_{46}^2 *$	$9_{46}^2 ++$	0	$\Sigma_{4,2}$
9_{47}^2	[4.595 4.634]	[4.638 4.672]	[-0.05 - 0.032]	$9_{47}^2 *$	$9_{47}^2 ++$	0	$\Sigma_{4,2}$
9_{48}^2	[4.745 4.84]	[4.682 4.766]	[0.047 0.089]	9_{48}^2	$\tau 9_{48}^2 *++$	2	$\Sigma_{2,1}$

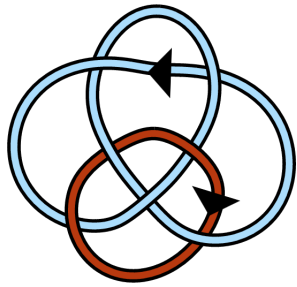
L	$\mathcal{S}_{200}(L++)$	$\mathcal{S}_{200}(L++, 1)$	$\mathcal{S}_{200}(L++, 2)$	Rolfesen	KP	lk(L)	Sym
9_{49}^2	[4.083 4.166]	[3.8 3.869]	[0.266 0.314]	9_{49}^2	$\tau 9_{49}^{2*+-}$	3	$\Sigma_{2,1}$
9_{50}^2	[2.539 2.576]	[2.949 2.98]	[-0.418 - 0.397]	9_{50}^{2*}	$\tau 9_{50}^{2+-}$	1	$\Sigma_{2,1}$
9_{51}^2	[2.646 2.673]	[3.008 3.03]	[-0.368 - 0.352]	9_{51}^2	$\tau 9_{51}^{2*+-}$	3	$\Sigma_{2,1}$
9_{52}^2	[4.12 4.151]	[3.762 3.788]	[0.351 0.37]	9_{52}^{2*}	$\tau 9_{52}^{2+-}$	1	$\Sigma_{2,1}$
9_{53}^2	[2.132 2.16]	[1.07 1.09]	[1.056 1.076]	9_{53}^2	9_{53}^{2*+-}	4	$\Sigma_{4,1}$
9_{54}^2	[1.348 1.401]	[0.681 0.723]	[0.651 0.693]	9_{54}^{2*}	9_{54}^{2+-}	1	$\Sigma_{4,1}$
9_{55}^2	[6.099 6.15]	[6.157 6.202]	[-0.067 - 0.044]	9_{55}^{2*}	9_{55}^{2++}	0	$\Sigma_{4,2}$
9_{56}^2	[4.696 4.744]	[4.65 4.692]	[0.038 0.06]	9_{56}^2	$\tau 9_{56}^{2*++}$	0	$\Sigma_{4,2}$
9_{57}^2	[0.563 0.593]	[0.897 0.922]	[-0.341 - 0.323]	9_{57}^{2*}	9_{57}^{2+-}	2	$\Sigma_{2,1}$
9_{58}^2	[2.171 2.193]	[1.84 1.859]	[0.326 0.339]	9_{58}^2	9_{58}^{2*+-}	2	$\Sigma_{2,1}$
9_{59}^2	[6.438 6.503]	[6.413 6.471]	[0.014 0.043]	9_{59}^{2*}	9_{59}^{2+-}	2	$\Sigma_{2,1}$
9_{60}^2	[4.326 4.397]	[4.379 4.442]	[-0.065 - 0.034]	9_{60}^2	9_{60}^{2*++}	2	$\Sigma_{2,1}$
9_{61}^2	[-0.024 0.014]	[0.886 0.913]	[-0.918 - 0.891]	9_{61}^2	9_{61}^{2++}	4	$\Sigma_{4,5}$

APPENDIX C

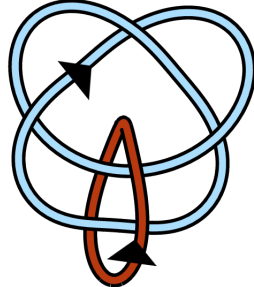
Oriented Labeled Link Table

Here the canonical link isotopy classes for L^{++} as described in Chapter 3 are presented. Next to each link name is its symmetry group, which may be cross-referenced with Table 2.1. For links lacking pure exchange symmetry, the lighter blue strand is component 1 and the darker red-orange strand is component 2.

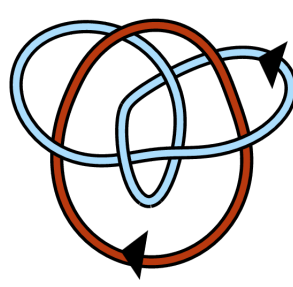




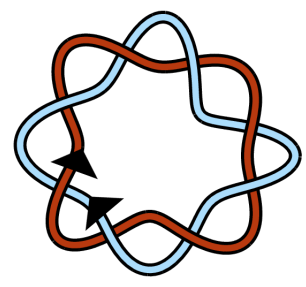
$7_6^2 \Sigma_{4,2}$



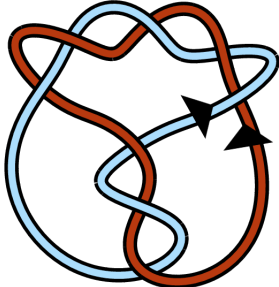
$7_7^2 \Sigma_{2,1}$



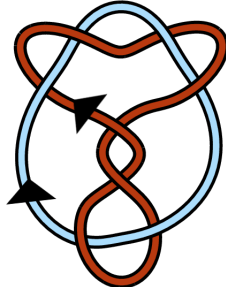
$7_8^2 \Sigma_{4,2}$



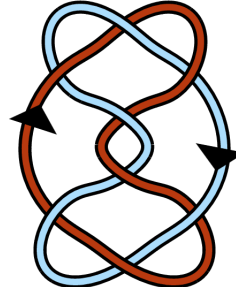
$8_1^2 \Sigma_{4,1}$



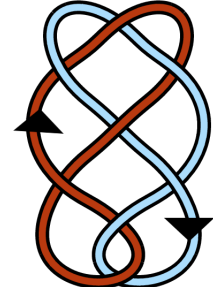
$8_2^2 \Sigma_{4,1}$



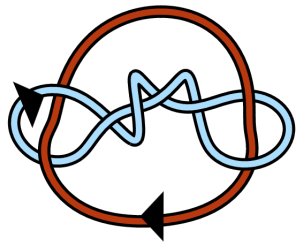
$8_3^2 \Sigma_{4,1}$



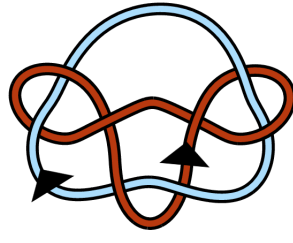
$8_4^2 \Sigma_{4,1}$



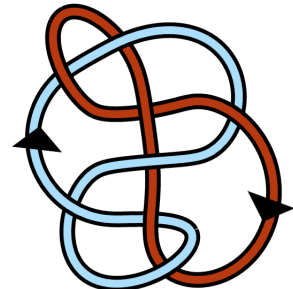
$8_5^2 \Sigma_{4,1}$



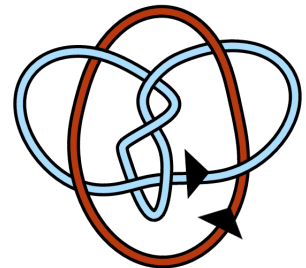
$8_6^2 \Sigma_{4,1}$



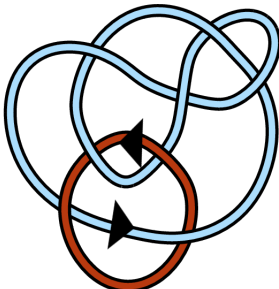
$8_7^2 \Sigma_{4,1}$



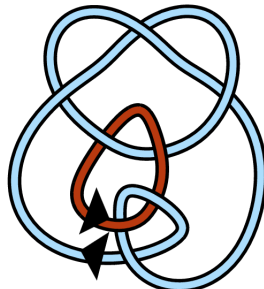
$8_8^2 \Sigma_{8,2}$



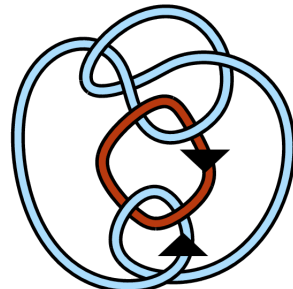
$8_9^2 \Sigma_{2,1}$



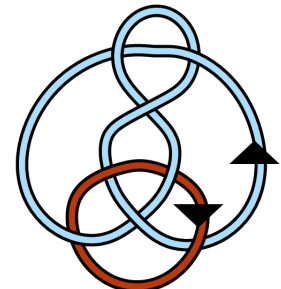
$8_{10}^2 \Sigma_{4,2}$



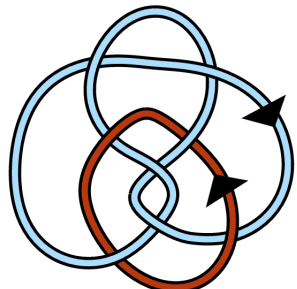
$8_{11}^2 \Sigma_{2,1}$



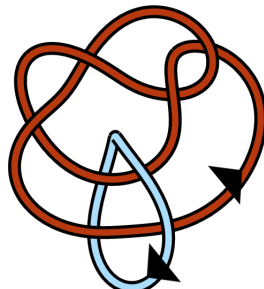
$8_{12}^2 \Sigma_{4,2}$



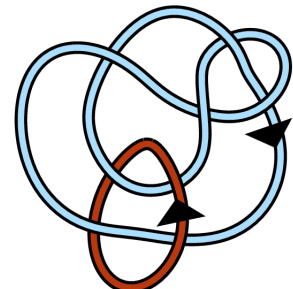
$8_{13}^2 \Sigma_{4,2}$



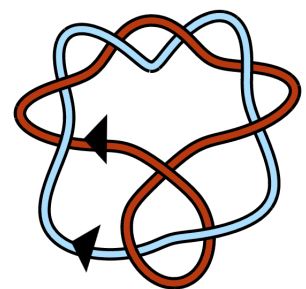
$8_{14}^2 \Sigma_{2,1}$



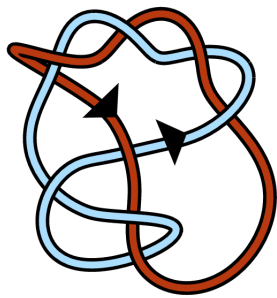
$8_{15}^2 \Sigma_{4,2}$



$8_{16}^2 \Sigma_{2,1}$



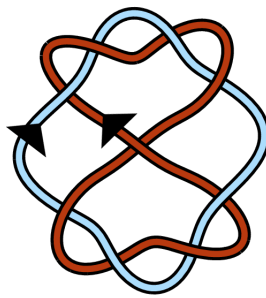
$9_1^2 \Sigma_{4,1}$



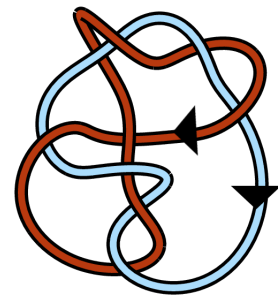
$9_2^2 \Sigma_{4,1}$



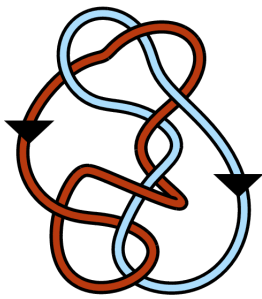
$9_3^2 \Sigma_{4,1}$



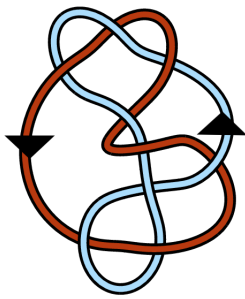
$9_4^2 \Sigma_{8,1}$



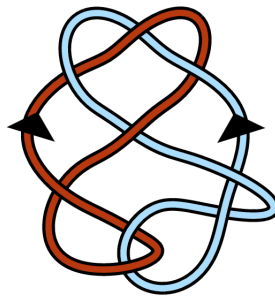
$9_5^2 \Sigma_{4,1}$



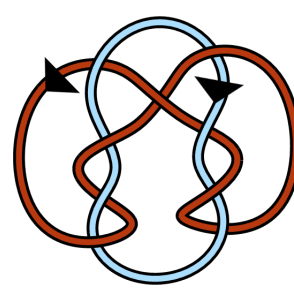
$9_6^2 \Sigma_{4,1}$



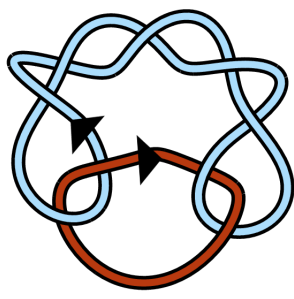
$9_7^2 \Sigma_{4,1}$



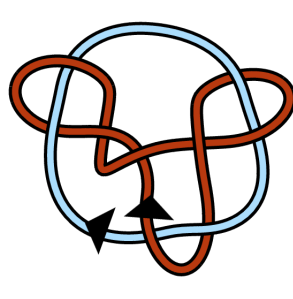
$9_8^2 \Sigma_{4,1}$



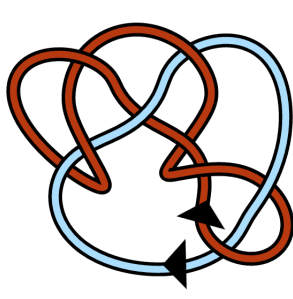
$9_9^2 \Sigma_{8,1}$



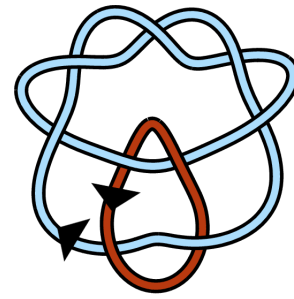
$9_{10}^2 \Sigma_{8,1}$



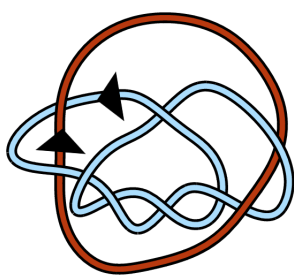
$9_{11}^2 \Sigma_{4,1}$



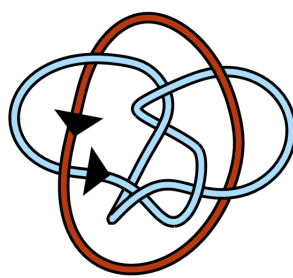
$9_{12}^2 \Sigma_{4,1}$



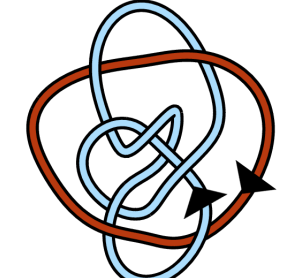
$9_{13}^2 \Sigma_{4,2}$



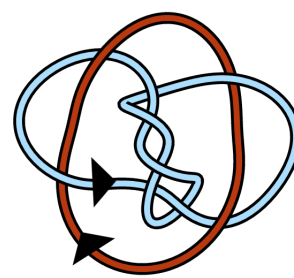
$9_{14}^2 \Sigma_{2,1}$



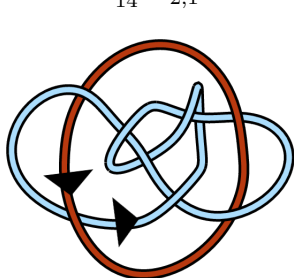
$9_{15}^2 \Sigma_{4,2}$



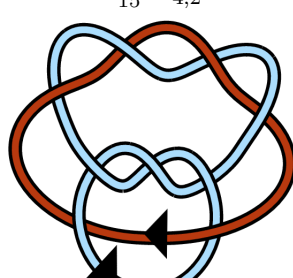
$9_{16}^2 \Sigma_{2,1}$



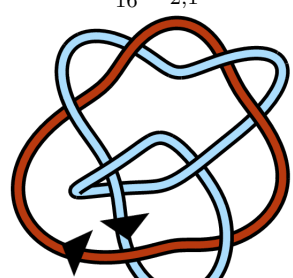
$9_{17}^2 \Sigma_{2,1}$



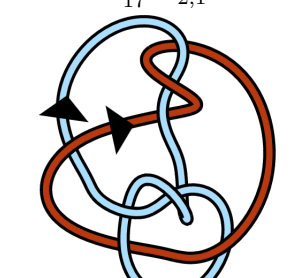
$9_{18}^2 \Sigma_{4,2}$



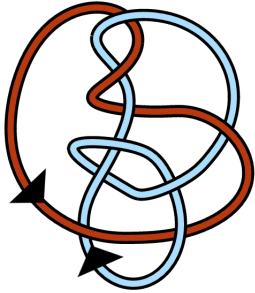
$9_{19}^2 \Sigma_{2,1}$



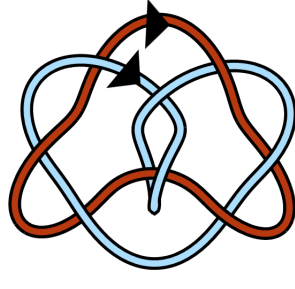
$9_{20}^2 \Sigma_{2,1}$



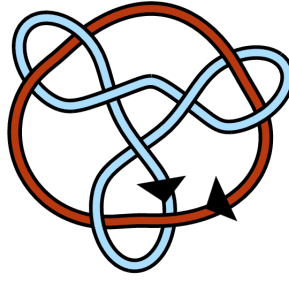
$9_{21}^2 \Sigma_{2,1}$



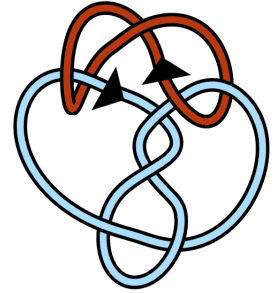
$9_{22}^2 \Sigma_{2,1}$



$9_{23}^2 \Sigma_{4,1}$



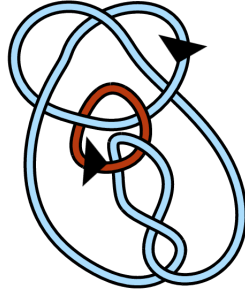
$9_{24}^2 \Sigma_{4,1}$



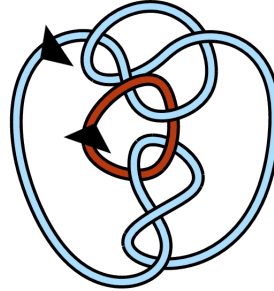
$9_{25}^2 \Sigma_{4,2}$



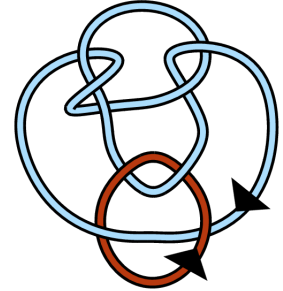
$9_{26}^2 \Sigma_{2,1}$



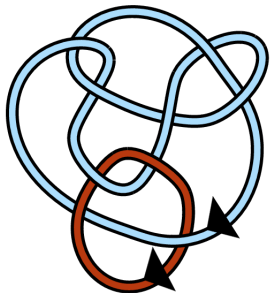
$9_{27}^2 \Sigma_{4,2}$



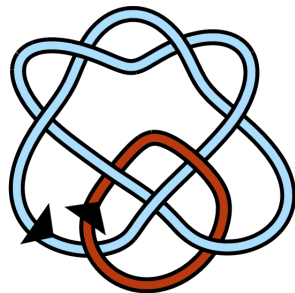
$9_{28}^2 \Sigma_{2,1}$



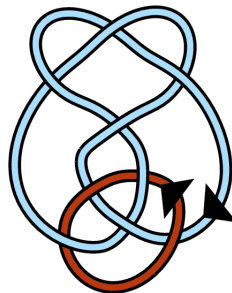
$9_{29}^2 \Sigma_{2,1}$



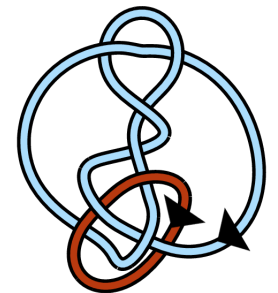
$9_{30}^2 \Sigma_{2,1}$



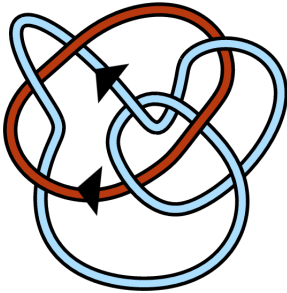
$9_{31}^2 \Sigma_{4,2}$



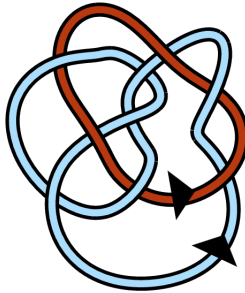
$9_{32}^2 \Sigma_{4,2}$



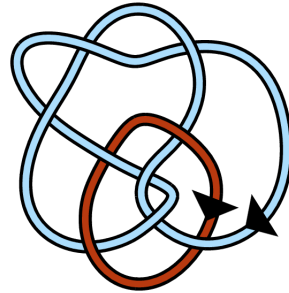
$9_{33}^2 \Sigma_{4,2}$



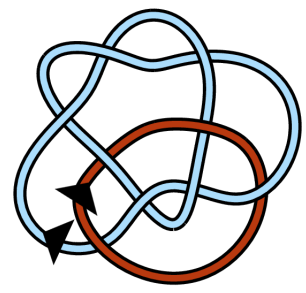
$9_{34}^2 \{e\}$



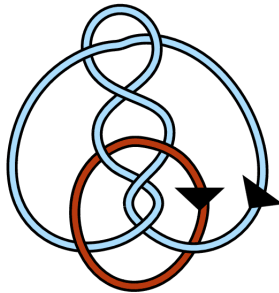
$9_{35}^2 \{e\}$



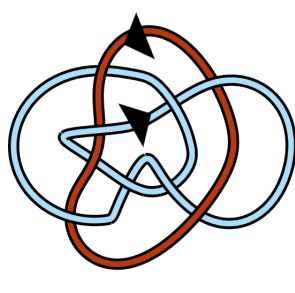
$9_{36}^2 \Sigma_{4,2}$



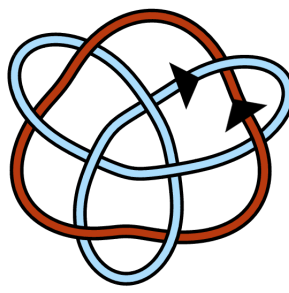
$9_{37}^2 \Sigma_{4,2}$



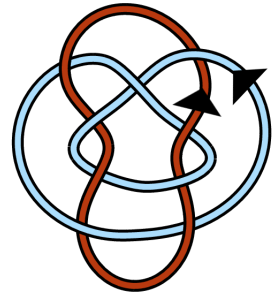
$9_{38}^2 \Sigma_{2,1}$



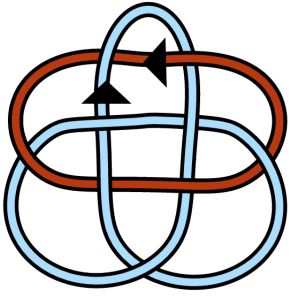
$9_{39}^2 \{e\}$



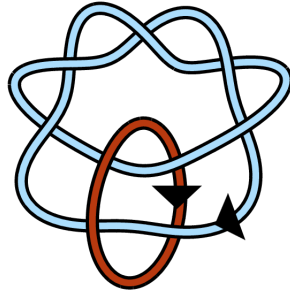
$9_{40}^2 \Sigma_{2,1}$



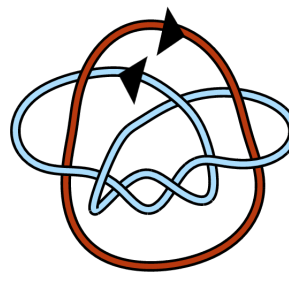
$9_{41}^2 \Sigma_{2,1}$



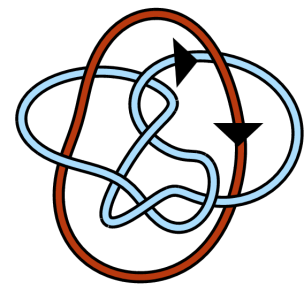
$9_{42}^2 \Sigma_{2,1}$



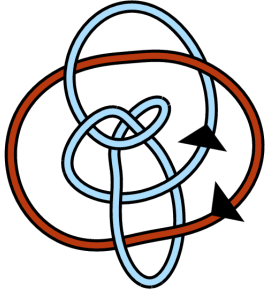
$9_{43}^2 \Sigma_{2,1}$



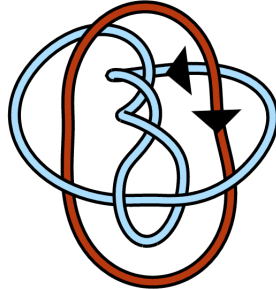
$9_{44}^2 \Sigma_{4,2}$



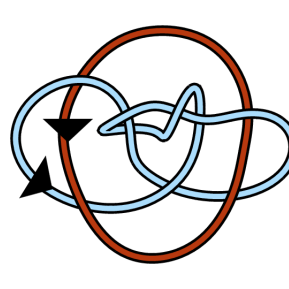
$9_{45}^2 \Sigma_{2,1}$



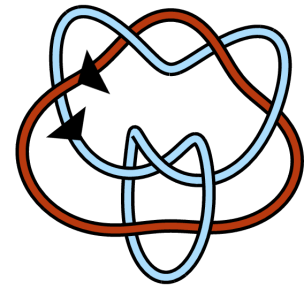
$9_{46}^2 \Sigma_{4,2}$



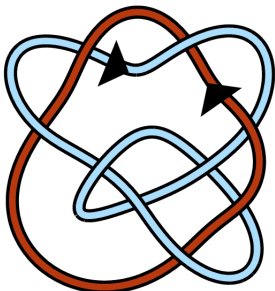
$9_{47}^2 \Sigma_{4,2}$



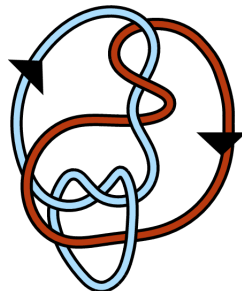
$9_{48}^2 \Sigma_{2,1}$



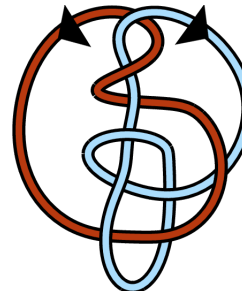
$9_{49}^2 \Sigma_{2,1}$



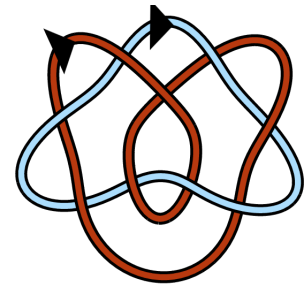
$9_{50}^2 \Sigma_{2,1}$



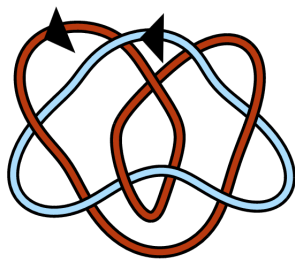
$9_{51}^2 \Sigma_{2,1}$



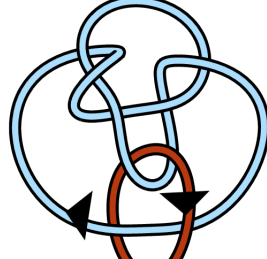
$9_{52}^2 \Sigma_{2,1}$



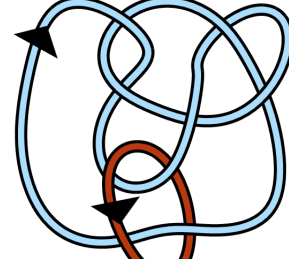
$9_{53}^2 \Sigma_{4,1}$



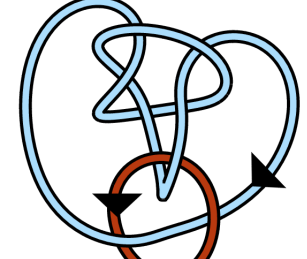
$9_{54}^2 \Sigma_{4,1}$



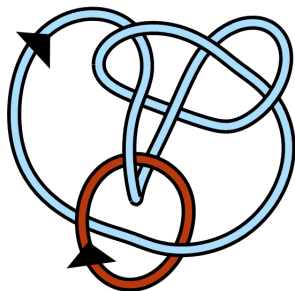
$9_{55}^2 \Sigma_{4,2}$



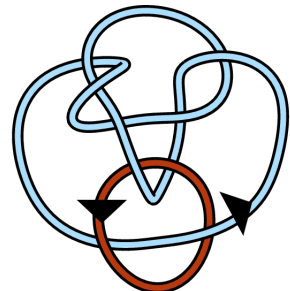
$9_{56}^2 \Sigma_{4,2}$



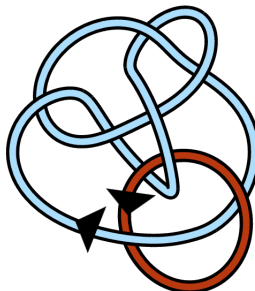
$9_{57}^2 \Sigma_{2,1}$



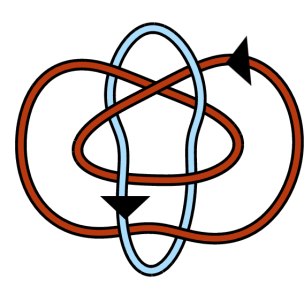
$9_{58}^2 \Sigma_{2,1}$



$9_{59}^2 \Sigma_{2,1}$



$9_{60}^2 \Sigma_{2,1}$



$9_{61}^2 \Sigma_{4,5}$

Bibliography

- [AB26] J. W. Alexander and G. B. Briggs, *On Types of Knotted Curves*, The Annals of Mathematics **28** (1926), no. 1/4, 562.
- [AB09] S. Arora and B. Barak, *Computational Complexity: A Modern Approach*, Cambridge University Press, 2009.
- [AC83] C. Aragão de Carvalho and S. Caracciolo, *A new Monte-Carlo approach to the critical properties of self-avoiding random walks*, Journal de Physique **44** (1983), no. 3, 323–331.
- [ACF83] C. Aragão de Carvalho, S. Caracciolo, and J. Fröhlich, *Polymers and $g|\phi|^4$ theory in four dimensions*, Nuclear Physics B **215** (1983), no. 2, 209–248.
- [BBM⁺05] A. D. Bates, S. Bates, A. Maxwell, H. Maxwell, and T. Maxwell, *DNA Topology*, Oxford bioscience, Oxford University Press, 2005.
- [BCC⁺12] M. Berglund, J. Cantarella, M. P. Casey, E. Dannenberg, W. George, A. Johnson, A. Kelley, A. LaPointe, M. Mastin, J. Parsley, J. Rooney, and R. Whitaker, *Intrinsic Symmetry Groups of Links with 8 and Fewer Crossings*, Symmetry **4** (2012), no. 1, 143–207, 1010.3234.
- [BCH⁺19] A. Barbensi, D. Celoria, H. A. Harrington, A. Stasiak, and D. Buck, *Grid diagrams as tools to investigate knot spaces and topoisomerase-mediated simplification of DNA topology*, arXiv.org (2019), 1–22, 1909.05937.
- [BF81] B. Berg and D. Foerster, *Random paths and random surfaces on a digital computer*, Physics Letters B **106** (1981), no. 4, 323–326.
- [BI15] D. Buck and K. Ishihara, *Coherent band pathways between knots and links*, Journal of Knot Theory and Its Ramifications **24** (2015), no. 02, 1550006.
- [BL12] S. Baldridge and A. M. Lowrance, *Cube Diagrams and 3-Dimensional Reidemeister-Like Moves for Knots*, Journal of Knot Theory and Its Ramifications **21** (2012), no. 05, 1250033, 0811.0225v2.
- [BM94] J. S. Birman and W. W. Menasco, *Special positions for essential Tori in link complements*, Topology **33** (1994), no. 3, 525–556.
- [BP07] R. E. Belardinelli and V. D. Pereyra, *Wang-Landau algorithm: A theoretical analysis of the saturation of the error*, The Journal of Chemical Physics **127** (2007), no. 18, 184105.
- [Bru97] H. Brunn, *Über Verknotete Kurven*, Mathematiker-Kongresses Zurich (1897), 256–259.
- [BSV13] R. Brasher, R. G. Scharein, and M. Vazquez, *New biologically motivated knot table*, Biochemical Society Transactions **41** (2013), no. 2, 606–611.

- [CCMP12] J. Cantarella, J. Cornish, M. Mastin, and J. Parsley, *The 27 Possible Intrinsic Symmetry Groups of Two-Component Links*, *Symmetry* **4** (2012), no. 1, 129–142.
- [CDGW] M. Culler, N. M. Dunfield, M. Goerner, and J. R. Weeks, *SnapPy, a computer program for studying the geometry and topology of 3-manifolds*, <http://snappy.computop.org> (01/11/2019).
- [Cha17] H. Chapman, *Asymptotic laws for random knot diagrams*, *Journal of Physics A: Mathematical and Theoretical* **50** (2017), no. 22, 225001, 1608.02638.
- [CN96] P. R. Cromwell and I. J. Nutt, *Embedding knots and links in an open book II. Bounds on arc index*, *Mathematical Proceedings of the Cambridge Philosophical Society* **119** (1996), no. 2, 309–319.
- [Cri00] N. J. Crisona, *Preferential relaxation of positively supercoiled DNA by E. coli topoisomerase IV in single-molecule and ensemble measurements*, *Genes & Development* **14** (2000), no. 22, 2881–2892.
- [Cro95] P. R. Cromwell, *Embedding knots and links in an open book I: Basic properties*, *Topology and its Applications* **64** (1995), no. 1, 37–58.
- [Cro98] P. Cromwell, *Arc presentations of knots and links*, *Banach Center Publications* **42** (1998), no. 1, 57–64.
- [Cul] M. Culler, *Gridlink, A tool for knot theorists*, <http://homepages.math.uic.edu/%7Eculler/gridlink/> (12/08/2019).
- [Del62] M. Delbrück, *Knotting Problems in Biology*, *Proceedings of Symposia in Applied Mathematics* **14** (1962), 55–68.
- [DH91] H. Doll and J. Hoste, *A tabulation of oriented links*, *Mathematics of Computation* **57** (1991), no. 196, 747–747.
- [Dia95] Y. Diao, *The Knotting of Equilateral Polygons in R^3* , *Journal of Knot Theory and Its Ramifications* **04** (1995), no. 02, 189–196.
- [DPS94] Y. Diao, N. Pippenger, and D. W. Sumners, *On Random Knots*, *Journal of Knot Theory and Its Ramifications* **03** (1994), no. 03, 419–429.
- [Dyn06] I. A. Dynnikov, *Arc-presentations of links: Monotonic simplification*, *Fundamenta Mathematicae* **190** (2006), 29–76, 0208153v3.
- [Erd45] P. Erdős, *On a lemma of Littlewood and Offord*, *Bulletin of the American Mathematical Society* **51** (1945), no. 12, 898–903.
- [EZHLN16] C. Even-Zohar, J. Hass, N. Linial, and T. Nowik, *Invariants of Random Knots and Links*, *Discrete & Computational Geometry* **56** (2016), no. 2, 274–314.
- [EZHLN18] C. Even-Zohar, J. Hass, N. Linial, and T. Nowik, *The distribution of knots in the Petaluma model*, *Algebraic & Geometric Topology* **18** (2018), no. 6, 3647–3667, 1706.06571.
- [Fis13] G. Fishman, *Monte Carlo: Concepts, Algorithms, and Applications*, *Springer Series in Operations Research and Financial Engineering*, Springer New York, 2013.
- [FW61] H. L. Frisch and E. Wasserman, *Chemical Topology*, *Journal of the American Chemical Society* **83** (1961), no. 18, 3789–3795.

- [GS09] C. M. Grinstead and J. L. Snell, *Grinstead and Snell's Introduction to Probability*, Titolo collana, University Press of Florida, 2009.
- [HKON14] K. Hong, H. Kim, S. Oh, and S. No, *Minimum lattice length and ropelength of knots*, *Journal of Knot Theory and Its Ramifications* **23** (2014), no. 07, 1460009, 1411.1845.
- [HLP99] J. Hass, J. C. Lagarias, and N. Pippenger, *The computational complexity of knot and link problems*, *Journal of the ACM* **46** (1999), no. 2, 185–211, 9807016v1.
- [HW92] S. R. Henry and J. R. Weeks, *Symmetry Groups of Hyperbolic Knots and Links*, *Journal of Knot Theory and Its Ramifications* **01** (1992), no. 02, 185–201.
- [Hyp] Hypnagogic Software, *KnotPlot*, <http://www.knotplot.com/> (10/24/2014).
- [IPS⁺17] K. Ishihara, M. Pouokam, A. Suzuki, R. Scharein, M. Vazquez, J. Arsuaga, and K. Shimokawa, *Bounds for minimum step number of knots confined to tubes in the simple cubic lattice*, *Journal of Physics A: Mathematical and Theoretical* **50** (2017), no. 21, 215601.
- [JW91] E. J. Janse van Rensburg and S. G. Whittington, *The BFACF algorithm and knotted polygons*, *Journal of Physics A: Mathematical and General* **24** (1991), no. 23, 5553–5567.
- [KT17] M. T. Keller and W. T. Trotter, *Applied Combinatorics*, 2017 editi ed., Mitchel T. Keller, William T. Trotter, 2017.
- [LCM96] C. Liang, C. Cerf, and K. Mislow, *Specification of chirality for links and knots*, *Journal of Mathematical Chemistry* **19** (1996), no. 3, 241–263.
- [Lic97] W. B. R. Lickorish, *An Introduction to Knot Theory*, Graduate Texts in Mathematics, Springer New York, 1997.
- [LS91] R. C. Lacher and D. W. Sumners, *Data structures and algorithms for computation of topological invariants of entanglements: link, twist and writhe*, 1991, pp. 365–373.
- [LS06] C. Laing and D. W. Sumners, *Computing the writhe on lattices*, *Journal of Physics A: Mathematical and General* **39** (2006), no. 14, 3535–3543.
- [ML07] A. N. Morozov and S. H. Lin, *Accuracy and convergence of the Wang-Landau sampling algorithm*, *Physical Review E - Statistical, Nonlinear, and Soft Matter Physics* **76** (2007), no. 2, 026701.
- [MOS09] C. Manolescu, P. Ozsváth, and S. Sarkar, *A combinatorial description of knot Floer homology*, *Annals of Mathematics* **169** (2009), no. 2, 633–660, 0607691.
- [MS13] N. Madras and G. Slade, *The Self-Avoiding Walk*, Probability and Its Applications, Birkhäuser Boston, 2013.
- [MT93] W. Menasco and M. Thistlethwaite, *The Classification of Alternating Links*, *The Annals of Mathematics* **138** (1993), no. 1, 113.
- [NT08] L. Ng and D. Thurston, *Grid Diagrams, Braids, and Contact Geometry*, Proceedings of Gökova Geometry-Topology Conference 2008, dec 2008, pp. 120–136, 0812.3665.
- [OEI19a] OEIS Foundation Inc., *The On-Line Encyclopedia of Integer Sequences, Sequence A008306*, <https://oeis.org/A008306>, 2019.

- [OEI19b] ———, *The On-Line Encyclopedia of Integer Sequences*, Sequence A010790, <https://oeis.org/A010790>, 2019.
- [OEI19c] ———, *The On-Line Encyclopedia of Integer Sequences*, Sequence A082491, <https://oeis.org/A082491>, 2019.
- [OSS15] P. S. Ozsváth, A. I. Stipsicz, and Z. Szabó, *Grid homology for knots and links*, vol. 208, American Mathematical Soc., 2015.
- [PDS⁺11] J. Portillo, Y. Diao, R. Scharein, J. Arsuaga, and M. Vazquez, *On the mean and variance of the writhe of random polygons*, *Journal of Physics A: Mathematical and Theoretical* **44** (2011), no. 27, 275004.
- [Per14] K. A. Perko, Jr., *Remarks on the history of the classification of knots*, *Banach Center Publications* **103** (2014), no. 2, 241–250.
- [Rei27] K. Reidemeister, *Elementare Begründung der Knotentheorie*, *Abhandlungen aus dem Mathematischen Seminar der Universität Hamburg* **5** (1927), no. 1, 24–32.
- [Rol76] D. Rolfsen, *Knots and Links*, *AMS/Chelsea Publication Series*, AMS Chelsea Pub., 1976.
- [Ros14] S. Ross, *A First Course in Probability*, 9th ed., Pearson, Boston, MA, 2014.
- [Ryb97] V. V. Rybenkov, *Simplification of DNA Topology Below Equilibrium Values by Type II Topoisomerases*, *Science* **277** (1997), no. 5326, 690–693.
- [SIA⁺09] R. Scharein, K. Ishihara, J. Arsuaga, Y. Diao, K. Shimokawa, and M. Vazquez, *Bounds for the minimum step number of knots in the simple cubic lattice*, *Journal of Physics A: Mathematical and Theoretical* **42** (2009), no. 47, 475006.
- [SW88] D. W. Sumners and S. G. Whittington, *Knots in self-avoiding walks*, *Journal of Physics A: Mathematical and General* **21** (1988), no. 7, 1689–1694.
- [SYB⁺17] R. Stolz, M. Yoshida, R. Brasher, M. Flanner, K. Ishihara, D. J. Sherratt, K. Shimokawa, and M. Vazquez, *Pathways of DNA unlinking: A story of stepwise simplification*, *Scientific Reports* **7** (2017), no. 1, 12420.
- [VCS05] M. Vazquez, S. D. Colloms, and D. W. Sumners, *Tangle Analysis of Xer Recombination Reveals only Three Solutions, all Consistent with a Single Three-dimensional Topological Pathway*, *Journal of Molecular Biology* **346** (2005), no. 2, 493–504.
- [WfV18] S. Witte, M. Flanner, and M. Vazquez, *A Symmetry Motivated Link Table*, *Symmetry* **10** (2018), no. 11, 604.
- [Wit19] S. Witte, *Java Code for Working With Grid Diagrams*, <https://github.com/Minirogue/grid-diagrams>, 2019.
- [WL01] F. Wang and D. P. Landau, *Determining the density of states for classical statistical models: A random walk algorithm to produce a flat histogram*, *Physical Review E* **64** (2001), no. 5, 056101.
- [ZB05] C. Zhou and R. N. Bhatt, *Understanding and improving the Wang-Landau algorithm*, *Physical Review E* **72** (2005), no. 2, 025701.